THE ROLE OF P73 IN BASAL KERATINOCYTE FUNCTION

By

John Scott Austin Beeler

Dissertation

Submitted to the Faculty of the

Graduate School of Vanderbilt University

in partial fulfillment of the requirements

for the degree of

DOCTOR OF PHILOSOPHY

in

Biochemistry

December 14, 2019

Nashville, Tennessee

Approved:

Jennifer A. Pietenpol, Ph.D.

David K. Cortez, Ph.D.

Scott W. Hiebert, Ph.D.

Christine M. Lovly, M.D., Ph.D.

Ian G. Macara, Ph.D.

To my parents and entire family,

and to Gaby

ACKNOWLEDGMENTS

A large number of people have played important roles, both professionally and personally, in allowing me to reach this point in my career. Growing up, I couldn't have imagined this path as a possibility for a kid from the middle of nowhere with parents who were just kids themselves. I plan to use this section to acknowledge some of the many people in my life that have played an important role in making this dissertation possible.

First off, I want to thank my mentor Dr. Jennifer Pietenpol. Without her unwavering support and guidance this dissertation would not have been possible. I was drawn to Jennifer's laboratory by her passion for science, proven track record of being an exceptional lifelong mentor, and the laboratory's focus on performing research that truly impacted human health. I am so thankful that Jennifer always pushed us to broaden our training so that we could be well-rounded scientists during our dissertation and in the future. Despite having a hectic schedule full of professional and administrative responsibilities, Jennifer was always a devoted mentor who made time for me. I consider myself particularly fortunate to have been able to witness such a great leader and mentor during graduate school, and hope that I can emulate Jennifer's approach during my professional career.

Another mentor who has made a huge impact on my life is Dr. Scott Hawley at the Stowers Institute for Medical Research. I joined Dr. Hawley's laboratory while I was an undergraduate student at the University of Missouri-Kansas City. My experience in his laboratory was wonderful and

instilled in me a passion for the scientific process. I am grateful for having such a positive training environment in my first research experience. I will forever appreciate Dr. Hawley's assistance in navigating the medical school applications process and always making me feel like a valued and important member of his research team, even as an undergraduate researcher.

I want to thank the members of my thesis committee: Dr. David Cortez, Dr. Scott Hiebert, Dr. Christine Lovly, and Dr. Ian Macara. They provided valuable insights and constructive feedback that tremendously improved the quality of my thesis project. I would also like to thank former members of the committee: Dr. William Pao and Dr. Carlos Arteaga.

I am grateful to current and former members of the Pietenpol laboratory for their support and assistance over the years. Kim Johnson, the laboratory mother, provided unwavering support and had a fix to any problem that arose, whether determining the best way to process a tissue for sectioning, obtaining out of stock reagents, or knowing who to contact to fix a water leak in the men's bathroom. Lynnette Stanton-Williams helped me find times for committee meetings that fit the busy schedules of Jennifer and my committee members. Hailing Jin is a talented experimentalist whose skills were incredibly beneficial in allowing me to finish up my research. Qing Zhang's assistance keeping the tissue culture area clean and organized was important for the many *in vitro* experiments presented in this dissertation. Spencer Lea, an undergraduate student in the laboratory,

made helpful contributions during experimental validation of the induced keratinocyte model system.

My fellow trainees in the Pietenpol laboratory have been key collaborators and provided significant assistance with my dissertation research. I truly appreciate the support each fellow trainee contributed scientifically, academically, and personally to me. I owe an immense amount of gratitude to Clayton Marshall. He spent a considerable amount of time introducing me to the p73-/- mouse model, discussing experimental results, and brainstorming future directions for my project. In addition, he was instrumental in performing the analyses described in this dissertation that used murine models. I would like to thank Bojana Jovanovic, Clayton Marshall, Tim Shaver, Gaby Santos, and Johanna Schaefer for allowing me to collaborate with them during graduate school and make team science a truly fun experience.

I am thankful to my collaborators and colleagues at Vanderbilt for their assistance with my project. Dr. Bryan Venters provided essential guidance to successfully perform ChIP-seq experiments. Dr. Paula Gonzalez Ericsson was instrumental in analyzing the skin of wild-type and p73-deficient mice during homeostasis and after injury. I really appreciate her willingness to take the time to educate me about the histology of the skin and image analysis software. The laboratories of Sandra Zinkel, David Cortez, and Christine Lovly contributed feedback during lab meetings that improved my research and helped determine which lines of investigation to

pursue. I am grateful to Dr. Olivia Koues, Dr. Yu Shyr, and Dr. Tiger Sheng for providing their assistance with next-generation sequencing applications.

I am grateful to current and past members of the Vanderbilt Medical Scientist Training Program (MSTP) leadership team for their guidance and support: Dr. Chris Williams, Dr. Lourdes Estrada, Dr. Megan Williams, Bryn Sierra, Melissa Krasnove, and Dr. Terry Dermody. I would like to thank the Vanderbilt Department of Biochemistry for their support during training: Dr. John York, Dr. Chuck Sanders, Patty Mueller, Jen Smith, and Marlene Jayne. My dissertation research was supported by NIH grants CA105436, CA070856, CA098131, and CA068485 to J.A.P. and NIH Vanderbilt Medical Scientist Training Program (GM007347) grant support to J.S.B.

I am incredibly thankful to my family and friends for all of the support they provided during my time in graduate school. Their unconditional support and belief in me meant the world and was essential in helping me get through the tough times when science wasn't going very well. In particular, I want to thank my parents for the sacrifices they made to raise me and the example they provided to me growing up. They always put my needs first, made sure I knew they loved me, and instilled in me a sense of dignity. I am also very grateful to my large extended family, who played an important role in raising me and getting me to the point where I was able to obtain a postgraduate degree. To all of my friends I made in Nashville and Kansas City, thank you so much for your support and helping me find wellness during my educational journey.

TABLE OF CONTENTS

LIST OF TABLES

LIST OF FIGURES

LIST OF ABBREVIATIONS

3’	3′-end (of a nucleic acid)
5’	5′-end (of a nucleic acid)
aa	Amino acid(s)
AEC	Ankyloblepharon-ectodermal defects-cleft lip/palate
Ana	Anagen
APM	Arrector pili muscle
ATCC	American Type Culture Collection
bp	Base pair(s)
Bu	Bulge (region of the hair follicle)
cDNA	Complementary DNA
CDS	Coding sequence
ChIP	Chromatin immunoprecipitation
CPI	Complete protease inhibitor
C-terminal	Carboxy-terminal
DAPI	4’,6-diamidino-2-phenylindole
DBD	DNA binding domain
DMEM	Dulbecco’s Modified Eagle’s Medium
DNA	Deoxyribonucleic acid
DP	Dermal papilla
E12.5	Mouse embryonic day 12.5
EX-E4	All p73/p63 exon junctions with exon 4 as the 3’ exon

E10-EX	All p73/p63 exon junctions with exon 10 as the 5' exon
ECL	Enhanced chemiluminescence
ENCODE	Encyclopedia of DNA Elements Project
ERCC	External RNA Controls Consortium
FACS	Fluorescence-activated cell sorting
FBS	Fetal bovine serum
FDR	False discovery rate
FLG	Filaggrin
GAPDH	Glyceraldehyde-3-phosphate dehydrogenase
GENCODE	Encyclopedia of Genes and Gene Variants Project
GO	Genome Ontology
GTEx	Genotype-Tissue Expression Project
h	Hour(s)
H&E	Hematoxylin and eosin
HB	Hair bulb
HDFn	Neonatal human dermal fibroblast(s)
HF	Hair follicle
HFSC	Bulge hair follicle stem cell(s)
HG	Hair germ
HK	Human keratinocyte(s)
HMEC	Human mammary epithelial cell(s)
HPA	Human Protein Atlas
HRP	Horseradish peroxidase

HS	Hair shaft
IACUC	Institutional Animal Care and Use Committee
IB	Immunoblotting
IF	Immunofluorescence
IFE	Interfollicular epidermis
IGV	Integrative Genomics Viewer
IHC	Immunohistochemistry
iKC	Induced basal keratinocyte(s)
iPSC	Induced pluripotent stem cell(s)
kb	Kilobase
kDa	Kilodalton
Ki67	Marker of proliferation Ki-67 (*MKI67*)
KRT14	Keratin 14
KRT5	Keratin 5
MDM2	Mouse double minute 2
mL	Milliliter
min	Minute(s)
mRNA	Messenger RNA
NBF	Neutral buffered formalin
NCBI	National Center for Biotechnology Information
NCI	National Cancer Institute
NIH	National Institutes of Health
nt	Nucleotide(s)

N-terminal	Amino-terminal
OD	Oligomerization domain
oligo(dT)	oligo(deoxythymine)
ORS	Outer root sheath
P1	Postnatal day 1 (murine age)
p21	Cyclin-dependent kinase inhibitor 1 (*CDKN1A*)
p53	Tumor protein p53
p53	*Trp53* (mice) or *TP53* (human) gene
p63	Tumor protein p63
p63	*Trp63* (mice) or *TP63* (human) gene
p73	Tumor protein p73
p73	*Trp73* (mice) or *TP73* (human) gene
PAGE	Polyacrylamide gel electrophoresis
PBS	Phosphate-buffered saline
PCA	Principal component analysis
PCR	Polymerase chain reaction
poly-A	Polyadenylation
PVDF	Polyvinylidene fluoride
qRT-PCR	Quantitative reverse transcription PCR
RAMPAGE	RNA Annotation and Mapping of Promoters for Analysis of Gene Expression
RIPA	Radioimmunoprecipitation assay
RNA	Ribonucleic acid

RNA-seq	RNA sequencing
RPMI	Roswell Park Memorial Institute
SAM	Sterile alpha motif
SC	Stem cell(s)
SD	Standard deviation
SDS	Sodium dodecyl sulfate
SEM	Standard error of the mean
SFN	Stratifin or 14-3-3 sigma
SG	Sebaceous gland
scRNA-seq	Single-cell RNA-sequencing
TA	Transactivation
TAC	Transit-amplifying cell(s)
TPM	Transcripts per million
TSA	Tyramide signal amplification
TSS	Transcriptional start site(s)
UMAP	Uniform Manifold Approximation and Projection
UTR	Untranslated region
VANTAGE	Vanderbilt Technologies for Advanced Genomics
v/v	Volume/volume percentage
WT	Wild-type
w/v	Weight/volume percentage

CHAPTER I

INTRODUCTION

The development, homeostasis, and repair of mammalian tissues is ultimately governed by transcription factors that bind DNA and regulate the transcription of genes. The composite effect of transcription factors on gene expression can be assessed by analyzing transcriptomes, the set of all RNA molecules and their quantity in a single cell or population of cells. Different cell types express unique transcriptional programs, and this variation underlies the wide range of physical, biochemical, and developmental differences seen among various cells and tissues. By performing comparative analyses on the transcriptional programs of different types of cells or tissues, researchers can gain a deeper understanding of what constitutes a specific cell type and how changes in the transcription of genes contribute to development and disease. In this chapter, the p53 family of transcription factors and their functions in mammalian tissues will be reviewed, with an emphasis on one family member, p73, and one specific tissue, the skin; and epidermal differentiation, homeostasis, and wound healing will be introduced. This dissertation primarily focuses on the role of p73 in basal keratinocytes of the skin and identifies p73 as a regulator of epidermal wound healing and keratinocyte gene expression.

p53 Family of Transcription Factors

Discovery

In 1979, p53 was discovered as a 53 kDa protein in complex with SV40 large T antigen in SV40-transformed cells (Lane and Crawford, 1979). Subsequent studies over several decades demonstrated that p53 is a tumor suppressor (Baker et al., 1989; Donehower et al., 1992; Malkin et al., 1990; Srivastava et al., 1990) and is the most frequently mutated gene in human cancers (Kandoth et al., 2013). p53 has been dubbed the "guardian of the genome" by its co-discoverer (Lane, 1992), Sir David Lane, for the important role it plays in coordinating the cellular response to DNA damage, through regulation of cell cycle arrest (Baker et al., 1990; Diller et al., 1990; Mercer et al., 1990), induction of apoptosis (Michalovitz et al., 1990; Yonish-Rouach et al., 1991), and cellular senescence (Serrano et al., 1997). The tumor suppressive activity of p53 is mediated by its ability to function as a sequence-specific transcription factor (Fields and Jang, 1990; Pietenpol et al., 1994; Raycroft et al., 1990) that binds and regulates the expression of target genes such as *CDKN1A* (which encodes p21, the cyclin-dependent kinase inhibitor) (el-Deiry et al., 1993; Kandoth et al., 2013) and *MDM2* (Barak et al., 1993; Wu et al., 1993). Mice lacking p53 (*p53*-/-) have a normal appearance, but develop a variety of spontaneous tumors by six months of age (Donehower et al., 1992). Similarly, inactivating mutations in human p53 gene (*TP53*) cause Li-Fraumeni

syndrome (Malkin et al., 1990; Srivastava et al., 1990), an autosomal dominant-inherited cancer predisposition syndrome that is characterized by the development of a variety of childhood and adult tumors.

It took almost two decades for a homologue of p53 to be identified. In 1997, Kaghad and colleagues (Kaghad et al., 1997) identified p73 as a false positive in a cDNA screen for sequences corresponding to the protein-binding domain of the insulin receptor substrate 1 (IRS-1; involved in insulin signaling). The investigators found that the gene of interest had 63% amino acid identity with the p53 DNA-binding domain and could induce expression of p21 protein (a canonical p53 target gene) (Kaghad et al., 1997). Much of the initial work on p73 focused on its role in tumor suppression given its similarity to p53. However, mice lacking p73 (*p73*-/-) had distinct phenotypes compared to *p53*-/- mice, exhibiting developmental defects including: hippocampal dysgenesis, hydrocephalus, chronic infections, pheromone sensory deficits, runting, and sterility (Yang et al., 2000). Unlike *p53*-/- mice, *p73*-/- did not exhibit an increase in spontaneous tumor formation (Yang et al., 2000). Only recently was a unifying mechanism identified to explain many of the diverse phenotypes observed in *p73*-/- mice (Marshall et al., 2016; Nemajerova et al., 2016); and the results leading to that mechanism will be discussed in further detail below.

One year after the discovery of p73, a third family member, p63, was discovered in a screen to identify additional genes belonging to the p53 family (Yang et al., 1998). Yang and colleagues reported that p63 had 60%

amino acid identity with the p53 DNA-binding domain and 85% identity with the p73 DNA-binding domain, and was expressed by the proliferating basal cells of the epithelial layers of the skin, cervix, urothelium, and prostate (Yang et al., 1998). The development of mice lacking p63 (*p63*-/-) revealed that p63 was essential for tissue development (Mills et al., 1999; Yang et al., 1999). *p63*-/- mice have major developmental defects including a lack of stratified squamous epithelia and glandular epithelial structures (hair follicles, sweat glands, mammary glands, prostate gland), defective limb and craniofacial developmental, and die shortly after birth (Mills et al., 1999; Yang et al., 1999). Consistent with the phenotype of *p63*-/- mice, mutations in the human p63 gene (*TP63*) were identified as causative for several human ectodermal dysplasia syndromes (van Bokhoven et al., 1999, 2001; Celli et al., 1999; Ianakiev et al., 2000; McGrath et al., 2001), which are characterized by the abnormal development of two or more ectodermal tissues (skin, hair, nails, teeth, and sweat glands) (Rinne et al., 2007).

These early observations led researchers to investigate the biological roles of p63 in epithelial development and homeostasis (versus in p53-like tumor suppressive functions). Subsequent studies have collectively shown that p63 regulates a transcriptional program that is essential for stem cell maintenance, proliferation, and development in stratified epithelial tissues (Mills et al., 1999; Senoo et al., 2007; Truong et al., 2006; Yang et al., 1999). In contrast with the function of p53 as a tumor

suppressor, elevated levels of p63 protein, resulting from *p63* gene amplification in select tumors (Hibi et al., 2000), are oncogenic in a significant fraction of human squamous cell carcinomas (in the lung, head and neck region, and esophagus) (Hu et al., 2002; Massion et al., 2003; Sniezek et al., 2004; Thurfjell et al., 2005; Weber et al., 2002).

Evolutionary History

A p53 family-like gene was first observed in single cell choanoflagellates and early metazoans sea anemone approximately one billion years ago (Belyi et al., 2010). A homologue of this gene is found in nearly all invertebrates, where it functions in protecting germ cells from DNA damage and prevents genomic instability (Belyi et al., 2010). The three canonical p53 family genes were first observed approximately 450 million years ago (Venkatesh et al., 2014) in early vertebrates as a result of two successive duplications of the ancestor p53 family-like gene (Belyi et al., 2010). This occurred at the time when vertebrates developed somatic stem cells with the capacity to maintain and repair tissues for the lifespan of an organism (Belyi et al., 2010). The initial gene duplication was observed in cartilaginous fish, yielding a p53-like gene and a p73/p63-like gene (Belyi et al., 2010). When bony fish diverged from cartilaginous fish shortly afterwards, a second gene duplication event (of the p73/p63-like gene) was observed, giving rise to separate p73-like and p63-like genes (Belyi et al., 2010). The presence of these three canonical p53 family genes is

conserved from bony fish through most all subsequent higher vertebrates, including: amphibians, mammals, reptiles, and birds (Belyi et al., 2010). Throughout vertebrate evolution, p53 family genes took on specialized functions, in addition to the ancestral role of the family in maintaining genomic integrity of the germline, including: (1) p53 - tumor suppression in somatic stem cells; (2) p63 - epithelial development, differentiation, and stem cell maintenance; and (3) p73 - formation of multiciliated cells as well as neural differentiation and cell maintenance (Belyi et al., 2010; Marshall et al., 2016; Nemajerova et al., 2016).

Gene and Protein Structure

p53 family members have a similar gene and protein structure (Blandino and Dobbelstein, 2004; Yang et al., 2002). Each gene contains multiple promoters, that enable the generation of transcripts encoding for protein products with different amino (N)-terminal sequences (Figure 1.1) (Bourdon et al., 2005; Kaghad et al., 1997; Yang et al., 1998, 2000). Proteins generated from the first promoter (P1) are longer and contain a full-length transactivation (TA) domain, which confers a more canonical p53-like function at target genes (Kaghad et al., 1997; Yang et al., 1998). In contrast, proteins generated from the second promoter (P2) are shorter and have a truncated TA domain (referred to as ΔN), which typically inhibits canonical p53-like functions (Bourdon et al., 2005; Yang et al., 1998, 2000).

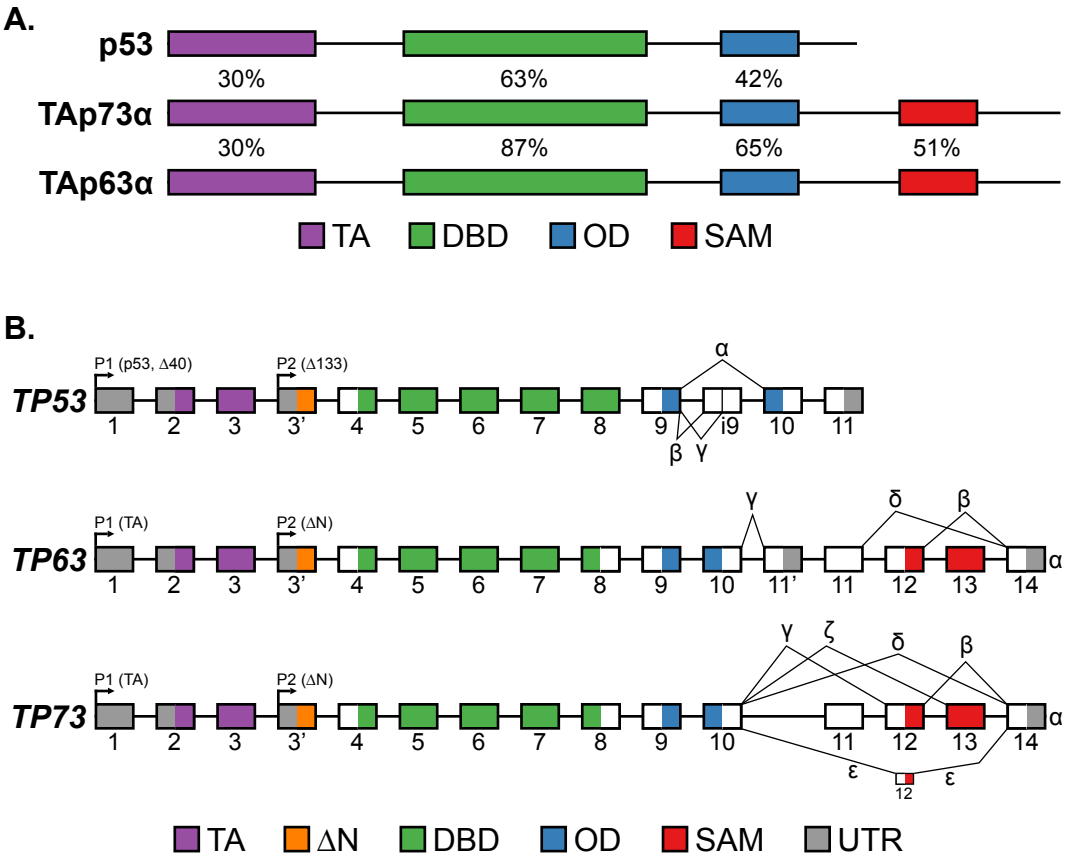

Figure 1.1. p53 Family Gene and Isoform Structure. (A) Schematic representation of the full-length p53 family proteins. Protein domains are labeled with color: transactivation (TA), purple; DNA-binding domain (DBD), green; oligomerization domain (OD), blue; and sterile alpha motif (SAM) domain, red. The percentage of amino acid sequence identify between the domains of p53 family members are listed. (B) Schematic representation of the structure of p53 family genes. Known promoters and mRNA splicing isoforms are annotated for each gene. Exons are labeled according to the protein domain they encode (same schema as in A) or the type of mRNA sequence: truncated transactivation domain (ΔN), orange; and untranslated region (UTR), gray.

However, the ΔN proteins of p73 and p63 also bind to and activate the expression of specific target genes, particularly ones important in development (Dohn et al., 2001; Ihrie et al., 2005; Liu et al., 2004; Wu et al., 2003). Family member genes also undergo 3' alternative splicing, producing transcripts with different 3' exons that encode for proteins with different carboxy (C)-terminal sequences (Figure 1.1), resulting in variable ability to transactivate target genes (Bourdon et al., 2005; Kaghad et al., 1997; Yang et al., 1998).

Each p53 family member gene encodes a central DNA-binding domain with greater than 60% amino acid identify with other family members (63% between p53 and p73, 60% between p53 and p63, and 87% between p73 and p63) (Yang et al., 2002). This high degree of sequence homology (in the DNA-binding domain) leads to structural conservation, resulting in the family members binding to and regulating overlapping target genes containing a canonical p53 consensus response element (Flores et al., 2002; Jost et al., 1997; Kaghad et al., 1997; Westfall et al., 2003) composed of two copies of RRRCWWGYYY (where R = purines, C = cytosine, W = adenine or thymine, G = guanine, and Y = pyrimidines) separated by a 0-13 bp spacer (el-Deiry et al., 1992). More detailed investigation of the p73 and p63 consensus DNA-binding sites showed that they are more degenerate than the p53 consensus site (Osada et al., 2005; Perez et al., 2007; Rosenbluth et al., 2011; Sasaki et al., 2005; Yang et al., 2010), likely reducing binding selectivity, which would

contribute to the differences observed in target genes (e.g. *JAG1*, *ING1*, and *PTPN14*) and biological functions between family members.

Each p53 family gene encodes for a conserved C-terminal oligomerization domain (Figure 1.1) that mediates the formation of tetramers [consist of a dimer of dimers (Coutandin et al., 2009; Jeffrey et al., 1995; Joerger et al., 2009; Kitayner et al., 2006; Natan and Joerger, 2012)], a process that increases the DNA-binding affinity and transcriptional activity of the transcription factor relative to monomeric or dimeric forms (Chène, 2001; Davison et al., 1999; Weinberg et al., 2004). The transcriptional activity of tetramers is also influenced by the isoforms of the monomers that make up each complex (e.g. generally TA isoforms are stronger inducers of canonical p53 target genes involved in the DNA damage response) (Nemajerova et al., 2018). Through the oligomerization domains, p73 and p63 can form heterodimers and heterotetramers with one another, but not with p53 (Davison et al., 1999).

The C-terminus of full-length α isoforms of p73 and p63 contain a sterile alpha motif (SAM) domain that is lacking from p53 (Figure 1.1) (Thanos and Bowie, 1999). SAM domains are found in proteins from a variety of organisms, from yeast to humans, and regulate a multitude of biological processes through protein-protein (Kim et al., 2001; Ponting, 1995) and protein-RNA (Aviv et al., 2003) interactions. The function of the p73 and p63 SAM domains are not well understood; however, early research linked a distinct ectodermal dysplasia syndrome [Hay-Wells or

ankyloblepharon-ectodermal defects-cleft lip/palate (AEC) syndrome] to specific mutations in the p63 SAM domain, suggesting that the domain might have a biological function in humans (McGrath et al., 2001). Indeed, Russo and colleagues found that AEC-associated mutations in the p63 SAM domain induced protein misfolding and aggregation, unlike the p63 mutations causative for other ectodermal dysplasia syndromes (Russo et al., 2018).

Regulation

Levels of p53 protein (and its transcriptional activity) are primarily regulated by post-translational modifications of the protein. MDM2, an E3 ubiquitin ligase, is critical in this regulation. In unstressed cells, MDM2 keeps cellular levels of p53 low by binding to and ubiquitinating p53, which marks p53 for degradation (Haupt et al., 1997). After cellular stress, p53 and MDM2 are modified by a series of post-translational modifications (including phosphorylation), which prevent MDM2 from binding to and inhibiting p53, resulting in increased levels of p53 protein and activity (Shieh et al., 1997). In addition, p53 binds to and increases the expression of MDM2 (Barak et al., 1993), which forms an autoregulatory feedback loop that keeps cellular levels of p53 tightly regulated.

The molecular details governing the regulation of p73 and p63 protein levels and transcriptional activity are less well understood than for p53, but occur through a complex combination of transcriptional and post-

transcriptional regulatory events. mRNA isoforms of p73 and p63 are expressed in a tissue-specific manner, suggesting that the genes are conditionally regulated in a cell type- and developmental-stage specific manner. Past studies have provided evidence to support this by identifying several transcription factors and signaling pathways that regulate the transcription of *p73* and *p63*. E2F-1 (Irwin et al., 2000; Seelan et al., 2002; Stiewe and Pützer, 2000), ZEB (Fontemaggi et al., 2001), YY1 (Wu et al., 2008), and CEBPA (Marabese et al., 2003) bind to the P1 promoter of *TP73* and regulate expression of TAp73 mRNA. TAp73 and p53 (Grob et al., 2001) bind to the P2 promoter of *TP73* and induce expression of ΔNp73 mRNA. NOTCH1 activation, epithelial-to-mesenchymal transition (EMT) transcription factors (SNAIL, SLUG, and ZEB1), and DNA damaging agents repress expression of ΔNp63 mRNA (Chua et al., 2007; Herfs et al., 2010; Higashikawa et al., 2007; Liefer et al., 2000; Nguyen et al., 2006); while FGF7 and STAT3 induce expression of ΔNp63 mRNA (Cheng et al., 2009). LEF1/TCF/β-catenin and CEBPD bind to the P2 promoter of *TP63* and induce expression of ΔNp63 mRNA (Barbaro et al., 2007; Borrelli et al., 2007; Chu et al., 2008; Ferretti et al., 2011). GLI3 (Li et al., 2008) and OCT4 (Ng et al., 2014) induce expression of TAp63; OCT4 through binding to the P1 promoter of *TP63*.

Similar to p53, the protein levels of p73 and p63 are regulated by protein-protein interactions and post-translational modifications. Proteins that bind to and regulate p73 and/or p63 include: (1) ITCH (E3 ubiquitin

ligase) that binds to and poly-ubiquitinates p73 and p63, promoting proteasomal degradation (Rossi et al., 2005, 2006); (2) YAP1 (Hippo signaling) that binds to and stabilizes p73α/β by inhibiting ITCH binding (Levy et al., 2007a); (3) PIRH2 (E3 ubiquitin ligase) that binds to and poly-ubiquitinates p73 and p63, promoting proteasomal degradation (Conforti et al., 2013; Jung et al., 2013; Wu et al., 2011) and (4) ASPP1 and ASPP2 that bind to p73 and p63, inducing transcriptional activity (Bergamaschi et al., 2004; Levy et al., 2007a)

The coordinate regulation of target genes by p53 family members (Flores et al., 2002; Jost et al., 1997; Kaghad et al., 1997; Westfall et al., 2003) occurs at multiple levels including: (1) p53 family proteins compete for access to the DNA-binding sites of shared target genes (DeYoung et al., 2006; Schavolt and Pietenpol, 2007; Serber et al., 2002; Stiewe and Pützer, 2000); (2) regulation of p53 family isoform expression, since different isoforms have variable transcriptional activity at many target genes (Bourdon et al., 2005; Kaghad et al., 1997; Yang et al., 1998, 2000); (3) p53 family proteins bind to and regulate the expression of other p53 family members (Grob et al., 2001; Harmes et al., 2003; Westfall et al., 2003) and themselves (Grob et al., 2001; Li et al., 2006; Nakagawa et al., 2002); (4) the activity of p53 family proteins is regulated by co-binding partners (Dobbelstein et al., 1999; Haupt et al., 1997; Levy et al., 2007a; Rossi et al., 2005, 2006; Zeng et al., 1999); and (5) p73 and p63 bind to one another through the oligomerization domains and form transcriptionally

active heterotetramers (Davison et al., 1999). A recent study found that heterotetramers of p73 and p63 are more stable *in vitro* than either homotetramer and provided evidence for their existence *in vivo* through immunoprecipitation studies in primary keratinocytes (Gebel et al., 2016). This study supported a previous publication that found p73 and p63 co-occupy DNA target sites *in vivo* (human ME180 cervical carcinoma cells) by sequential chromatin immunoprecipitation (Yang et al., 2010). The function of p73 and p63 heterotetramers is not well understood, but will be important for understanding the role of each family member in the many tissues (Puig et al., 2003) and cancers (DeYoung et al., 2006; Leong et al., 2007; Rocco et al., 2006) that co-express both proteins. The complex regulation amongst p53 family members and of each family member protein by itself makes it difficult to interpret the results from any given study in which investigators limited their scope of study to one protein of the p53 family in isolation. The studies presented in Chapters III and IV begin to address this complexity and present results of experiments in which p73 and p63 are coordinately investigated at the transcript and protein level.

Biological Roles of p73 from Knockout Mouse Models

p73-/- mouse models have provided significant insight to the biological roles of p73. Development and characterization of the first *p73*-/- mouse model was reported in 2000 (Yang et al., 2000). The model was

generated by deletion of exons 5 and 6 (encode for part of the DNA-binding domain) and each tissue in the mice was functionally deficient for all p73 isoforms (Yang et al., 2000). The *p73*-/- mice exhibited developmental defects including: hippocampal dysgenesis, hydrocephalus, chronic infections and inflammation, runting, female sterility, male infertility, gastrointestinal bleeding, and abnormal pheromone sensory pathways (Yang et al., 2000). In this report and for 15 years afterwards, the diverse phenotypes observed in *p73*-/- mice lacked a clear and unifying hypothesis. In 2016, the Pietenpol laboratory described the generation of another *p73*-/- mouse model, through deleting exons 7-9 (encode for part of the DNA-binding domain and the oligomerization domain), and discovered that p73 is essential for the formation of multiciliated cells (Marshall et al., 2016). Many of the phenotypes observed in all the *p73*-/- mouse models reported to date can be explained by a loss of multiciliated cell function in tissues including: hydrocephalus - lack of multiciliated ependymal cells in the central nervous system to regulate cerebrospinal fluid; chronic infections - lack of multiciliated in the airway to clear foreign agents; female sterility - lack of multiciliated in the oviduct to regulate the passage of eggs from the ovaries to the uterus; and male sterility - sperm in the testis lack flagella). p73 regulates a transcriptional program in multiciliated cells that includes key transcriptional modulators of multiciliogenesis (e.g. *Foxj1* and *Myb*) (Marshall et al., 2016; Nemajerova et al., 2016). Other studies of *p73*-/- mice have uncovered additional roles for p73 in diverse processes

including: survival and maintenance of cortical neurons (p73 prevents premature apoptosis) (Pozniak et al., 2002); neural stem cell maintenance (p73 promotes self-renewal and proliferation as well inhibits premature senescence) (Talos et al., 2010); and ovarian follicle development (p73 regulates a transcriptional program involved in cell-to-cell adhesion and migration) (Santos Guasch et al., 2018).

Isoform specific *p73* knockout mouse models have been useful in determining the biological roles of individual p73 isoforms in development, homeostasis, and tumorigenesis. TAp73-/- mice, which were generated by deletion of exons 2 and 3 (Figure 1.1), have less severe developmental defects than *p73*-/- mice (Tomasini et al., 2008). TAp73-/- mice exhibit many phenotypes that overlap with *p73*-/- mice (but were milder) including: hippocampal dysgenesis, infertility, and chronic infections and inflammation (Tomasini et al., 2008). TAp73-/- mice develop spontaneous and carcinogen-induced tumors at an increased rate (not observed in *p73*-/- mice), indicating that TAp73 functions as a tumor suppressor (Tomasini et al., 2008), in part through binding with and modulating the activity of protein involved in the spindle assembly checkpoint, which promotes proper chromosome segregation and helps prevent aneuploidy (Tomasini et al., 2009). Ensuing studies using TAp73-/- mice have discovered additional functions for TAp73 in: antioxidant defense (TAp73 protects against aging, premature senescence, and reactive oxygen species accumulation by inducing the expression of *Cox4i1*, a subunit of cytochrome C oxidase, the

final enzyme in the electron transport chain) (Rufini et al., 2012); glucose metabolism (TAp73 induces expression of glucose-6-phosphate dehydrogenase, the rate-limiting enzyme of the pentose phosphate pathway, which supports cell proliferation) (Du et al., 2013; Jiang et al., 2013); spermatogenesis (TAp73 prevents the premature loss of immature germ cells by regulating an adhesion-related transcriptional program) (Holembowski et al., 2014; Inoue et al., 2014); and multiciliogenesis (TAp73 functions as a central regulator of multiciliated cell differentiation by directly activating the expression of numerous ciliary genes) (Nemajerova et al., 2016; Wildung et al., 2019).

ΔNp73-/- mice, which were generated by deletion of exon 3' (Figure 1.1), have a milder phenotype than TAp73-/- mice (Tissir et al., 2009; Wilhelm et al., 2010). ΔNp73-/- mice have a normal life span, are fertile, and lack the severe chronic infections observed in *p73*-/- mice (Tissir et al., 2009; Wilhelm et al., 2010). However, both ΔNp73-/- and *p73*-/- mice share select neuronal phenotypes including hypoplasia of the cortex, choroid plexus, vomeronasal organ, and Cajal-Rezius cells (Tissir et al., 2009; Wilhelm et al., 2010). The hypoplasia observed in these p73 expressing neuronal cell populations is due, in part, to increased apoptosis (Tissir et al., 2009) and suggests a role for ΔNp73 in neuronal cell survival as a negative regulator of p53- and/or TAp73-dependent apoptosis. This role is supported by work showing that primary thymocytes from ΔNp73-/- mice exhibit increased apoptosis in response to DNA-damage (γ-irradiation) in a

p53-dependent manner (i.e. phenotype reverses in a *p53*-null background) (Wilhelm et al., 2010).

The reduced severity or absence of phenotypes across tissue types in isoform-specific knockout mice (TAp73-/- and ΔNp73-/-) compared to global knockouts (*p73*-/-) (Wilhelm et al., 2010) suggest that the isoform classes have overlapping or interacting functions within individual tissues and cells. This is an important factor to consider when studying the roles of a p73 isoform in a given tissue in isolation. Determining which p73 isoforms are normally expressed in a given tissue during homeostasis is required for assessing the functional role of p73 in that given tissue. The expression pattern of p73 isoforms in normal tissues and cell types has not been well understood due to a lack of p73 isoform-specific antibodies and challenges associated with accurately quantifying RNA isoforms in genes with characteristics like *p73*, including: expression of an array of RNA isoforms through alternative promoter usage and alternative splicing (Figure 1.1), transcript length > fragment length of sequencing library, and relatively low expression levels (Sarantopoulou et al., 2019). We have started to address these challenges in the studies described in Chapters III and IV.

During our prior study linking p73 to multiciliogenesis, we discovered that 50% of p63-expressing basal epithelial cells in the trachea co-express p73 and that tracheas from *p73*-/- mice exhibit a 35% reduction in the number of basal epithelial cells [despite the loss of the most common cell type (multiciliated cell) in the tissue] (Marshall et al., 2016). Co-expression

of p73 and p63 has been previously observed in the basal cell populations of other epithelial tissues (Puig et al., 2003), but little was known about the role of p73 in these basal progenitor cells including which isoforms they express. Unlike *p63*-/- mice (Mills et al., 1999; Yang et al., 1999), *p73*-/- mice develop stratified epithelia including the skin epidermis, indicating that p73 is not required for proper epidermal morphogenesis. p73 expression is also a marker of the basal epidermal stem cell population located near hair follicles (scale-like skin) (Sada et al., 2016). Numerous other studies have also linked p73 to stem cell activity in a variety of biological contexts including: neuronal stem cells (Agostini et al., 2010; Gonzalez-Cano et al., 2010; Talos et al., 2010), induced pluripotent stem cells (Alexandrova et al., 2013; Lin et al., 2012; Martin-Lopez et al., 2017), cancer cells (Meier et al., 2016), and aging (Rufini et al., 2012).

Collectively, observations from our laboratory and others, led us to hypothesize that p73 plays a role in the maintenance of basal epithelial cells and/or regulates the stem cell activity of basal progenitor cells. We tested this hypothesis through a series of experiments described in Chapters III and IV of this dissertation. To determine levels and types of p73 isoforms expressed by basal cells across different tissues, we developed an algorithm to quantify p73 isoform expression in a large-scale dataset of tissue-specific gene expression (53 tissues, 714 individuals, 11,688 RNA-seq samples) (Carithers et al., 2015; GTEx Consortium, 2013) as described in Chapter III. In Chapter IV, we focused on a specific tissue,

the skin, which we discovered predominantly expresses ΔNp73 and analyzed p73 in relation to p63 in basal epithelial cells. We discovered that *p73*-/- mice exhibit delayed wound healing, p73 is expressed by the stem cell populations of the skin that govern wound healing, and that ΔNp73 regulates the expression of a gene network involved in basal keratinocyte biology (Beeler et al., 2019).

Epithelial Skin Biology

Epidermal Differentiation and Homeostasis

The skin functions as a barrier to protect the body from physical, microbial, and chemical assaults as well as unregulated loss of water and solutes (Proksch et al., 2008a). It has two primary layers, the epidermis and dermis (Figure 1.2). The epidermis is the outermost layer of the skin and is a stratified squamous epithelium. It consists of an inner layer of proliferative basal keratinocytes (connected to an underlying basement membrane) and outer layers of differentiating keratinocytes (Figure 1.2). The dermis is located beneath the epidermis, anchored to it by adhesion molecules within the basement membrane, and primarily composed of connective tissue that plays important roles in mechanical support, sensation, and thermoregulation. Epidermal appendages, including hair follicles and sweat glands as well as blood vessels that supply the epidermis, are located in the dermis.

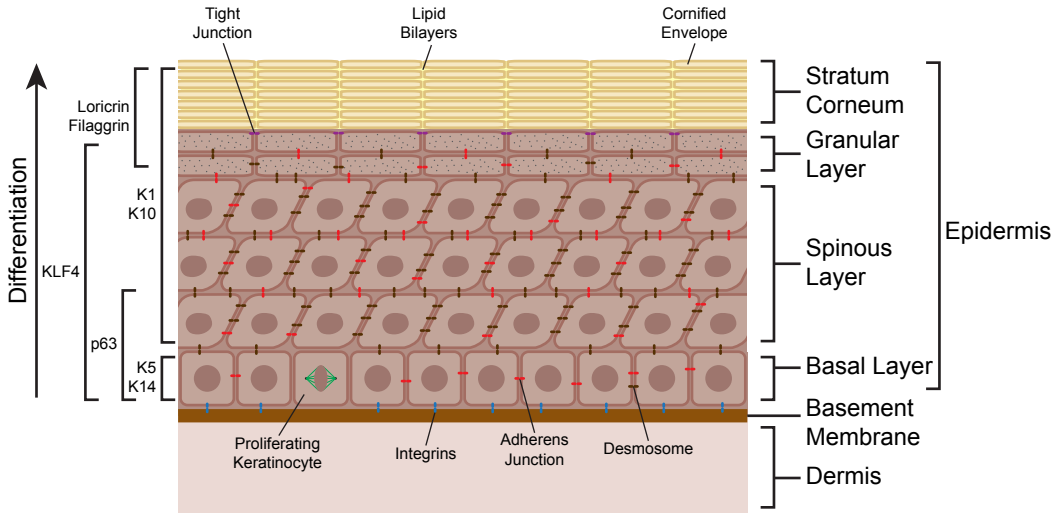

Figure 1.2. Schematic of Epidermal Differentiation and Markers. The epidermis is the outermost layer of the skin and provides most of the barrier function to the organ. It is a stratified squamous epithelium composed of epidermal keratinocytes organized into four main layers, which each have a different morphological appearance and differentiation status. Periodically, keratinocytes in the basal layer (progenitor population of the tissue) detach from the underlying basement membrane and migrate towards the surface of the skin while undergoing a terminal differentiation program, resulting in the production of dead squames that make up the stratum corneum. The expression of genes that mark different stages of epidermal differentiation and layers of the epidermis are shown on the left side of the diagram.

Homeostasis is generally understood as the physiological process that maintains the structure and function of a tissue (Stark et al., 2006). To achieve homeostasis, the epidermis has to maintain a constant number of cells through balancing of the rates of proliferation and cell loss within the tissue. This process is coordinated by the stem cells of the epidermis, which are located in the innermost basal layer. Periodically, basal cells detach from the underlying basement membrane and execute a terminal differentiation program while migrating upward toward the surface of the skin (Figure 1.2). In the first step of this process, keratinocytes transition from the basal to the suprabasal (or spinous) layer. During this transition, cells undergo dynamic changes in gene expression including decreased expression of basal keratinocyte markers (*KRT5* and *KRT14*) and increased expression of spinous markers (*KRT1* and *KRT10*) (Fuchs and Green, 1980). These gene expression changes result in cells with a network of intermediate filaments reinforced with increased numbers of desmosomes, which gives these cells their spinous-like appearance when stained with H&E (Johnson et al., 2014).

As cells migrate upward into and through the granular layer, they lose their nuclei and organelles, and form keratohyalin and lamellar (lipid rich) granules, which gives their cytoplasm a granular appearance by H&E staining. In the final stages of terminal differentiation, granular cells undergo extensive enzymatic protein crosslinking to form the cornified envelope (proteinaceous sac filled with keratin filaments) and extrude their

lamellar granules into the extracellular space (Blanpain and Fuchs, 2009). The result of this process is the formation of flat and dead stratum corneum cells (also called squames), which provide most of the barrier function of the skin and are eventually shed from the surface of the skin. In humans, it takes approximately four weeks for basal cells to undergo this differentiation process and be shed from the surface of the skin (Fuchs, 2016).

Roles of p63

p63 was established as a master regulator of epidermal development, differentiation, and homeostasis through the phenotypes of the *p63*-/- mouse models (Mills et al., 1999; Yang et al., 1999) and human diseases caused by p63 mutations (van Bokhoven et al., 1999, 2001; Celli et al., 1999; Ianakiev et al., 2000; McGrath et al., 2001). The findings from studies analyzing p63 isoform-specific knockout mouse models support ΔNp63 being the major functional isoform in the epidermis and other epithelial tissues, whereas a role for TAp63 in the epidermis is disputed (Romano et al., 2012; Su et al., 2009; Suh et al., 2006). ΔNp63-/- mice, which largely phenocopy *p63*-/- mice, fail to develop proper stratified epithelia during embryonic development, indicating that ΔNp63 is essential for epidermal development (Romano et al., 2012). ΔNp63 is highly expressed by keratinocytes in the basal layer of epidermis (same cell type in the skin that expresses p73), the progenitor cell population of the tissue,

during homeostasis (Yang et al., 1998) and is essential for maintaining the proliferative potential of this stem cell population (Senoo et al., 2007; Truong et al., 2006).

The molecular roles of ΔNp63 have been extensively investigated in epidermal keratinocytes. ΔNp63 binds to and regulates the expression of a gene expression program with important roles in biological processes of the epidermis such as proliferation, adhesion, differentiation, and stem cell maintenance (Carroll et al., 2006; Pellegrini et al., 2001; Truong et al., 2006). Key direct p63 target genes and gene groups in these processes include: *PERP* (Ihrie et al., 2005), *KRT14* (Romano et al., 2007), *CDKN1A* (p21) (Westfall et al., 2003), integrins (*ITGA3*, *ITGA6*, *ITGA5*, *ITGB4,* and *LAMC2*), *CDH3* (P-cadherin) (Shimomura et al., 2008), and desmosomal components (*DSC3*, *DSP*, and *DSG1*) (Ferone et al., 2013). ΔNp63 also regulates gene expression in epidermal keratinocytes through modulation of the global chromatin structural state. *SATB1* (Fessing et al., 2011) and *BRG1* (Mardaryev et al., 2014) are p63 target genes and chromatin modifiers, with important roles in inducing expression of genes within the epidermal differentiation complex (EDC), a keratinocyte lineage-specific gene locus, during skin development. In addition, ΔNp63 binds to and regulates the chromatin state and activity of epidermal enhancers, possibly through acting as a pioneer factor to open compact chromatin and allow binding by other transcription factors (Bao et al., 2015; Kouwenhoven et al., 2015; Rinaldi et al., 2016).

Given the knowledge gained from the molecular studies of ΔNp63 function and the essential roles of ΔNp63 in epidermal cell fate commitment, Chen and colleagues performed a screen to identify skin lineage-specific transcription factors that could convert non-epithelial cells to the epidermal fate when co-expressed with ΔNp63 (Chen et al., 2014). The authors demonstrated co-expression of ΔNp63 and KLF4 could reprogram fibroblasts to the epidermal basal keratinocyte cell fate (Chen et al., 2014). In Chapter IV, we leverage the learning from this model and deploy it to explore the function of ΔNp73 in epidermal programming and discovered that ΔNp73 enhances p63-mediated expression of keratinocyte genes involved in skin development, proliferation, and wound healing.

Wound Healing

Following wounding, it is essential to quickly repair the epidermis and restore the barrier function of the skin. The wound healing process is generally divided into four overlapping phases: (1) blood clotting, (2) inflammation, (3) proliferation, and (4) remodeling (Gonzales and Fuchs, 2017; Gurtner et al., 2008). Immediately after an injury, platelets aggregate in the wound and form a blood clot, which stops the bleeding and provides a temporary barrier. In the next phase (inflammation), resident T cells are activated and phagocytes (macrophages, monocytes, and neutrophils) are recruited to the wound to assist in clearing out dead cells and pathogens. During the next stage (proliferation) cells in the wound proliferate and begin

the repair of the tissue (blood vessels, extracellular matrix, and epidermis). Basal keratinocytes near the wound are activated to express a transactional program (e.g. *KRT6*, *KRT16*) that reduces cell-cell and cell-substrate adhesion, allowing the cells to migrate into the wound and participate in re-epithelialization of the epidermis (Figure 1.3) (Coulombe, 1997). The basal keratinocytes behind the migrating epidermal front are also involved in re-epithelialization by undergoing proliferation (Figure 1.3) (Werner and Grose, 2003). In the final stage of wound healing (remodeling), the dermis is repaired and its collagen is remodeled to increase its tensile strength.

The importance of p63 in wound healing was first exemplified by the healing deficits observed in patients with ectodermal dysplasias caused by mutations in the human *TP63* gene (van Bokhoven et al., 1999, 2001; Celli et al., 1999; Ianakiev et al., 2000; McGrath et al., 2001). Kotster and colleagues went on to demonstrate a role for ΔNp63 in wound healing using an epidermal-specific inducible ΔNp63 knockdown mouse model (Koster et al., 2007, 2009). Upon induction of ΔNp63 knockdown, the mice developed severe skin erosions and exhibited an impaired ability to heal full-thickness skin wounds including a failure to undergo terminal differentiation (Koster et al., 2007, 2009). A study of cutaneous wound healing in humans reported that keratinocytes at the wound edge, migrating epidermal tongue, and regenerating epidermis (basal and parabasal cells)

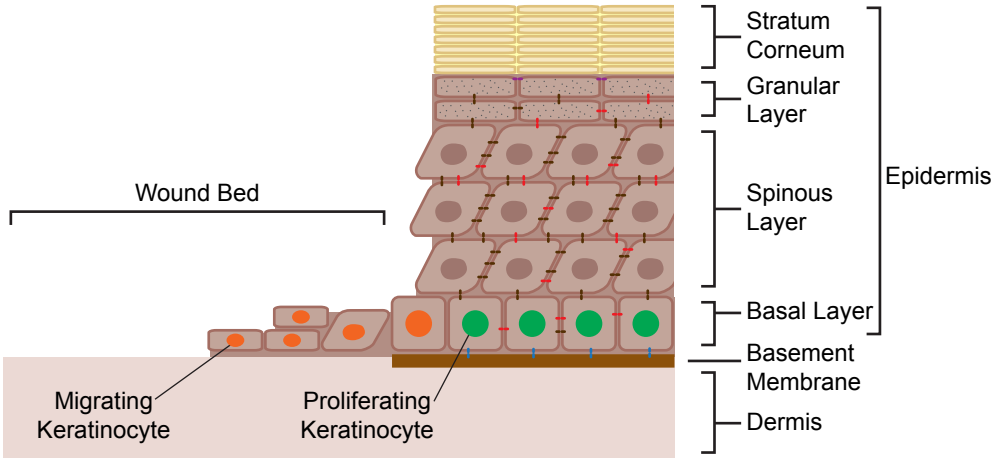

Figure 1.3. Schematic of Epidermal Keratinocyte Functions During Wound Re-epithelialization. After cutaneous injury, basal keratinocytes near the wound edge are activated to express a transcriptional program (e.g. *KRT6*, *KRT16*) that results in reduced cell-cell and cell-substrate adhesion and a change in cellular morphology, allowing the cells to migrate into the wound bed and fill in the gap (cells labeled with orange nuclei). In addition, basal keratinocytes located behind the migrating epidermal front assist with re-epithelialization by undergoing proliferation (cells labeled with green nuclei).

express p63 (Kurokawa et al., 2006). p63 also regulates wound repair in human airway epithelial basal cells (Warner et al., 2013).

Stem cells in the skin, which express ΔNp63, coordinate the wound healing process (Ge and Fuchs, 2018). When an injury occurs, nearby epidermal and hair follicle (HF) stem cells are recruited to the wound to re-epithelialize the epidermis (Ito et al., 2005). During this process, HF stem cells express markers of both HF and epidermal stem cells (Ge et al., 2017). This “mixed lineage” state is transient and resolves by the end of wound healing (i.e., HF stem cells in the wound adopt an epidermal stem cell fate) (Ge et al., 2017). In Chapter IV, we explored the functions of p73 in epidermal wound healing and found that *p73*-/- mice exhibit delayed wound healing due in part to reduced proliferation, and that *p73* is expressed by the cell types that govern wound healing (epidermal and hair follicle stem cells) (Beeler et al., 2019).

Global Transcriptional Profiling

Importance

Despite having the same genotype, different cell types in the body have distinct phenotypes and gene expression profiles due to differential gene regulation. In eukaryotes, regulation of gene expression is complex and occurs at multiple steps including chromatin accessibility, transcription, RNA processing, RNA stability, translation, and protein activity.

Transcription factors, like the p53 family, play a key role in the regulation of gene expression; they bind to specific DNA sequences or other transcription factors and induce or repress transcription of nearby genes. Gene expression is commonly studied at the level of transcription (i.e., RNA) because it is an important step in the regulation of many genes and can be studied genome-wide with modern technologies. The RNA molecules present in a biological system reflect the genes being expressed at the time and can be used to infer the biological processes that are active in the system. Global transcriptional profiling has become a widely used approach in biomedical research and has provided insight into the transcription factors that regulate epithelial biology including: ΔNp63 (Carroll et al., 2006; Koster et al., 2007; Kouwenhoven et al., 2015; Truong et al., 2006), KLF4 (Chen et al., 2003), IRF6 (Ingraham et al., 2006), GRHL3 (Gordon et al., 2014; Klein et al., 2017; Yu et al., 2006), FOXN1 (Janes et al., 2004), and FOXO1 (Mori et al., 2014). We previously combined global transcriptional profiling with chromatin immunoprecipitation sequencing (ChIP-seq), a technology used to identify transcription factor binding-sites genome-wide, to identify genes that are regulated by p73 in multiciliated cells (Marshall et al., 2016). In Chapter IV, we used global transcriptional profiling to study the function of ΔNp73 in epidermal programming and discovered that ΔNp73 regulates a transcriptome similar to ΔNp63.

Development of the RNA-seq Technology

Over the past ten years, short-read RNA-seq has supplanted microarrays as the preferred technology for performing global transcriptional profiling because of a number of advantages with the technology including: (1) can identify novel transcripts at a single-base resolution; (2) has a low background signal and a large dynamic range of expression; (3) can distinguish different isoforms, and (4) requires little input RNA (Wang et al., 2009). The laboratory-based steps in a standard short-read RNA-seq experiment consist of: RNA extraction, poly-A mRNA enrichment, cDNA synthesis, library preparation (ligation of adapters to the cDNA ends), and library sequencing (10-30 million times per sample). The Illumina platform is by far the most commonly used short-read sequencing technology for RNA-seq (Leinonen et al., 2011) and a typical experiment involves sequencing 50-150 bp from one (singe-end) or both (paired-end) ends of the cDNA fragments in the library. Subsequent computational steps include: align sequencing reads to a reference genome or transcriptome, quantify sequence alignments (at the gene, exon, or transcript level), and model differential expression. Long-read (1-50 kb) RNA-seq technologies (Pacific Biosciences and Oxford Nanopore) have also been developed that can sequence entire mRNA transcripts, but are currently not widely used because they have a much lower throughput and higher error rate than the Illumina short-read technology (Stark et al., 2019).

In the past five years, RNA-seq methods for studying gene expression in single cells (scRNA-seq) have been quickly adopted by investigators and undergone a rapid pace of advancement (Stark et al., 2019). Single-cell analysis has allowed investigators to discover rare cell types with roles in the pathology of human diseases that would not have been identifiable using bulk RNA-seq, which measures the mean gene expression of a population of cells (Montoro et al., 2018). The workflow of scRNA-seq methods is built heavily on methods developed for bulk RNA-seq and includes: isolation of single cells from samples, cell lysis, cDNA synthesis and tagging, PCR amplification, and Illumina sequencing. The recommended number of cells to sequence (published range = 10s to 100,000s of cells) and how deeply to sequence them (typical range = 1e4-1e6 reads per cell) in a scRNA-seq experiment vary depending on the aims of the experiments, the sample type, and the library preparation method (Hwang et al., 2018; Olsen and Baryawno, 2018). scRNA-seq data contains a lot of technical variance (i.e. it is noisy) and presents unique challenges for data analysis (Olsen and Baryawno, 2018). Novel algorithms and statistical methods are being actively developed to address these issues, but they are less mature than the methods used for bulk RNA-seq data analysis. Recent studies have used scRNA-seq to study cellular heterogeneity in the murine epidermis and hair follicle, and discovered 25 distinct cell populations and heterogeneity within the progenitor cell populations of the tissue (Joost et al., 2016; Yang et al., 2017). In addition,

Joost and colleagues used scRNA-seq to study how skin stem cells from different niches respond during epidermal wounding (Joost et al., 2018). In Chapter IV, we leveraged these skin-related scRNA-seq datasets to explore *p73* expression in different populations of keratinocytes in the murine skin, including epidermal and hair follicle stem cells.

mRNA Isoform Quantification by RNA-seq

The majority of the publicly available RNA-seq datasets were generated using the Illumina short-read sequencing technology (Leinonen et al., 2011). Short reads are typically 50-150 bp long and obtained by sequencing both ends of 200-500 bp cDNA fragments. A large proportion of mRNA transcripts are longer than 1 kb. Short-reads lack the information to associate differences in the sequence of mRNA isoforms (e.g. alternative promoter usage and splicing) that are separated by more than the length of the fragment (Sarantopoulou et al., 2019). As a consequence, it is difficult to accurately quantify full-length mRNA isoforms from short-read RNA-seq, particularly for genes with long transcripts and many isoforms such as *p73* and *p63*.

Quantifying the expression of p73 and p63 mRNA isoforms is challenging for additional reasons. mRNA isoforms of p73 and p63 have a long 3' UTR (~3,500 bp for p73 and ~3,000 bp for p63), which results in: (1) reduced effectiveness in generating full-length cDNA during oligo(dT) priming due to RNA degradation and/or enzymatic errors during reverse

transcription, resulting in the underrepresentation of 5' RNA sequences after poly-A selection and reduced sequencing coverage at the 5' ends of genes (Wang et al., 2009); and (2) only a small fraction, if any, of the sequencing reads aligning to *p73* and *p63* containing information that can be used to analyze promoter usage and splicing. In addition, studying p73 mRNA isoforms is particularly challenging because the gene is expressed at relatively low levels (<10 TPM) in cell and tissue types in which it has important biological functions during homeostasis (Marshall et al., 2016; Nemajerova et al., 2016; Santos Guasch et al., 2018). In Chapter III, we developed a methodology to address these challenges and used it to quantity the expression of the p73 and p63 isoforms.

CHAPTER II

MATERIALS AND METHODS

Cultured Cells

Cell Culture

CAL148 and MDA-MB-453 were grown in DMEM (Thermo Fisher Scientific, 11965-092) with 1 µg/mL EGF and 10% FBS (Gemini Bio Products, 100-106). HCC1806 (ATCC, CRL-2335) and HCC70 (ATCC, CRL-2315) cells were grown in RPMI + GlutaMAX (Thermo Fisher Scientific, 61870-036) with 10% FBS (Gemini Bio Products, 100-106). MCF10 (ATCC, CRL-10317) and HMEC cells were grown as previously described (Hearnes et al., 2005). HaCaT (Cell Line Services, 300493), HaCaT C2 (single cell clone derived from parental HaCaT), HaCaT p63α-/- (lack p63α expression as a result of CRISPR-Cas9 genomic editing of HaCaT C2 cells), 293FT (Thermo Fisher Scientific, R70007), and MDA-MB-231 (ATCC, HTB-26) cells were grown in DMEM (Thermo Fisher Scientific, 11965-092) with 10% FBS (Gemini Bio Products, 100-106). Neonatal human dermal fibroblasts (HDFn) cells (ATCC, PCS-201-010) were grown in Medium 106 (Thermo Fisher Scientific, M-106-500) with 2% (v/v) Low Serum Growth Supplement (Thermo Fisher Scientific, S-003-10). All cell lines were grown in 100 U/mL Penicillin:Streptomycin (Gemini Bio Products, 400-109) and tested routinely for mycoplasma (Lonza, LT07-418) to ensure that all experiments were

performed on mycoplasma-free cultures. HDFn cells were passaged using ATCC Trypsin-EDTA for Primary Cells (PCS-999-003) and ATCC Trypsin Neutralizing Solution (PCS-999-004). All other cells were passaged using Thermo Fisher Scientific 0.25% Trypsin-EDTA (25200-056).

Cloning Lentiviral Expression Vectors

The coding sequences of KLF4, ΔNp63α, ΔNp73α, and ΔNp73β was amplified independently by PCR (while adding a restriction site to each end of the DNA) and cloned into pCDH-CMV-3xMCS-EF1-copGFP-T2A-puro by *Nhe*I (New England BioLabs, R3131S) and *Sal*I (New England BioLabs, R3138S) restriction digestion and T7 DNA ligation (New England BioLabs, M0318S). Each expression vector was sequenced using the Sanger method to ensure the coding sequence matched Encyclopedia of Genes and Gene Variants Project (GENCODE) annotations (Frankish et al., 2019). Further detail on all vectors including the source of the template DNA for each coding sequence is provided in Table 2.1.

Lentivirus Production

Lentivirus was produced in 293FT cells through transfection of second-generation lentiviral vectors (Zufferey et al., 1997). Cells were plated in T-175 flasks and grown to 80-90% confluency. For each lentivirus produced, the following vectors were diluted in 1.2 mL of Opti-MEM (Thermo Fisher Scientific, 31985-070): pMD2.G (1.68 pmol or 6.5 µg; Addgene, 12259),

ID	Full Name	Source
psPAX2	psPAX2	Addgene (Plasmid # 12259)
pMD2.G	pMD2.G	Addgene (Plasmid # 12260)
pSB1	pCDH-CMV-3xMCS-EF1-copGFP-T2A-puro	Systems Biosciences (Catalog # CD513B-1)
pSB25	pSB1-KLF4	PCR cloning using the CDS of LZRS-KLF4 (George Sen laboratory) with with NheI (5') & SalI (3') restriction sites
pSB26	pSB1-ΔNp63α	PCR cloning using the CDS of pMCS.71/2272-ΔNp63α (Pietenpol laboratory) with NheI (5') & SalI (3') restriction sites
pSB45	pSB1-ΔNp73β	PCR cloning using the CDS of FG12-CMV-ΔNp73β-HA (Pietenpol laboratory) with NheI (5') & SalI (3') restriction sites
pSB47	pSB1-ΔNp73α	PCR cloning using the CDS of pcDNA3-ΔNp73α-HA (Pietenpol laboratory) with NheI (5') & SalI (3') restriction sites

Table 2.1. Vectors Used in this Dissertation. The table lists the ID, full name, and source of each vector.

pxPAX2 (3.03 pmol or 21.4 µg; Addgene, 12260), and lentiviral transfer vector (3.83 pmol). Lipofectamine 2000 (140 µL; Thermo Fisher Scientific, 11668500) was diluted in 1.2 mL of Opti-MEM and incubated at room temperature for five minutes. Diluted DNA was added to the diluted Lipofectamine 2000 dropwise and incubated at room temperature for 30 minutes. Flasks of 293FT cells were switched to antibiotic-free media and the DNA-lipid complexes were added dropwise to the side of the flask. Fourteen to sixteen hours later the transfection media was removed, and fresh media containing antibiotics was added. Virus was harvested 48 and 72 hours after transfection. Viral supernatant was centrifuged at 1,000 rpm for 5 min, passed through a 0.45 µm syringe filter (Sarstedt, 83.1826), and stored at -80°C. Lentivirus was titered using the Lenti-X qRT-PCR Titration Kit (Takara Bio).

Lentiviral Infections

Lentivirus was stored at -80°C in aliquots prior to infection and was limited to one freeze-thaw cycle before use. Target cells were grown to 33-66% confluency in 6-well or 12-well plates before infection. For every infection condition, equivalent copy numbers of each virus were used in the presence of 6 µg/mL polybrene. Each plate was spun at 2,000 rpm for one hour at room temperature. The spinfection procedure was repeated 24 hours later and fresh media was added at 48 hours. Cells were grown for a

total of 3-6 days after the initial infection before collection and the media was changed every other day.

Immunoblotting

Cell pellets were collected by trypsinization and lysed in RIPA buffer supplemented with protease inhibitors (Sigma-Aldrich, 11697498001). Murine tissues were homogenized in RIPA buffer supplemented with protease inhibitors (Sigma-Aldrich, 11697498001) using a Diagenode Bioruptor with protein extraction beads (Diagenode, C20000021). The protein concentration of cell and tissue extracts was quantified using the DC Protein Assay (Bio-Rad, 500-0116). Protein samples (30-50 µg for cells and 100 µg for tissues) were separated on 10% SDS-PAGE gels and transferred to polyvinylidene fluoride (PVDF) membranes (MilliporeSigma, IPVH00010). Membrane blocking and antibody incubations were conducted in 1X TBST with 5% w/ nonfat dry milk. Primary antibody incubations were performed overnight at 4°C with KLF4 (R&D Systems AF3460; 1:2,000), p63α H-129 (Santa Cruz Biotechnology sc-8344; 1:500), p73 EP436Y (Abcam ab40658; 1:1,000), and GAPDH (Merck Millipore MAB374; 1:10,000). Further detail on all primary antibodies used in immunoblotting is provided in Table 2.2. Secondary antibody incubations were performed 24-26 hours later for 1 hour at room temperature using species-appropriate HRP-conjugated secondary antibodies (Thermo Fisher Scientific; 1:5,000). Membranes were incubated in ECL substrate (Thermo Fisher Scientific,

Epitope	Company	Catalog #	Species	IB	IF	IHC	ChIP
p73 (EP436Y)	Abcam	ab40658	rabbit	1:1,000	1:1,000*		10 µg
p63α (H-129)	Santa Cruz	sc-8344	rabbit	1:500			10 µg
p63 (AF1916)	R&D Systems	AF1916	goat	1:200			10 µg
GAPDH	Merck Millipore	MAB374	mouse	1:10,000			
KLF4	R&D Systems	AF3640	goat	1:2,000			
p63α (D2K8X)	Cell Signaling	13109	rabbit		1:1,000*		
Keratin 5	Fitzgerald	20R-CP003	guinea pig		1:200		
Keratin 14	Fitzgerald	20R-CP002	guinea pig		1:200		
E-Cadherin	BD	610181	mouse		1:1,000		
Keratin 10	Abcam	ab76318	rabbit		1:100		
Ki67	BD	550609	mouse		1:1,000*		
γH2AX	Novus	NB100-2280	rabbit			1:1,000	

Table 2.2. Antibodies Used in this Dissertation. The table lists the epitope, company, catalog number (#), and species of each antibody, as well as dilution the antibody was used at in applicable applications including: immunoblotting (IB), immunofluorescence (IF), immunohistochemistry (IHC), and chromatin immunoprecipitation (ChIP). IF dilutions with an asterisk indicate that tyramide signal amplification (TSA) was used to enhance fluorescent signal detection. ChIP experiments were performed using 25-50 million cells.

32106) for 1-2 minutes and chemiluminescent signal was captured with X-ray film or Amersham Imager 600 (GE Healthcare Life Sciences, 29083461).

RNA Isolation

Total RNA was harvested from HDFn and MDA-MB-231 cell pellets that had been generated by cell trypsinization and frozen at -20°C. RNA for qRT-PCR analysis was isolated using the Aurum Total RNA Mini Kit (Bio-Rad, 732-6820). Samples were treated with DNase I for 30 minutes at room temperature. RNA for RNA sequencing (RNA-seq) analysis was isolated using the RNAqueous-Micro Total RNA Isolation Kit (Thermo Fisher Scientific, AM1931). Samples were treated with DNase I for 20 minutes at room temperature. All RNA samples were quantified and assessed for quality using a NanoDrop One Spectrophotometer (Thermo Fisher Scientific, ND-ONE-W). Samples for RNA-seq were also analyzed using the Qubit RNA assay and BioAnalyzer 2100 or TapeStation system (Agilent).

Quantitative Reverse Transcription PCR (qRT-PCR)

cDNA was generated from 750 ng of total RNA using MultiScribe Reverse Transcriptase (Thermo Fisher Scientific, 4311235) and oligo(dT) primer (Thermo Fisher Scientific, N8080128). Quantitative PCR was performed using the CXF96 Touch Real-Time PCR Detection System (BioRad,

1855195) with iQ SYBR Green Supermix (BioRad, 1708880). An annealing temperature of 60°C was used for each primer set. Samples were run in triplicate and normalized to *GAPDH*. The ΔΔCt method was used to calculate relative gene expression between samples (Livak and Schmittgen, 2001). Primer sequences for *KRT14*, *KRT5*, *FLG*, *SFN*, and *GAPDH* are listed in Table 2.3.

Human Dermal Fibroblast Induced Keratinocyte (iKC) RNA-seq

RNA-seq was performed on HDFn cells after iKC reprogramming at the Vanderbilt Technologies for Advanced Genomics (VANTAGE) core. Stranded RNA-seq libraries were prepared from total RNA using poly-A enrichment and the TruSeq RNA Library Preparation Kit (Illumina). Libraries were sequenced on an Illumina NovaSeq 6000 or NextSeq 500 using a paired-end 150 base pair protocol. RNA-seq reads were trimmed to remove adapter sequences with Flexbar v3.4.0 (Dodt et al., 2012) and aligned to hg19 (GRCh37 Primary Assembly) with STAR v2.6.1a (Dobin et al., 2013) using default parameters and GENCODE v28lift37 annotations (Frankish et al., 2019). The number of reads mapped to GENCODE for each gene was quantified with featureCounts v1.6.2 (Liao et al., 2014) and used with DESeq2 v1.14.1 (Love et al., 2014) to perform differential expression analysis between samples. Overrepresentation enrichment analysis was conducted on differentially expressed genes [DESeq2 false discovery rate (FDR) < 0.1] using WebGestaltR v0.1.1 (Wang et al., 2017).

Name	Sequence
KRT14-qPCR-1-F	GTCCTTCGCACCAAGAACTG
KRT14-qPCR-1-R	GGGATCTTCCAGTGGGATCT
KRT5-qPCR-1-F	GCTGGAGGGCGAGGAATGC
KRT5-qPCR-1-R	ACCGAGGCCACCGCCATA
FLG-qPCR-F	GGCAAATCCTGAAGAATCCA
FLG-qPCR-R	TGCTTTCTGTGCTTGTGTCC
SFN-qPCR-1-F	CGAAACCTGCTCTCAGTAGCCT
SFN-qPCR-1-R	CCTCCTCGTTGCTTTTCTGCTC
GAPDH-qPCR-1-F	CATGTTCCAATATGATTCCAC
GAPDH-qPCR-1-R	CCTGGAAGATGGTGATG

Table 2.3. Primers Used in this Dissertation. The table lists the name and sequence of each primer used in qRT-PCR experiments. The primer pairs were designed to amplify a 80-200 bp product and have a Tm value of ~60°C.

Transcript abundance [units = transcripts per million (TPM)] was estimated using Kallisto v0.44.0 (Bray et al., 2016). FASTQ files for RNA-seq data from this analysis were deposited in the NCBI SRA under the BioProject ID PRJNA540145.

Chromatin Immunoprecipitation Sequencing (ChIP-seq)

For each p63 ChIP, 25-50 million cells were crosslinked with formaldehyde (1-1.5%) for ten minutes at room temperature, collected by scraping, and sonicated to yield approximately 300 base pair DNA fragments using a Diagenode Bioruptor. ChIP was performed with HaCaT and HCC1806 using 10 µg of p63α H-129 (Santa Cruz Biotechnology, sc-8344) antibody or with HaCaT C2 using 10 µg of p63 (AF1916, R&D Systems) antibody. Input control samples were collected from sonicated samples prior to performing ChIP. ChIP-seq libraries were prepared as described previously (Marshall et al., 2016). Sequencing of ChIP-seq libraries was performed at the Vanderbilt VANTAGE core using the Illumina platform with a single-end 50 or 75 base pair protocol. ChIP-seq reads were trimmed to remove adapter sequences using Flexbar v3.4.0 (Dodt et al., 2012) and aligned to hg19 (GRCh37 Primary Assembly) using BWA v0.7.17-r1188 (Li and Durbin, 2009) with default parameters (BWA-backtrack for 50 base pair reads and BWA-MEM for 75 base pair reads). Duplicate reads were identified using the Picard v2.17.11 tool “MarkDuplicates”. Samtools v1.9 (Li et al., 2009) was used to filter out duplicate, multimapping, improperly

paired, and mitochondrial reads. Peak calling was performed with MACS2 (Li et al., 2009; Zhang et al., 2008) using input samples as a control and a FDR q-value threshold of 0.01. Motif enrichment analysis was performed with MEME-ChIP (Machanick and Bailey, 2011) on the genomic sequences at detected p63 peaks (length = 500 base pair) as a QC step to ensure that the canonical p63/p73 DNA-binding motif was identified and the ChIP was successful. Analysis of p73 and p63α genomic-binding profiles in HCC1806 cells was conducted using deepTools (Ramírez et al., 2014). p63/p73-binding sites within 50 kb of the transcription start sites (TSS) of the set of 44 genes involved in iKC reprogramming were determined by manually reviewing the MACS2-identified peaks in the Integrative Genomics Viewer (IGV) (Thorvaldsdóttir et al., 2013). Genes were marked as containing a p63/p73-binding site (in Figure 4F) if an overlapping p63/p73 ChIP-seq peak was detected within 50 kilobases of the TSS in two out of three basal cell models analyzed [HK (Kouwenhoven et al., 2015), HaCaT, and HCC1806 (Santos Guasch et al., 2018)] and the overlapping peak contained a canonical p63/p73 DNA-binding motif. FASTQ files for ChIP-seq data generated as part of this analysis were deposited in the NCBI SRA under the BioProject ID PRJNA540145. Further detail on all primary antibodies used in the ChIP analyses is provided in Table 2.2.

Murine Model

Animal Model

We used the previously described *p73*+/+ and *p73*-/- mice (Marshall et al., 2016) in a BALB/c congenic background (Santos Guasch et al., 2018) for all experiments requiring murine tissue. The research using mice described herein was carried out in strict accordance with the recommendations in the Guide for the Care and Use of Laboratory Animals of the National Institutes of Health (NIH). The protocol was approved by the Institutional Animal Care and Use Committee (IACUC) of Vanderbilt University Medical Center (Protocol Number: M08636). All surgery was performed under controlled-dose isoflurane anesthesia, and all efforts were made to minimize suffering.

Immunofluorescence (IF) and Immunohistochemistry (IHC)

Immunostaining of tissue sections was performed as previously described (Marshall et al., 2016). Murine skin tissues were fixed in 10% neutral buffered formalin (NBF) and embedded in paraffin for sectioning. De-identified human skin sections were obtained from pre-existing formalin-fixed paraffin-embedded tissue blocks. These blocks were prepared from excess tissue remaining after evaluation and diagnosis at the time of a surgical procedure. The Vanderbilt University Medical Center Institutional Review Board considers these tissues exempt since they were pre-existing and de-identified. IF was conducted using the following antibodies: p73

EP436Y (Abcam ab40658; 1:1,000), p63α D2K8X (Cell Signaling Technology #13109; 1:1,000), Keratin 5 (Fitzgerald Industries International 20R-CP003; 1:200), Keratin 14 (Fitzgerald Industries International 20R-CP002; 1:200), E-cadherin (BD Biosciences 610181; 1:1,000), Keratin 10 (Abcam ab76318; 1:100), and Ki67 B56 (BD Biosciences 550609; 1:1,000). p73, p63, and Ki67 were detected using TSA Plus Fluorescence Amplification Kit (PerkinElmer). Keratins (5, 10, 14) and E-cadherin were detected using species-appropriate Alexa Fluor secondary antibodies at 1:200 (Thermo Fisher Scientific). IHC was conducted using γH2AX (Novus Biologicals NB100-2280; 1:1,000) antibody. Further detail on all primary antibodies used in immunostaining is provided in Table 2.2.

Cutaneous Wounding Assay

Mice (8-12 months old; ~1:1 ratio of males and females) were anesthetized using a controlled dose of isoflurane and four full-thickness wounds were made in the back skin using a 0.5 cm biopsy punch following Vanderbilt IACUC-approved protocols. Mice were monitored daily after wounding. Samples were collected at 0 (immediately after wounding), 3, 7, and 10 days after wounding with a total of eight wounds from two mice collected per time point. During sample collection, wounds were measured with calipers [wound area = (length/2) x (width/2) x π] and the back skin was harvested, fixed overnight in 10% NBF, and paraffin-embedded for further analysis. Whole tissue sections were digitally acquired using an AxioScan

Z1 slide scanner (Carl Zeiss Canada). Automated semiquantitative scoring of staining in wounded and unwounded skin was performed on whole slide images by a pathologist who had not been informed of the study hypothesis using QuPath software (Bankhead et al., 2017). Wound and unwounded areas were manually annotated. At least two areas of skin were analyzed for each condition (minimum total area = 1.94 mm^2) with the quantification algorithm to produce a semiquantitative score based on the percentage of stained nuclei (Ki67 IF) or the percentage of stained nuclei and staining intensity (p73 IF and γH2AX IHC). For the latter qualifications, H-scores were calculated using the following equation: H-score = 3*(% of 3+ intensity cells) + 2*(% of 2+ intensity cells) + 1*(% of 1+ intensity cells) (McCarty et al., 1985). Each selected region was visually assessed to verify correct performance of the quantification algorithm.

Computational Analyses

Genotype-Tissue Expression (GTEx) RNA-seq

RNA-seq data for 11,688 human samples (51 normal tissue sites and 2 primary cell lines) was downloaded from the GTEx Portal on January 1, 2018 (V7 Release) (Carithers et al., 2015; GTEx Consortium, 2013). The RNA-seq libraries were generated from total RNA using the Illumina TruSeq RNA Library Preparation Kit (non-stranded, poly-A capture) and sequenced on the Illumina HiSeq 2000 or 2500 (>50 million 76 base pair

paired-end reads per sample). Sequencing reads were aligned to hg19 with STAR v2.4.2a (Dobin et al., 2013) using GENCODE v19 (Harrow et al., 2012) annotations. Gene-level expression (units = TPM) were quantified using RNA-SeQC v1.1.8 (DeLuca et al., 2012) and junction read counts using STAR v2.4.2a (Dobin et al., 2013). For each sample, the number of reads spanning each *TP73* and *TP63* exon-exon junction were calculated, normalized to the counts per million (read counts / total number of aligned reads / 1e6), and used to determine isoform expression for the 5'-end (5') and 3'-end (3') of transcripts independently (see Figure 3.1 for an overview). The percentage of 5' or alternative promoter usage isoform expression for both genes was determined by the relative amounts of normalized junction counts for exon 3 to exon 4 (E3-E4; corresponds to the TA isoform) versus exon 3' to exon 4 (E3-E4; corresponds to the ΔN isoform). For *TP73*, the relative amount of exon 3a to exon 4 (E3a-E4; corresponds to the I3a isoform) was also incorporated into the analysis. The GTEx junction count quantification dataset did not contain information on the exon-spanning junctions corresponding to three previously identified 5' isoforms (Ex2p73, Ex2/3p73, ΔNp73') (Murray-Zmijewski et al., 2006), suggesting they are expressed at low levels in human tissues. Junction counts for *TP63* corresponding to exon 4 skipping (exon 3 or exon 3' to exon 5) and an additional 216 base pair exon (located in the intron between exons 4 and 5) were detected at very low levels and thus excluded from the analysis (lacked tissue specific expression, expression simply correlated

with *TP63* expression). 3' or alternative splicing isoform expression for both genes was calculated in a similar manner, with slight modifications for each gene to account for differences in alternative splicing between them. The percentage of p73α + β [exon 10 to exon 11 (E10-E11)], p73γ + ε [exon 10 to exon 12 (E10-E12)], p73ζ [exon 10 to exon 13 (E10-E13)], and p73δ [exon 10 to exon 14 (E10-E14)] was calculated by analyzing normalized exon-exon junction counts starting at exon 10 (E10). The relative expression of p73α versus β was determined by comparing normalized exon 12 to exon 13 (E12-E13; corresponds to the α isoform) versus exon 12 to exon 14 (E12-E14; corresponds to the β isoform) junction counts. The percentage of p63γ [exon 10 to exon 11a (E10-E11a)] versus non-p63γ (E10-E11) was calculated by analyzing normalized exon-exon junction counts starting at E10. The percentage of p63δ [exon 11 to exon 14 (E11-E14)] versus non-p63δ (E11-E12) expression was calculated, including normalization for the previously determined percentage of p63γ expression (multiplied relative percentages of p63δ and non-p63δ by the non-p63γ from the prior calculation). The percentage of p63β (E12-E14) and p63α (E12-E13) was calculated using the same methodology as for p63δ. Isoform expression for each tissue was calculated as the mean isoform expression for all samples belonging to a given tissue.

Encyclopedia of DNA Elements (ENCODE) TSS

RAMPAGE (RNA Annotation and Mapping of Promoters for the Analysis of Gene Expression) (Batut and Gingeras, 2013; Batut et al., 2013) data for human adult and embryonic tissues with *TP73* and/or *TP63* expression (n = 17) was downloaded from the ENCODE Project Portal (Davis et al., 2018) on July 1, 2019. TSS identified by the ENCODE RAMPAGE pipeline were manually reviewed in IGV (Thorvaldsdóttir et al., 2013) for each sample to validate that the signal for unique reads at the *TP73* and *TP63* genomic loci was consistent with TSS calls.

Cell Line RNA-seq

RNA-seq data for cell lines (MBA-MB-453, CAL148, and HaCaT) generated as part of previous unpublished studies in the Pietenpol laboratory was obtained. Total RNA had been isolated with Aurum Total RNA Mini Kit (Bio-Rad, 732-6820). Library preparation and sequencing was performed by VANTAGE. RNA-seq libraries were made using the Illumina TruSeq RNA Library Preparation Kit (stranded, poly-A capture) and sequenced using the Illumina HiSeq platform (>30 million 76 base pair paired-end reads per sample). Sequencing reads were pooled and aligned to hg19 (GRCh37 Primary Assembly) with STAR v2.6.1a (Dobin et al., 2013) using default parameters and GENCODE v28lift37 annotations (Harrow et al., 2012). Exon and exon-exon junction counts were quantified with FeatureCounts v1.6.2 (Liao et al., 2014) using the following parameters: “-F GTF -t exon -

Q 10 -s 2 -T 8 -g gene_name -f -O -p -B -C -J -G genome.fa -a gencode.gtf". Determination of *TP73* and *TP63* isoform expression was performed in the same manner described in the methods of the GTEx RNA-seq analysis. Transcript abundance was estimated with Kallisto v0.44.0 (Bray et al., 2016) and gene-level abundance was calculated as the sum of the TPM values for all protein-coding transcripts of a gene.

Human Protein Atlas (HPA) RNA-seq

RNA-seq transcript abundance data for 172 human samples across 37 tissue sites was downloaded from the HPA website on August 3, 2018 (version 18) (Uhlen et al., 2010). Transcript abundance had been estimated with Kallisto v0.42.4 (Bray et al., 2016) and gene-level abundance calculated as the sum of the TPM values for all protein-coding transcripts of a gene.

Tabula Muris Single-Cell RNA-seq

Single-cell RNA-seq **(**scRNA-seq) count data from 2,310 murine back skin cells was downloaded from the Tabula Muris Consortium (Tabula Muris Consortium et al., 2018) on May 29, 2018. RNA-seq libraries were prepared from individual FACS-sorted cells (Itga6+ and/or Cd34+) using the Smart-Seq2 protocol and sequenced on the Illumina NovaSeq 6000 (100 base pair paired-end protocol). Sequencing reads were aligned to the mm10plus genome using STAR v2.5.2b (Dobin et al., 2013) and gene

counts calculated with HTSEQ v0.6.1p1 (Anders et al., 2015). scRNA-seq count data was analyzed with Seurat v2.3.4 (Butler et al., 2018). Cells with less than 900 unique genes detected, less than 75,000 total gene counts, or more than 12% External RNA Controls Consortium (ERCC) RNA Control reads were excluded from the analysis. Expression data was log normalized and scaled to a mean of zero and variance of one for each gene. Regression analysis was performed on the gene expression data for each cell to account for variation due only to the total number of gene counts detected or the percentage of ERCC reads. Principal component analysis (PCA) was performed with the top 2,000 highly variable genes and the number of significant PCs for clustering analysis was determined using the JackStraw procedure and elbow plot analysis. Seurat analysis identified a total of seven clusters using the first 33 principal components and a resolution of 0.4. Two-dimensional visualization of scRNA-seq data was performed with UMAP (Becht et al., 2018) using the first 33 principal components. UMAP parameters used included: n_neighbors = 15 and min_dist = 0.2. The expression of skin cell type markers (e.g. *Cd34*, *Ly6a*, *Fgf18*, *Krt14*, *Mki67*, *Krt10*) was analyzed for each cluster and used to assign cluster annotations. Cells were classified as expressing *Trp63* or *Trp73* if they had a log-normalized expression greater than or equal to 0.5.

Hair Follicle Single-cell RNA-seq

scRNA-seq gene expression data from 1,119 murine hair follicle cells (Yang et al., 2017) were downloaded from the National Center for Biotechnology Information (NCBI) Gene Expression Omnibus database (GSE90848). Sequencing reads were aligned to the mm10 using Bowtie2 v2.2.9 (Langmead and Salzberg, 2012) and gene-level expression (TPM) quantified with RSEM (Li and Dewey, 2011). Cells were classified as expressing *Trp63* or *Trp73* if they had expression greater than or equal to 1 TPM.

Murine Stem Cell RNA-seq

RNA-seq data on murine bulge HF (GSM2656733 and GSM2656734) and epidermal (GSM2656735 and GSM2656736) stem cells isolated by FACS with marker-based sorting (Ge et al., 2017) were downloaded from the NCBI Sequence Read Archive (SRA) on November 2, 2018 (SRP093638). FASTQ files were processed as described in the HDFn iKC RNA-seq methods section except mm10 genome and GENCODE vM17 annotations (Frankish et al., 2019) were used.

Human Keratinocyte RNA-seq

RNA-seq data on primary human keratinocytes grown and differentiated *in vitro* (Cavazza et al., 2016; Kouwenhoven et al., 2015) were downloaded from the NCBI SRA on October 24, 2018 (SRP044925 and SRP070902).

FASTQ files were processed as described in the HDFn iKC RNA-seq methods section. Differentiated samples used in the analysis were limited to those collected 6 or 7 days after the induction of differentiation.

Statistical

All statistical analyses and graphical representations were conducted using R (version 3.5.2 or 3.5.3) unless otherwise noted. The Spearman correlation between *TP63* and *TP73* expression across human tissues (GTEx and HPA RNA-seq datasets) and its statistical significance were calculated using the "cor.test" function in R. Wound closure and qRT-PCR expression data are presented as the mean +/- SEM. The two-way ANOVA test was used to compute the mean difference in percentage wound closure between *p73*+/+ and *p73*-/- mice over days 0, 3, 7, and 10 (calculated with the R “aov” function using the genotype and days after wounding as factors). Student’s t-test was used to calculate statistical significance for wound closure on individual days, IF scores, IHC scores, and qRT-PCR expression (calculated with the R “t.test” function using the following parameters: two-sided, unpaired). Differences were considered significant when $P < 0.05$ and asterisks indicate: * = $P < 0.05$, ** = $P < 0.01$, and *** = $P < 0.001$.

CHAPTER III

p73 AND p63 ISOFORM EXPRESSION IN HUMAN AND MURINE EPITHELIAL TISSUE

Introduction

The p73 and p63 knockout mouse models (global and isoform-specific knockout of the genes) have enabled investigators to discover cellular and physiological contexts in which these transcription factors function *in vivo* and highlighted the distinct biological properties associated with the different protein isoforms encoded by a single gene (Nemajerova et al., 2016; Romano et al., 2012; Su et al., 2009; Wilhelm et al., 2010). Determining which p73 and p63 isoforms are expressed in a given cell or tissue model is an important step in deciphering the functional roles of the transcription factors overall. Unfortunately, analyzing p73 and p63 isoform expression is challenging, due to the lack of isoform-specific antibodies and the large number of potential isoforms that can be generated from each gene. The latter has likely contributed to the contradictory findings in past studies. The development of high-throughput or next-generation sequencing technologies and their application to global transcriptional profiling [RNA-sequencing (RNA-seq)], has made it possible to survey entire steady-state mRNA pools, including novel and known isoforms, at single base resolution in a high-throughput and quantitative manner (Wang et al., 2009). Sethi and colleagues recently clarified past contradictions in

p63 isoform expression by using RNA-seq datasets to perform a large-scale analysis of p63 isoform expression in human cell lines and tissues with high levels of *p63* expression (Sethi et al., 2015). There was an unmet need to perform a similar analysis for *p73*, given how poorly its isoform expression patterns in cells and tissues were understood, and that was the goal of the studies described in this Chapter.

Quantifying the expression of p73 and p63 mRNA isoforms is challenging for a number of reasons. The *p73* and *p63* genes have a complex structure that generates multiple isoforms through 5' alternative promoter usage and 3' alternative splicing (Figure 3.1). Both genes have two promoters (P1 and P2), which give rise to isoforms with distinct functions in transcriptional regulation (Kaghad et al., 1997; Yang et al., 1998, 2000). Isoforms transcribed from P1 contain a full-length transactivation (TA) domain (Kaghad et al., 1997; Yang et al., 1998), while isoforms transcribed from P2 contain a truncated TA domain (ΔN) (Yang et al., 1998, 2000). The *p73* and *p63* genes also undergo 3' alternatively splicing, which gives rise to a number of splice forms (termed α, β, γ, etc.) with differing transcriptional activity (Kaghad et al., 1997; Yang et al., 1998). The long length (~2000-5000 bp) of p73 and p63 transcripts also complicates quantification of isoform expression (Oshlack and Wakefield, 2009). All p73 and p63 isoforms contain a ~1,000 bp sequence in the middle (encoding the DNA-binding and oligomerization domains) that separates the variable 5' and 3' ends of each isoform (Figure 3.1), making

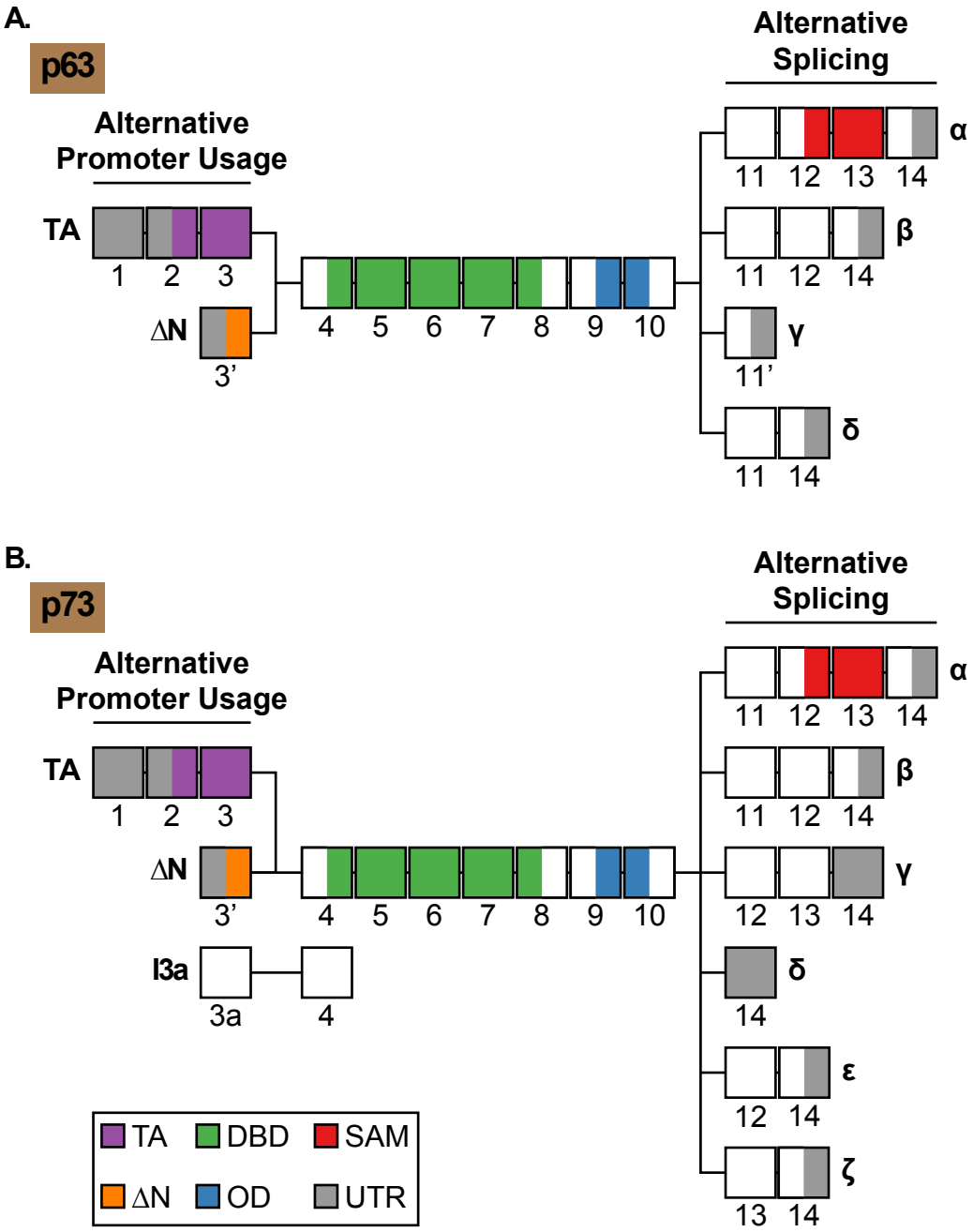

Figure 3.1. Exon Structure of p63 and p73 mRNA Isoforms. Schematic representation of the exon structure of p63 (A) and p73 (B) mRNA isoforms. This information was used to develop an algorithm to quantify the mRNA expression of p63 and p73 alternative promoter usage and splicing isoforms by analyzing RNA-seq reads that span exon-exon junctions. Exons are labeled with color according to the protein domain they encode or the type of mRNA sequence: full-length transactivation (TA), purple; truncated transactivation domain (ΔN), orange; DNA-binding domain (DBD), green; oligomerization domain (OD), blue; sterile alpha motif (SAM) domain, red; and untranslated region (UTR), gray.

it very challenging to directly associate the variation at each end of the isoform by standard approaches (e.g. qRT-PCR, microarray, RNA-seq). In addition, p73 and p63 mRNA isoforms have a long 3' UTR (~3,500 bp for p73 and ~3,000 bp for p63), which results in: (1) difficulty generating full-length cDNA by oligo(dT) priming (standard approach in transcriptional studies) and a consequential reduction in coverage at the 5' end of genes; and (2) only a small portion, if any, of the sequencing reads aligning to *p73* and *p63* provide information to assess promoter usage and splicing. Studying p73 mRNA isoforms is also made challenging because the gene is expressed at relatively low levels (<10 TPM) in cells and tissues in which it has important biological functions during homeostasis (Marshall et al., 2016; Nemajerova et al., 2016; Santos Guasch et al., 2018).

p73 is co-expressed with p63 in the basal cell populations of many epithelial tissues (Puig et al., 2003), but little is known about p73 in these cells including which isoforms are expressed during homeostasis. We recently discovered that 50% of basal epithelial cells in the trachea (progenitor cell population) express p73 and that tracheas from *p73*-/- mice have reduced numbers (35%) of basal cells despite the loss of the most common cell type (multiciliated cell) in the epithelium (Marshall et al., 2016). In addition, *p73* expression is a marker of one of the two main basal epidermal stem cell populations (the one located near hair follicles in scale-like skin) (Sada et al., 2016). These results collectively suggest a role for

p73 in basal epithelial cells and catalyzed our interest in determining which p73 isoforms are expressed in basal cells across different tissues.

To determine which p73 isoforms are expressed in basal epithelial cell populations, we performed a large-scale analysis of p73 isoform expression using human tissue RNA-seq data from the GTEx Project (Carithers et al., 2015; GTEx Consortium et al., 2017). GTEx is an ideal dataset for this analysis because: (1) tissue collection, RNA isolation, library preparation, and sequencing were performed using rigorous standard operating procedures to ensure the generation of high-quality data; (2) it contains 11,688 samples from 714 donors across 53 non-diseased tissue sites; and (3) RNA-seq was performed on each sample using a paired-end protocol and at a high depth of coverage (>50 million reads). We also analyzed p63 isoforms to gain insight to the relationship between p73 and p63 isoform expression; and the results served as a control, since the expression pattern of p63 isoforms in epithelial tissues is known (Sethi et al., 2015). In addition, we included non-epithelial tissues in the analysis to provide a resource for the research community. Finally, to overcome the challenges associated with quantifying the expression of p73 and p63 mRNA isoforms, we developed an algorithm to analyze exon junction-spanning reads and independently quantify alternative promoter usage and splicing isoforms for *p73* and *p63*.

In the analysis described in this Chapter, we determined the expression patterns of p73 and p63 isoforms across a panel of 53 human

tissues. We found that expression of *TP73* and *TP63* was correlated across tissues, with most tissues expressing either both genes or neither gene. For both p73 and p63, the predominant alternative promoter usage isoform (TA versus ΔN) varied between tissues, whereas the predominant alternative splicing isoform was α in nearly all tissues (with the exception of p63γ being predominant in skeletal muscle). Epithelial tissues with basal cell populations (e.g. skin, esophagus, and vagina) expressed high levels of *TP73* and *TP63*. These tissues almost exclusively expressed ΔNp63 mRNA, consistent with previous studies (Sethi et al., 2015), whereas the expression of p73 alternative promoter usage isoforms was heterogeneous between tissues. We performed a series of analyses to explore the heterogeneous p73 alternative promoter usage isoform expression in epithelial tissues and provide evidence suggesting the existence of a previously unreported p73 transcription start site (TSS) in them.

Results

p73 and p63 Gene Expression in Human Tissue

To study the expression patterns of *p73* and *p63* in human tissue during homeostasis, we analyzed RNA-seq data from the GTEx Project, an atlas of RNA expression from healthy human donor tissue (11,688 total samples) (Carithers et al., 2015; GTEx Consortium et al., 2017). We observed a significant correlation (r_s = 0.49, p = 0.0003) between *TP73* and

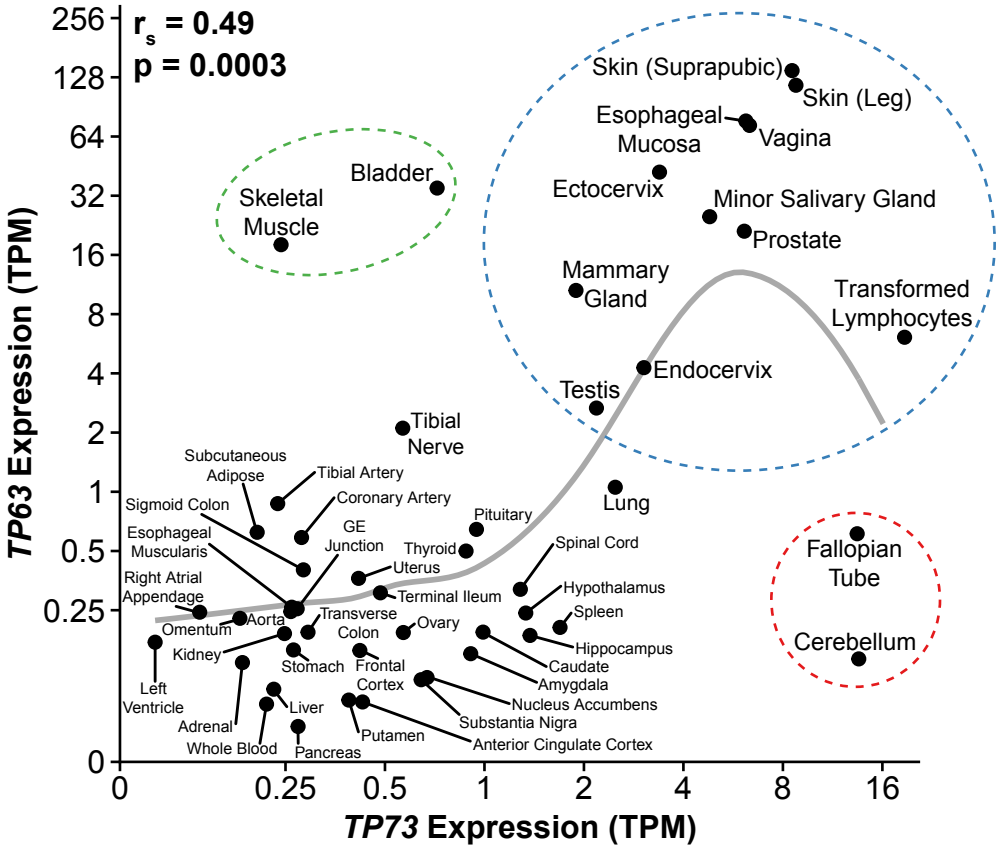

Figure 3.2. p73 and p63 Gene Expression in Human Tissue. Scatter plot of *TP73* versus *TP63* mRNA expression (TPM) by human tissue type from the GTEx dataset. Mean expression (TPM + 0.1) for each tissue is plotted on a log2 scale with a LOESS smooth local regression line (gray). Correlation between *TP73* and *TP63* was quantified using Spearman's rank correlation coefficient (r_s). Tissues were divided into four groups based on the patterns of p73/p63 expression: (1) dual p73/p63-positive (blue dotted line); (2) single p73-positive (red dotted line); (3) single p63-positive (green dotted line); and (4) dual p73/p63-negative.

TP63 expression (Figure 3.2). Overall, p63 mRNA was expressed at higher levels in tissues than p73 (Figure 3.2). We identified four patterns of p73/p63 expression across tissues. The majority of tissues expressed low levels (<2 TPM) of both *TP73* and *TP63* (referred to as dual p73/p63 negative group henceforth) (Figure 3.2). The other large group of tissues expressed at least moderate levels (>2 TPM) of both *TP73* and *TP63* (referred to as the dual p73/p63-positive group henceforth) and included many tissues that have abundant basal cell populations (e.g. skin, esophagus, vagina, prostate; Figure 3.2, blue dashed line). A small number of tissues preferentially expressed either *TP73* (cerebellum and fallopian tube) or *TP63* (skeletal muscle and bladder), which we refer to henceforth as the single p73- and p63-positive groups respectively (Figure 3.2; red and green dashed lines, respectively). These results indicate that *TP73* and *TP63* are differentially expressed between tissue types.

p73 and p63 Protein Expression in Murine Tissue

Our past research examining the roles of p73 was primarily performed in mice (Beeler et al., 2019; Marshall et al., 2016; Santos Guasch et al., 2018). In contrast, the GTEx Project analyzed the transcriptomes of human tissue. In order to determine if the *p73* and *p63* tissue-specific gene expression patterns observed in GTEx (Figure 3.2) were similar in mice and if cell type-specific expression occurs within a given epithelial tissue, we analyzed p73 and p63α protein expression by

immunofluorescence (IF) in various epithelial tissues from wild-type mice including skin, tongue, esophagus, vagina, mammary gland, and trachea. In the tissues analyzed, p73 co-localized with p63α in the nuclei of cells located in regions of the epithelium where basal cell populations typically reside (Figure 3.3). These results are consistent with the tissue gene expression patterns observed in the human GTEx samples and our prior murine studies (Beeler et al., 2019; Marshall et al., 2016).

In addition, we analyzed p73 and p63α protein expression by immunoblotting in various epithelial tissue from wild-type mice. Overall, the murine immunoblot data (Figure 3.4) were consistent with the human tissue mRNA expression from GTEx (Figure 3.2). Murine skin, tongue, esophagus, and vagina expressed both p73 and p63α protein, with ΔNp63α and ΔNp73α likely being the predominant isoforms based on the molecular weights of the protein ladders and human isoform controls (Figure 3.4). Murine bladder tissue expressed p63, but not p73 (Figure 3.4), consistent with it being one of only two tissues in the GTEx dataset that expressed only p63 (Figure 3.2). Skeletal muscle was included in the immunoblot to serve as a negative control for p73 and p63α protein expression. Skeletal muscle expresses p63, but it is an isoform of p63 (γ) (Mangiulli et al., 2009) that is not recognized by the antibody we used in immunoblotting.

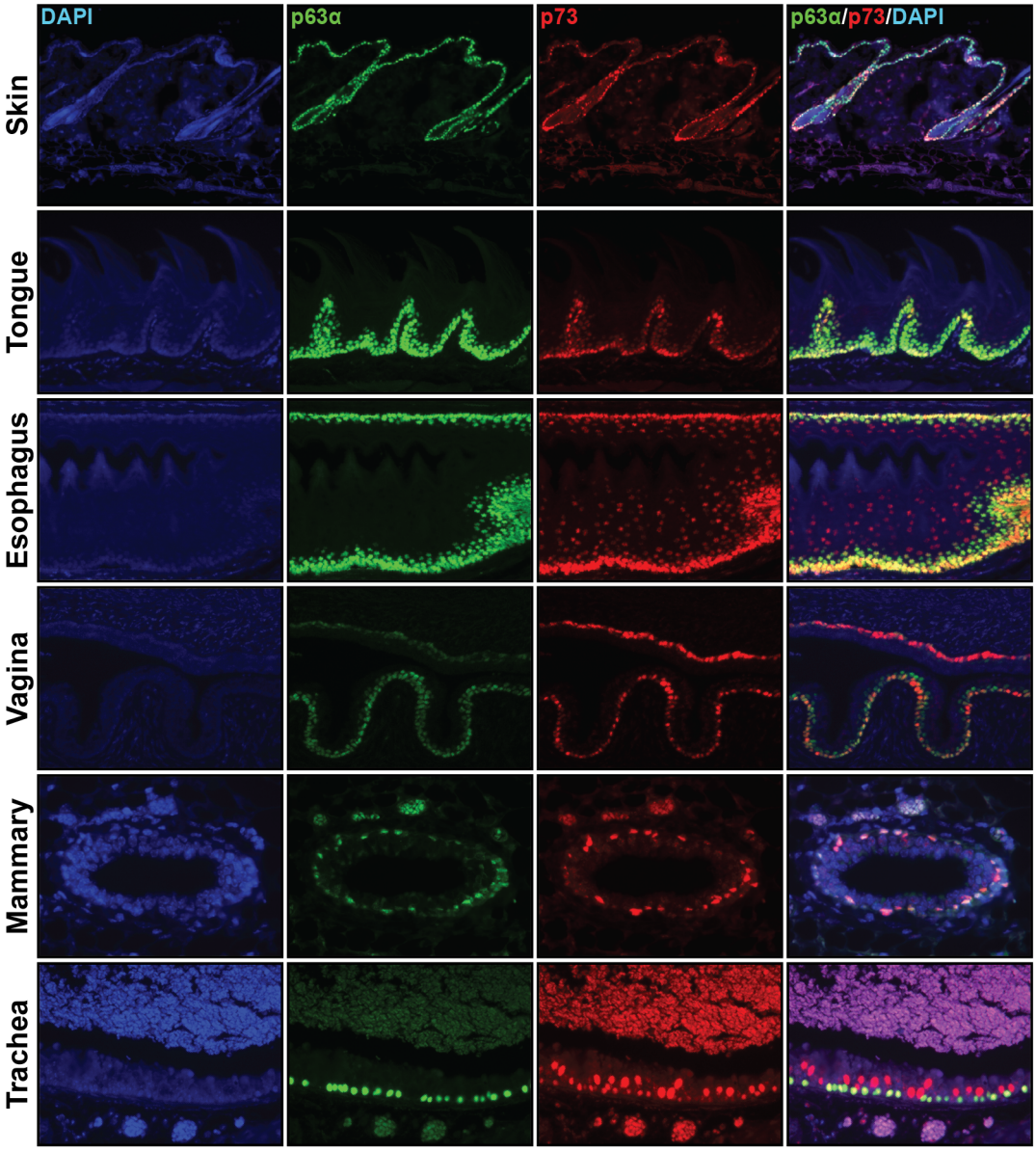

Figure 3.3. p73 and p63α Protein Expression and Localization in Murine Epithelial Tissue. Representative micrographs of IF staining in murine tissues from wild-type mice for DAPI (blue), p63α (red), and p73 (green). All data represented was collected by Clayton Marshall.

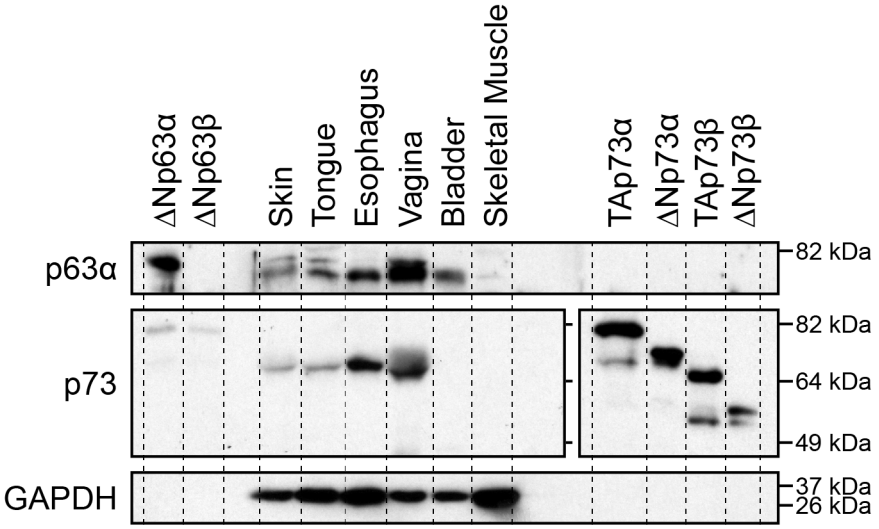

Figure 3.4. p73 and p63α Protein Expression in Murine Epithelial Tissue. Immunoblot analysis for p73 and p63α was performed on tissue lysate harvested from wild-type mice. Human p73 and p63 isoform controls were included to assess antibody sensitivity and specificity, and aid in the interpretation of tissue isoform expression. Murine tissue lysate was collected by Clayton Marshall.

mRNA Expression of p73 and p63 Alternative Promoter Usage Isoforms in Human Tissue

Current methodologies to quantify full-length mRNA isoform expression are not accurate for genes with characteristics like *p73* and *p63* (encode several isoforms, have long transcripts and lower expression levels) (Sarantopoulou et al., 2019). To overcome this challenge and determine p73 and p63 isoform expression in human tissue during homeostasis, we developed an algorithm to independently quantify 5' alternative promoter usage and 3' alternative splicing isoform expression for *p73* and *p63* in individual samples by analyzing exon junction-spanning reads from RNA-seq data (refer to Chapter II, GTEx Project RNA-seq for the full details). We applied our algorithm to the GTEx dataset and quantified the isoform expression of *p73* and *p63* for each sample, summarizing the results by the mean of each tissue. Alternative promoter usage isoform expression was quantified by analyzing the number of RNA-seq reads that span the following exon-exon junctions: (1) exon 3 to 4 (corresponds to TA isoforms); (2) exon 3' to 4 (corresponds to ΔN isoforms), and (3) exon 3a to 4 (corresponds to I3a isoform, *p73* specific) (Figure 3.1). ΔNp63 was the predominant isoform (80-100%) in most tissues from the dual p73/p63-positive group in Figure 3.1, which includes the skin, esophageal mucosa, vagina, and prostate (Table 3.1, column 6). Exceptions were the testis and transformed lymphocytes, which both

Tissue	n	*TP63*				*TP73*				
		Gene TPM	EX-E4 Reads	% TA	% ΔN	Gene TPM	EX-E4 Reads	% TA	% ΔN	% I3a
Skin (Suprapubic)	387	138.4	51,389	2	98	8.5	943	20	80	0
Skin (Leg)	473	116.6	59,324	3	97	8.8	1,122	13	87	0
Esophageal Mucosa	407	76.7	39,845	0	100	6.2	455	83	17	0
Vagina	115	72.9	9,127	1	99	6.3	72	81	19	0
Prostate	152	21.1	2,307	2	98	6.1	170	74	27	0
Ectocervix	6	42.2	232	2	98	3.4	3	68	32	0
Endocervix	5	4.3	19	20	80	3.0	9	67	33	0
Minor Salivary Gland	97	25.0	3,771	6	94	4.8	155	49	51	0
Mammary Gland	290	10.6	3,655	3	97	1.9	325	35	65	1
Transformed Lymphocytes	130	6.1	1,657	99	1	18.6	5,551	98	2	0
Testis	259	2.7	560	96	4	2.2	2,331	4	1	95
Cerebellum	173	0.14	27	59	41	13.6	1,864	97	3	0
Fallopian Tube	7	0.61	2	65	35	13.4	80	76	25	0
Skeletal Muscle	564	18.0	29,796	100	0	0.24	26	32	66	3
Bladder	11	35.0	474	0	100	0.72	4	54	27	19
Lung	427	1.1	436	38	62	2.5	1,375	65	35	0
Tibial Nerve	414	2.1	782	94	6	0.57	15	95	0	5
Spleen	162	0.20	31	64	36	1.7	274	95	5	0
Pituitary Gland	183	0.64	148	68	32	0.95	117	88	12	0
Thyroid Gland	446	0.50	218	70	30	0.88	384	94	6	0
Tibial Artery	441	0.87	465	74	26	0.24	14	94	7	0
Spinal Cord (C-1)	91	0.32	44	70	30	1.3	32	59	41	0
Hypothalamus	121	0.24	57	88	13	1.3	154	31	69	0
Hippocampus	123	0.19	40	73	27	1.4	149	46	54	0
Caudate	160	0.19	68	80	21	0.99	196	58	42	0
Amygdala	100	0.15	35	89	11	0.91	78	52	48	0
Nucleus Accumbens	147	0.11	29	73	28	0.67	99	50	50	0
Frontal Cortex	158	0.16	42	77	23	0.42	7	82	18	0
Subcutaneous Adipose	442	0.62	326	56	44	0.21	20	74	20	6
Terminal Ileum	137	0.31	55	84	16	0.48	59	100	0	0
Uterus	111	0.36	41	71	30	0.42	8	100	0	0
Ovary	133	0.19	28	64	36	0.57	18	100	0	0
Transverse Colon	274	0.19	94	78	22	0.29	75	97	3	0
Stomach	262	0.16	52	46	54	0.26	42	95	2	2
Pancreas	248	0.06	34	27	73	0.27	122	93	7	0
Liver	175	0.10	30	59	41	0.23	44	100	0	0
Whole Blood	407	0.08	42	61	39	0.22	137	97	3	0

Table 3.1. mRNA Expression of p73 and p63 Alternative Promoter Usage Isoforms in Human Tissue. The table lists the number (n) of RNA-seq samples for each human tissue type in GTEx as well as the total gene abundance (units = TPM) and expression of alternative promoter isoforms for *TP73* and *TP63*. Alternative promoter usage isoform expression was calculated through analysis of exon-exon junction-spanning reads (see Figure 3.1 for details). For both genes, the total number of exon junction-spanning reads corresponding to alternative promoter usage (EX-E4) and the mean percentage expression (rounded to nearest whole number) of each alternative promoter isoform is listed by tissue type. I3a (column 11) is a p73 isoform results from the use of an alternative TSS located between exons 3' and 4 of *TP73*.

predominantly expressed TAp63 (96% and 99% respectively) (Table 3.1, column 5). Among the tissues from the single p63-positive group in Figure 3.1, skeletal muscle expressed TAp63 (100%) and the bladder expressed ΔNp63 (100%) (Table 3.1, columns 5 and 6). TAp63 isoforms were more highly expressed in tissues with low levels (<1 TPM) of *TP63* expression, except for lung, pancreas, and stomach (Table 3.1, columns 5 and 6).

Among the tissues from the single p73-positive group in Figure 3.1, which all had high levels of *TP73* expression (>10 TPM), TAp73 was the predominant isoform (cerebellum, 97%; fallopian tubes, 76%) (Table 3.1, column 9). Tissues from the dual p73/p63-positive group had variable p73 alternative promoter usage isoform expression patterns (Table 3.1, columns 9 and 10). Most of these tissues expressed more TAp73 than ΔNp73 and included: esophageal mucosa (83%), vagina (81%), prostate (74%), ectocervix (68%), endocervix (67%), and transformed lymphocytes (98%) (Table 3.1, column 9). In contrast, ΔNp73 had higher expression levels in the skin (80% to 87%) and the mammary gland (65%) (Table 3.1, column 10). The testis was unique in expressing high levels (95%) of a transcript that appears to result from the use of an alternative transcriptional start site (TSS) located between exons 3' and 4 of *TP73* (Table 3.1, column 11). This testis-enriched isoform (referred to as I3a henceforth) was typically composed of the exon (referred to as exon 3a henceforth) starting at the I3a putative TSS, exon 4, and the ~750 bp of the intronic sequence immediately following exon 4 (Figure 3.1B). TAp73 was

expressed at higher levels than ΔNp73 in the testis (Table 3.1, columns 9 and 10), consistent with the critical role for TAp73 in sperm maturation (Holembowski et al., 2014; Inoue et al., 2014). TAp73 was more highly expressed in tissue with low levels (<1 TPM) of *TP73* expression, except for skeletal muscle, hypothalamus, and hippocampus (Table 3.1, column 9).

mRNA Expression of p73 and p63 Alternative Splicing Isoforms in Human Tissue

We quantified the mRNA expression of alternative splicing isoforms for p73 and p63 by analyzing the number of RNA-seq reads that span exon junctions from exons 10 through 14 (Figure 3.1). For both *TP73* and *TP63*, there was less variability in alternative splicing isoform expression as compared to alternative promoter usage isoform expression between tissue types (Tables 3.1 and 3.2). In all tissues but one, p63α was predominant (67-97%) alternative splicing isoform expressed (Table 3.2, column 5). p63β was the second highest expressed isoform in epithelial tissue with high (>10 TPM) *TP63* expression and included: skin (19 and 21%), esophageal mucosa (19%), vagina (17%), prostate (11%), ectocervix (16%), minor salivary gland (14%), mammary gland (5%), and bladder (14%) (Table 3.2, column 6). Skeletal muscle expressed a high percentage of p63γ (85%), making it the only tissue in which p63α was not the most highly expressed alternative splicing isoform (Table 3.2, column 7). p63γ

Tissue	n	*TP63*						*TP73*						
		Gene TPM	E10-EX Reads	% α	% β	% γ	% δ	Gene TPM	E10-EX Reads	% α	% β	% γ+ε	% δ	% ζ
Skin (Suprapubic)	387	138.4	88,201	79	19	1	1	8.5	6,054	74	21	5	0	0
Skin (Leg)	473	116.6	99,042	78	21	0	1	8.8	8,258	75	20	4	0	0
Esophageal Mucosa	407	76.7	60,286	79	19	1	2	6.2	4,085	85	11	3	0	0
Vagina	115	72.9	13,200	82	17	1	2	6.3	1,033	79	16	5	0	0
Prostate	152	21.1	3,668	86	11	2	1	6.1	1,201	79	17	4	0	0
Ectocervix	6	42.2	365	82	16	2	0	3.4	27	87	13	0	0	0
Endocervix	5	4.3	28	97	3	0	0	3.0	16	84	9	7	0	0
Minor Salivary Gland	97	25.0	5,509	79	14	6	1	4.8	846	76	19	4	1	1
Mammary Gland	290	10.6	5,765	93	5	1	1	1.9	994	66	27	4	1	1
Transformed Lymphocytes	130	6.1	2,943	95	4	1	1	18.6	5,827	61	31	9	0	0
Testis	259	2.7	1,318	95	1	4	1	2.2	422	90	2	8	0	1
Cerebellum	173	0.14	43	81	4	15	0	13.6	2,553	80	11	8	0	0
Fallopian Tube	7	0.61	4	87	13	0	0	13.4	106	94	4	3	0	0
Skeletal Muscle	564	18.0	43,054	15	0	85	0	0.24	49	48	36	16	0	0
Bladder	11	35.0	650	86	14	0	0	0.72	9	81	19	0	0	0
Lung	427	1.1	687	85	11	3	1	2.5	1,183	72	22	6	0	0
Tibial Nerve	414	2.1	1,145	94	2	3	1	0.57	12	34	39	28	0	0
Spleen	162	0.20	45	86	9	4	2	1.7	337	72	20	8	0	0
Pituitary Gland	183	0.64	166	92	7	1	0	0.95	162	77	16	6	0	0
Thyroid Gland	446	0.50	327	84	7	8	1	0.88	213	71	22	7	0	0
Tibial Artery	441	0.87	683	79	7	14	1	0.24	38	70	25	2	0	3
Spinal Cord (C-1)	91	0.32	52	89	3	5	2	1.3	66	51	30	18	2	0
Hypothalamus	121	0.24	62	88	0	10	3	1.3	298	59	21	14	2	3
Hippocampus	123	0.19	52	79	5	16	0	1.4	329	61	23	15	1	0
Caudate	160	0.19	67	87	1	6	6	0.99	290	60	25	14	1	0
Amygdala	100	0.15	20	90	0	11	0	0.91	215	51	30	18	1	0
Nucleus Accumbens	147	0.11	38	71	7	22	0	0.67	187	62	25	13	0	0
Frontal Cortex	158	0.16	56	95	3	2	0	0.42	88	38	33	28	2	0
Subcutaneous Adipose	442	0.62	525	86	9	5	1	0.21	32	63	31	6	0	0
Terminal Ileum	137	0.31	78	82	9	9	0	0.48	50	71	24	5	0	0
Uterus	111	0.36	55	93	4	3	0	0.42	9	72	28	0	0	0
Ovary	133	0.19	43	87	7	5	0	0.57	16	57	39	4	0	0
Transverse Colon	274	0.19	135	91	4	5	0	0.29	84	76	18	6	0	0
Stomach	262	0.16	108	80	15	4	1	0.26	48	69	20	9	0	3
Pancreas	248	0.06	50	80	14	6	0	0.27	105	88	9	3	1	0
Liver	175	0.10	35	81	9	10	0	0.23	46	83	15	2	0	0
Whole Blood	407	0.08	88	67	9	24	0	0.22	157	46	45	8	1	0

Table 3.2. mRNA Expression of p73 and p63 Alternative Splicing Isoforms in Human Tissue. The table lists the number (n) of RNA-seq samples for each human tissue type in GTEx as well as the total gene abundance (units = TPM) and expression of alternative splicing isoforms for *TP73* and *TP63*. Alternative splicing isoform expression was calculated through analysis of exon-exon junction-spanning reads (see Figure 3.1 for details). For both genes, the total number of exon junction-spanning reads corresponding to alternative splicing (E10-EX) and the mean percentage expression (rounded to nearest whole number) of each alternative splicing isoform is listed by tissue type. The expression of p73γ and p73ε (column 13) are presented as the sum of the two isoforms because they have an exonic structure that is difficult to differentiate with our methodology.

was expressed at much lower relative amounts (0-24%) in other tissues, with the highest levels of p63γ tending to occur in tissue with low levels (<1 TPM) of *TP73* expression (Table 3.2, column 7). Low levels of p63δ expression were detected in all tissues (Table 3.2, column 8).

p73 exhibited greater diversity in alternative splicing isoform expression than p63 (Table 3.2). Across tissues with at least moderate levels (>2 TPM) of *TP73* expression, p73α was the predominantly expressed alternative splicing isoform and included: skin (74 and 75%), esophageal mucosa (85%), vagina (79%), prostate (79%), ectocervix (87%), endocervix (84%), minor salivary gland (76%), transformed lymphocytes (61%), testis (90%), cerebellum (80%), and fallopian tubes (94%) (Table 3.2, column 11). Among these same tissues, p73β was the second highest expressed (4-31%) isoform (Table 3.2, column 12). We analyzed p73γ + p73ε in tandem because they have an exonic structure that is difficult for our methodology to differentiate (Figure 3.1). p73γ + p73ε was the third most expressed isoform in most tissues, with the highest levels observed in tissues with low levels (<1 TPM) of *TP73* expression (Table 3.2, column 13). Minimal expression levels of p73δ and p73ζ were detected in all tissues (Table 3.2, columns 14 and 15).

p63 Exon 8 mRNA Isoform Expression in Human Tissue

Through analysis of p63 isoform expression, we noted two different types of junction-spanning reads between exons 8 and 9. One type (E8)

contained the full-length sequence of exon 8 (E8) while the other (E8s) lacked the last 12 bp of exon 8, which encode 4 amino acids located between the DNA-binding and oligomerization domains of p63 (Figure 3.1). The p63 E8s isoform was previously identified in mice (Rizzo et al., 2015), but little is known about its functions. Across tissues, we found that E8 was the predominant isoform expressed (~70%) and that E8s was expressed at lower levels (~30%) (Table 3.3, columns 5 and 6). Among tissues with high levels (>10 TPM) of *TP63* expression, the percentage of E8 expression was consistent (63-77%) and did not appear to be expressed in a tissue-specific manner like p63γ in skeletal muscle (Table 3.3, columns 5).

Analysis of p73 Alternative Promoter Usage in Human Tissue

During analysis of the 5' isoform expression of p73 (Table 3.1), we noted a large variation in isoform expression between epithelial tissues from the dual p73/p63-positive group. For instance, the skin predominantly expressed ΔNp73 (87 and 80%) while the esophageal mucosa predominantly expressed TAp73. We were intrigued by this observation because of the differences in the biological functions of TAp73 and ΔNp73 and the commonalities between the two tissues including both: (1) consisting of a stratified squamous epithelium composed of multiple layers of keratinocytes; (2) expressing similar gene co-expression networks (identified in a prior analysis using the GTEx dataset) (Saha et al., 2017); (3) co-expressing p73 and p63α protein in the basal epithelial layer by IF

Tissue	n	*TP63*			
		Gene TPM	EX-E9 Reads	%	
				E8	E8s
Skin (Suprapubic)	387	138.4	90,394	74	26
Skin (Leg)	473	116.6	104,144	77	23
Esophageal Mucosa	407	76.7	65,808	70	30
Vagina	115	72.9	13,656	67	34
Prostate	152	21.1	3,949	63	37
Ectocervix	6	42.2	344	66	34
Endocervix	5	4.3	28	83	17
Minor Salivary Gland	97	25.0	6,109	70	30
Mammary Gland	290	10.6	6,189	65	35
Transformed Lymphocytes	130	6.1	3,206	70	30
Testis	259	2.7	1,464	70	30
Cerebellum	173	0.14	53	56	44
Fallopian Tube	7	0.61	3	67	33
Skeletal Muscle	564	18.0	49,802	70	30
Bladder	11	35.0	726	63	38
Lung	427	1.1	768	73	27
Tibial Nerve	414	2.1	1,215	75	25
Spleen	162	0.20	45	66	34
Pituitary Gland	183	0.64	230	70	30
Thyroid Gland	446	0.50	375	74	26
Tibial Artery	441	0.87	793	73	27
Spinal Cord (C-1)	91	0.32	61	75	25
Hypothalamus	121	0.24	77	64	36
Hippocampus	123	0.19	58	49	51
Caudate	160	0.19	86	59	41
Amygdala	100	0.15	33	62	38
Nucleus Accumbens	147	0.11	52	69	31
Frontal Cortex	158	0.16	79	68	32
Subcutaneous Adipose	442	0.62	568	78	23
Terminal Ileum	137	0.31	97	75	25
Uterus	111	0.36	62	63	37
Ovary	133	0.19	38	78	22
Transverse Colon	274	0.19	121	70	30
Stomach	262	0.16	118	77	23
Pancreas	248	0.06	59	77	23
Liver	175	0.10	42	83	17
Whole Blood	407	0.08	87	73	27

Table 3.3. p63 Exon 8 Isoform Expression in Human Tissue. The table lists the number (n) of RNA-seq samples for each human tissue type in GTEx as well as the total gene abundance (units = TPM) and exon 8 isoform expression for *TP63*. Exon 8 isoform expression was calculated through analysis of exon-exon junction-spanning reads between exons 8 and 9. The total number of reads spanning exons 8 and 9 (EX-E9) and the mean percentage expression (rounded to nearest whole number) of each exon 8 isoform is listed for each tissue type. E8s (column 6) is a p63 isoform that lacks the final 12 bp of exon 8.

(Figure 3.3); and (4) expressing one similarly-migrating immuno-reactive band by immunoblot that is consistent with the molecular weight of the ΔNp73α protein control (Figure 3.4).

To explore the difference in p73 alternative promoter usage isoform expression between epithelial tissue from the dual p73/p63-positive group, we determined if the results presented in Table 3.1, which were generated by analyzing only exon-junction spanning reads, were supported by the total number of reads aligning to each exon associated with alternative promoter usage isoforms (Figure 3.1). The results of this analysis for select epithelial and non-epithelial tissue is presented in Figure 3.5. In each tissue, the relative number of log2 normalized counts for the exons that encode for the TA (exon 3) and ΔN (exon 3') isoforms of p73 and p63 (Figure 3.5) were consistent with our previous analysis using only exon junction-spanning reads (Table 3.1). While analyzing the exon expression data, we noticed that the expression level of *TP73* exon 4 (E4, shared by all p73 isoforms) was much higher than the combined expression of exons 3 (E3) and 3' (E3') in epithelial tissue (skin, esophageal mucosa, vagina, and prostate) (Figure 3.5, top). We did not observe a similar difference in the expression levels of E4 versus E3+E3' for *TP63* in these same epithelial tissues (Figure 3.5, top), or for either gene in non-epithelial tissue (transformed lymphocytes, skeletal muscle, and cerebellum) that predominantly express high levels (>10 TPM) of TAp63 and/or TAp73 (Figure 3.5, bottom row). A decrease of RNA-seq coverage in the 5' end of

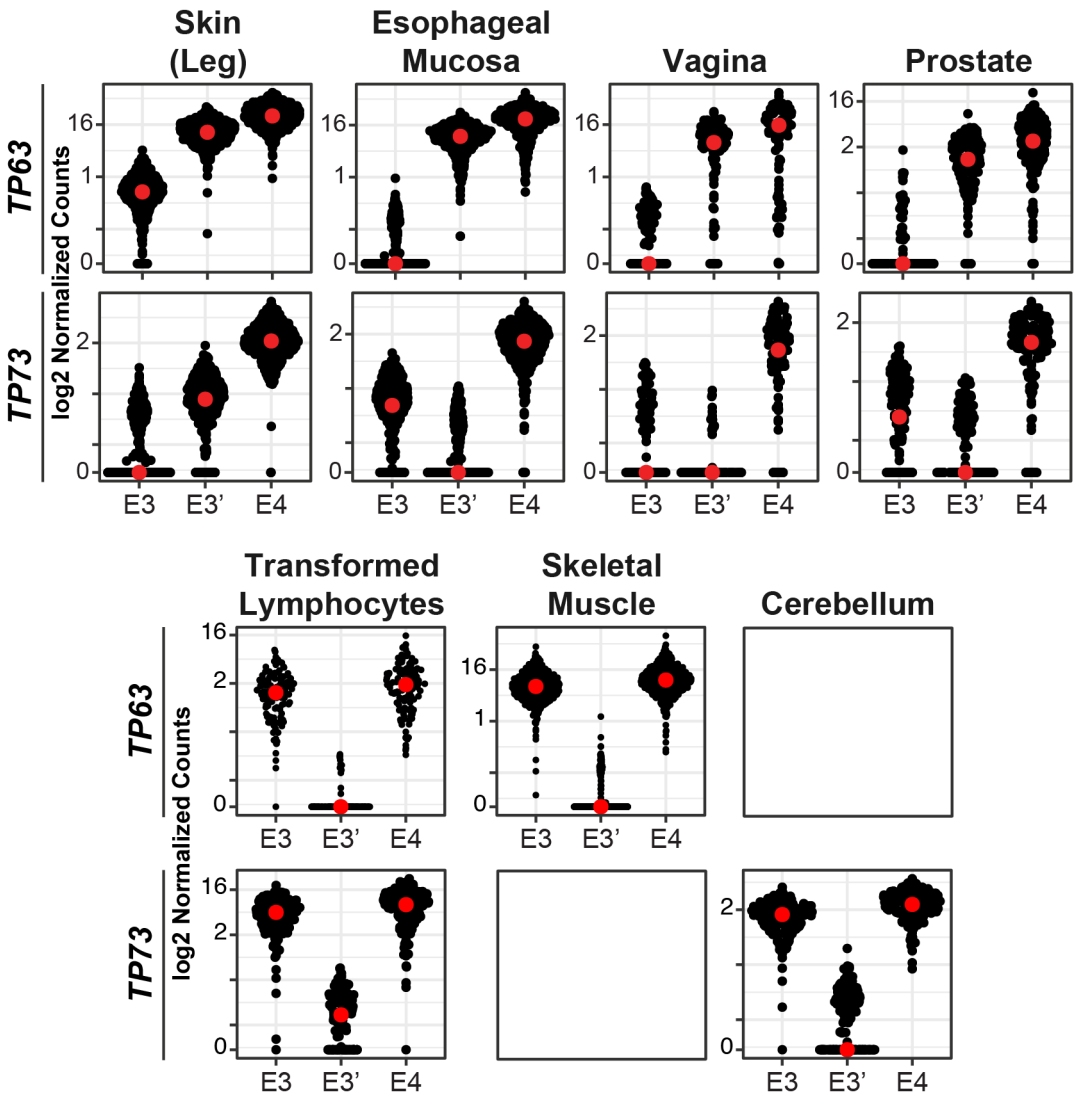

Figure 3.5. p73 and p63 Exon Expression in Human Tissue. Sina plots of *TP73* and *TP63* counts for exons 3, 3', and 4 by human tissue type from GTEx. Exon counts are normalized by exon length and sequencing depth, and plotted on a log2 scale (normalized counts + 0.01). Each black dot represents the expression level of one sample and each red dot indicates the median value of the population.

genes in a particular tissue could result from the use of lower quality RNA for library preparation, due to the inability to generate full-length cDNA from degraded RNA transcripts during oligo(dT) priming. We did not find evidence that the epithelial tissue with reduced expression of *TP73* E3+E3' versus E4 had lower quality RNA as assessed by the RNA integrity number (RIN) and the post-mortem interval (time from death to tissue collection) (Ferreira et al., 2018). In addition, we analyzed the genomic sequence of *TP73* E3' to verify that it had similar "mappability scores" (measure of the ability to align short-reads to a sequence) as other exons in the gene.

To explore the reduction in expression of *TP73* E3+E3' versus E4 we observed in epithelial tissue in Figure 3.5, we quantified the difference in *TP73* expression between the exon junctions corresponding to alternative promoter usage (EX-E4) and exon junctions shared by all isoforms (E5-E10). We calculated this metric for *TP73* and *TP63* in each tissue (Table 3.4) using the following equation: (sum of EX-E4 normalized expression) / (mean normalized expression of exon junctions between E5-E10) * 100. Consistent with the results of the exon expression analysis in Figure 3.5, we observed a ~10-fold decrease in the expression of *TP73* alternative promoter usage exon junctions compared to junctions between exons 5-10 in epithelial tissue from the dual p73/p63-positive group (Table 3.4). In the same epithelial tissue, we only observed a ~25% decrease in *TP63* alternative promoter usage exon junction expression (mostly ΔNp63), an amount consistent with the degree of 3' bias (higher sequencing

Tissue	n	*TP63*				*TP73*				
		EX-E4 Reads	%			EX-E4 Reads	%			
			TA	ΔN	EX-E4 / μ(E5-E10)		TA	ΔN	I3a	EX-E4 / μ(E5-E10)
Skin (Suprapubic)	387	51,389	2	98	72	943	20	80	0	13
Skin (Leg)	473	59,324	3	97	73	1,122	13	87	0	12
Esophageal Mucosa	407	39,845	0	100	78	455	83	17	0	9
Vagina	115	9,127	1	99	82	72	81	19	0	5
Prostate	152	2,307	2	98	73	170	74	27	0	12
Ectocervix	6	232	2	98	77	3	68	32	0	8
Endocervix	5	19	20	80	81	9	67	33	0	60
Minor Salivary Gland	97	3,771	6	94	80	155	49	51	0	14
Mammary Gland	290	3,655	3	97	74	325	35	65	1	29
Transformed Lymphocytes	130	1,657	99	1	71	5,551	98	2	0	80
Testis	259	560	96	4	53	2,331	4	1	95	NA
Cerebellum	173	27	59	41	68	1,864	97	3	0	64
Fallopian Tube	7	2	65	35	40	80	76	25	0	74
Skeletal Muscle	564	29,796	100	0	79	26	32	66	3	55
Bladder	11	474	0	100	82	4	54	27	19	45
Lung	427	436	38	62	75	1,375	65	35	0	81
Tibial Nerve	414	782	94	6	81	15	95	0	5	60
Spleen	162	31	64	36	82	274	95	5	0	76
Pituitary Gland	183	148	68	32	88	117	88	12	0	62
Thyroid Gland	446	218	70	30	72	384	94	6	0	138
Tibial Artery	441	465	74	26	75	14	94	7	0	31
Spinal Cord (C-1)	91	44	70	30	95	32	59	41	0	73
Hypothalamus	121	57	88	13	99	154	31	69	0	61
Hippocampus	123	40	73	27	87	149	46	54	0	61
Caudate	160	68	80	21	110	196	58	42	0	71
Amygdala	100	35	89	11	117	78	52	48	0	54
Nucleus Accumbens	147	29	73	28	87	99	50	50	0	77
Frontal Cortex	158	42	77	23	88	7	82	18	0	13
Subcutaneous Adipose	442	326	56	44	69	20	74	20	6	46
Terminal Ileum	137	55	84	16	80	59	100	0	0	68
Uterus	111	41	71	30	77	8	100	0	0	80
Ovary	133	28	64	36	67	18	100	0	0	84
Transverse Colon	274	94	78	22	108	75	97	3	0	77
Stomach	262	52	46	54	65	42	95	2	2	68
Pancreas	248	34	27	73	89	122	93	7	0	91
Liver	175	30	59	41	93	44	100	0	0	86
Whole Blood	407	42	61	39	65	137	97	3	0	70

Table 3.4. Analysis of p73 Alternative Promoter Exon-Exon Junction Expression in Human Tissue. The table lists the number (n) of RNA-seq samples for each human tissue type in GTEx as well as the expression of alternative promoter isoforms for *TP73* and *TP63* (same data presented in Table 3.1). In addition, for each gene, alternative promoter exon-exon junction expression (EX-E4) was divided by the mean (μ) exon-exon junction expression of exons 5-10 (and multiplied by 100) in order to determine if the expression of sequences corresponding to p73 alternative promoter isoforms was reduced relative to sequences shared by all p73 isoforms. *TP73* expression in the testis was excluded from this analysis because the tissue abundantly expressed a p73 isoform lacking exons 5-10.

coverage at the 3' ends of genes) seen in a typical high-quality RNA-seq experiment utilizing poly-A capture (i.e., 3' bias will occur when poly-A capture is used) (Table 3.4). In addition, we observed a similar ~30% decrease in *TP73* alternative promoter usage exon junction expression in tissue (cerebellum, fallopian tube, transformed lymphocytes) that express predominantly TAp73 at high levels (>10 TPM) (Table 3.4). In sum, these findings suggest that the decrease in *TP73* alternative promoter usage exon junction expression is specific to epithelial tissue from the dual p73/p63-positive group and not simply due to tissue-specific characteristics, since a similar decrease in alternative promoter usage exon junction expression was not observed for *TP63*.

Analysis of p73 TSS in Human Epithelial Tissue

Having determined that select epithelial tissue express reduced levels of *TP73* alternative promoter usage exons (compared to exons shared by all isoforms), we considered various possibilities that could lead to generation of this result. One possibility is the presence of an additional TSS in the *TP73* locus located at or upstream of exon 4 that could yield a transcript encoding a protein similar in size and function to ΔNp73. To study it, we used RAMPAGE (RNA Annotation and Mapping of Promoters for the Analysis of Gene Expression), an RNA-seq sequencing method that can identify TSS at single-base resolution with a high signal-to-noise ratio across the genome (Batut and Gingeras, 2013). We analyzed human tissue

(adult and embryonic) RAMPAGE data produced by ENCODE Project, which included several adult tissue samples that were also analyzed by the GTEx Project. We identified a predicted TSS in the *TP73* gene, located immediately upstream (~7 bp) of the 5' end of exon 4, in multiple tissue types: skin (leg and suprapubic), embryonic skin, tongue, esophagus, and vagina (Figure 3.6). This TSS has not been previously described to our knowledge. Other epithelial tissue (embryonic tongue and prostate) had RAMPAGE reads (specifically the 5' ends) align to the same E4 TSS, but it did not reach genome-wide significance (Figure 3.6). We did not find evidence of the E4 TSS in the testis (Figure 3.6) or tissue with low (<2 TPM) levels of *TP73* expression (embryonic skeletal muscle, embryonic spinal cord, embryonic frontal cortex, ovary) (data not shown). Consistent with our analysis of p73 alternative promoter usage isoform expression using GTEx RNA-seq (Table 3.1), we detected a predicted TSS at the 5' end of *TP73* exon 3a (Figure 3.6). Among the epithelial tissue in Figure 3.6, only leg skin and embryonic tongue contained a RAMPAGE-predicted TSS at the site of the canonical ΔNp73 TSS (5' end of E3'), but all the other tissue except vagina had RAMPAGE reads aligning to the TSS (Figure 3.6). None of epithelial tissue had a predicted TSS at the canonical TAp73 TSS E1 (data not shown).

A transcript produced from the putative E4 TSS (E4p73) would contain a 34 bp 5' UTR and a start codon 27 bp downstream of the 5' end of exon 4. This transcript could potentially encode a ΔNp73-like protein

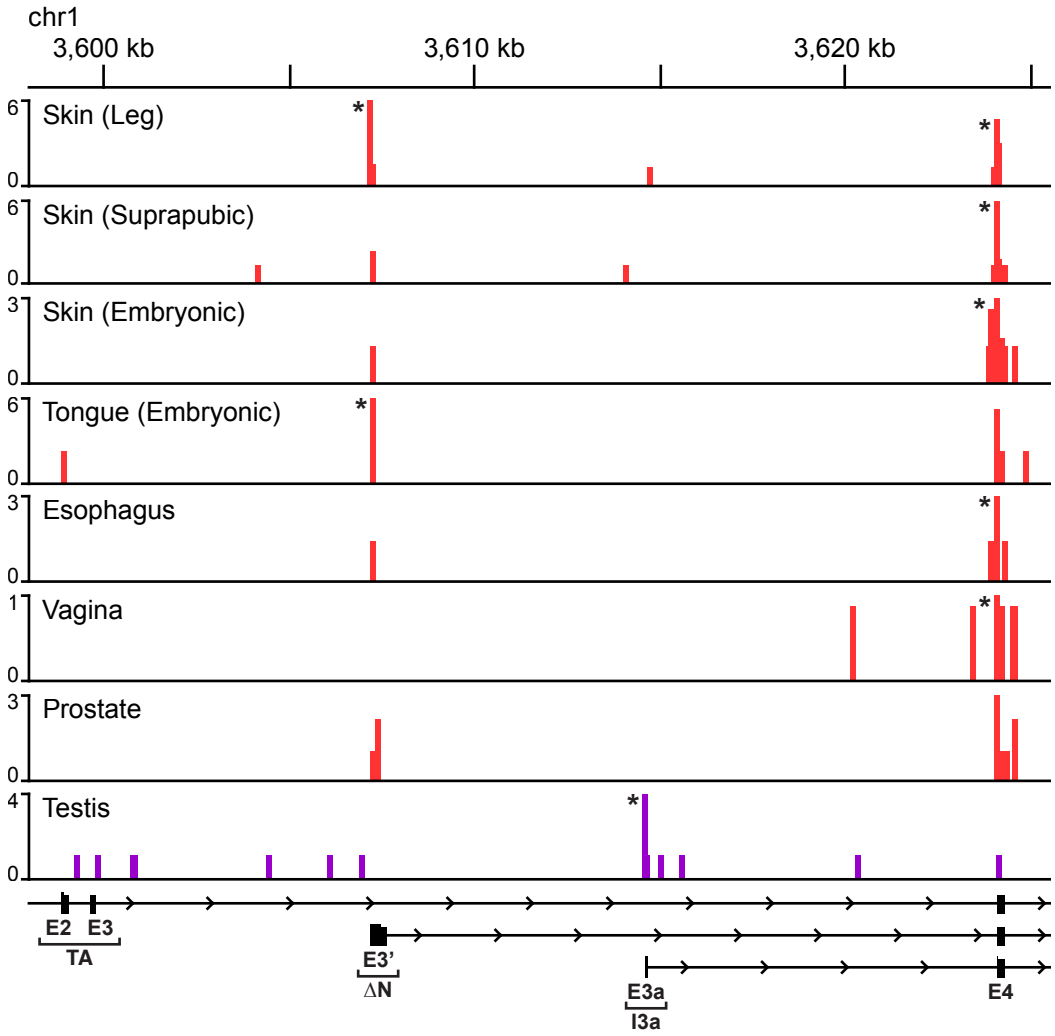

Figure 3.6. Analysis of p73 TSS in Human Epithelial Tissue. Genome browser view of human tissue RAMPAGE data (from ENCODE Project) at the 5' end of the *TP73* genomic locus. RAMPAGE identifies TSS across the genome at single-base resolution. Each track shows the density of RAMPAGE read 5' ends and is auto-normalized (the scale is listed to the left of each track). RAMPAGE peaks (i.e. RAMPAGE TSS) were identified using the ENCODE peak detection methodology for RAMPAGE data and are marked with an asterisk.

product with a N-terminal truncation of the first 22 amino acids (~Δ2 kDa) (Figure 3.7). A previous study confirmed that the E4 start codon in ΔNp73α can initiate translation and produce the expected ΔNp73-like protein product using *in vitro* translation and cell-based overexpression studies (Grob et al., 2001). By immunoblot analysis, the migration of this isoform would be difficult to distinguish from ΔNp73; and, could help explain why the epithelial tissue in Figure 3.4 express a similar sized immuno-reactive p73 protein band. A similar finding was reported for p63. Rinne and colleagues discovered three patients with an AEC-like syndrome, caused by mutations in the exons of *TP63* that encode the ΔN domain, that express a truncated ΔNp63 protein by translation re-initiation at the first methionine in exon 4 (Rinne et al., 2008). Collectively, these results provide preliminary evidence supporting the existence of a previously unreported p73 TSS in select epithelial tissue.

p73 and p63 Isoform Expression in Human Epithelial Cells

To generate further evidence supporting the existence of E4p73 transcript and protein, we performed immunoblot and RNA-seq analyses on immortalized, transformed, and primary epithelial cell cultures originating from tissues that express p73. ΔNp63α was the predominant isoform detected in all cell lines analyzed (Figure 3.8A). These results were consistent with the corresponding RNA-seq data from HaCaT cells, which

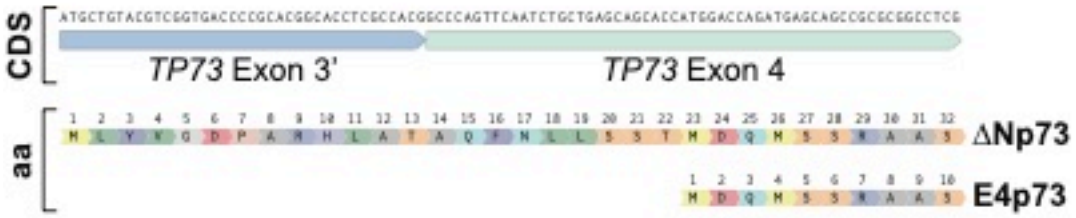

Figure 3.7. Comparison of N-terminal Amino Acid Sequences of ΔNp73 and E4p73. The figure includes the coding sequence (CDS) and the amino acid (aa) sequence of the first 32 aa of ΔNp73 as well the aa sequence of the putative E4p73 isoform.

A.

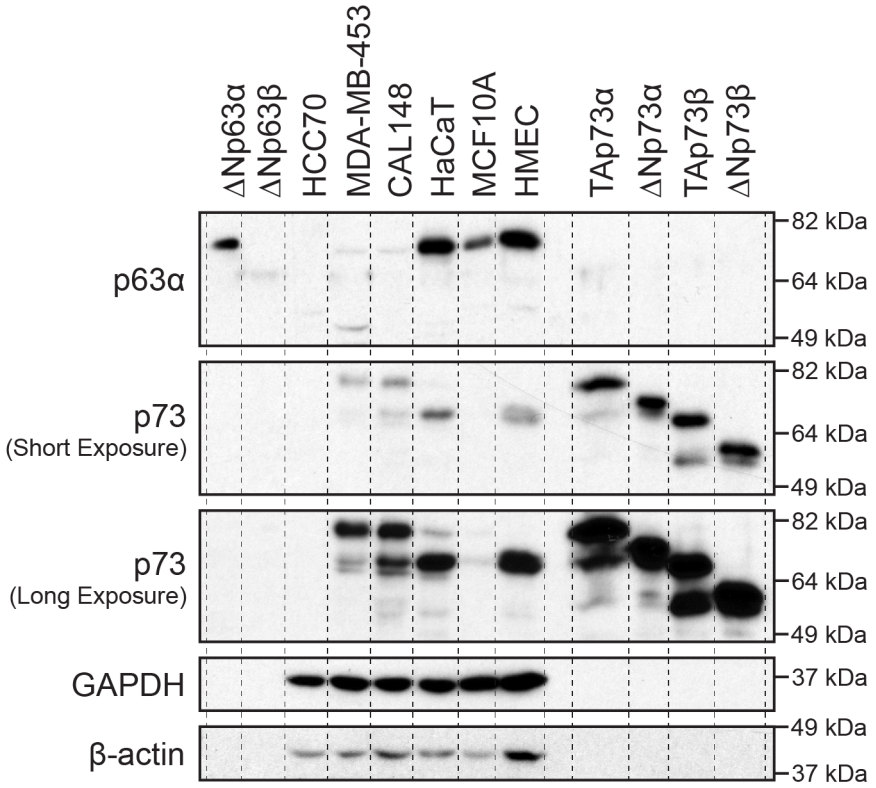

B.

	TP63							*TP73*						
	Gene	%		%				Gene	%		%			
Sample	**TPM**	**TA**	**ΔN**	**α**	**β**	**γ**	**δ**	**TPM**	**TA**	**ΔN**	**α**	**β**	**γ+ε**	**δ**
MDA-MB-453	1.2	ND	ND	ND	ND	ND	ND	12.5	100	0	82	15	3	0
CAL148	3.1	100	0	ND	ND	ND	ND	19.4	91	9	84	11	5	0
HaCaT	57.1	1	99	84	12	2	2	1.6	100	0	91	9	0	0

Figure 3.8. p73 and p63 Isoform Expression in Human Epithelial Cells. (A) Immunoblot analysis for p73 and p63α was performed on cellular lysate harvested from immortalized, transformed, and primary epithelial cell cultures originating from tissues that express p73. Human p73 and p63 isoform controls were included to assess antibody sensitivity and specificity, and aid in the interpretation of tissue isoform expression. HCC70 lack expression of p73 mRNA, and used as a negative control. (B) For each cell line analyzed by RNA-seq (n = 3), the table lists the total gene abundance (units = TPM) and expression of alternative promoter and splicing isoforms for *TP73* and *TP63*. Isoform expression was calculated through analysis of exon-exon junction-spanning reads. Samples lacking a sufficient number of exon junction-spanning reads (n = 5) to quantify isoform expression are marked as ND.

found that ΔNp63 (99%) and p63α (84%) were the predominant alternative promoter usage and alternative splicing isoforms expressed respectively (Figure 3.8B).

TAp73α was the predominant expressed isoform in transformed cells (CAL148 and MDA-MB-453) by immunoblotting (Figure 3.8A) and this matched the corresponding RNA-seq data for the cells (Figure 3.8B). By immunoblot, HaCaT cells had multiple immunoreactive bands for p73: (1) a major band that migrated between the ΔNp73α and TAp73β controls; and (2) a minor band that migrated similar to the TAp73α control (Figure 3.8A). In the RNA-seq data from HaCaT cells, 100% (5/5) of the p73 alternative promoter usage exon junction-spanning reads corresponded to the TAp73 isoform and 0% to the ΔNp73 isoform (Figure 3.8B). Furthermore, we did not even detect any reads aligning to the *TP73* exon (E3') unique to ΔNp73 isoforms (out of a total of 1,016 reads aligning to *TP73*). Also, we noted in HaCaT cells that the number of reads aligning to exons 3 and 3' of *TP73* was much lower than the number aligning to exon 4 (6 + 0 versus 45 respectively; 6/45 = 13%), similar to our observations in epithelial tissue from Figure 3.5. We did not observe this large of a difference in the number of reads aligning to *TP73* exons 3 and 3' versus 4 for MDA-MB-453 (67 + 2 versus 145; 48%) or CAL148 (112 + 46 versus 205; 77%) cells. Finally, in HaCaT cells, p73α was the major (91%; 10/11 exon junction-spanning reads) and p73β was the minor (9%, 1/11) alternative splicing isoform expressed. Based on the protein and mRNA expression data from HaCaT

cells we can conclude that: (1) the major immunoreactive band for p73 is more likely to be ΔNp73α (or a ΔNp73α-like protein) than TAp73β given the lack of p73β expression by RNA-seq; (2) the molecular weight of the major immunoreactive band for p73 is consistent with size E4p73α in a previous study (Grob et al., 2001); and (3) the expression of E4p73α by HaCaT cells would help explain the differences observed in alternative promoter usage isoform expression at the mRNA and protein levels.

We also analyzed p73 protein expression in primary cultures of human basal mammary epithelial cells (HMECs) (Hearnes et al., 2005). HMECs expressed one major immunoreactive band for p73 that had a molecular weight similar to the major p73 band in HaCaT cells.

Conclusion

To date, this study is the largest comprehensive bioinformatic analysis of p73 and p63 mRNA isoform expression. Given the rigorous standard operating procedures for tissue procurement and RNA-seq used by the GTEx Project (Carithers et al., 2015), the analysis presented in this Chapter should be a useful resource to investigators interested in tissue-specific expression and the function of the various p73 and p63 isoforms.

The p73 and p63 gene-level expression data from GTEx was largely consistent with previously published tissue-specific gene expression analyses (Di Como et al., 2002; Grespi et al., 2012; Puig et al., 2003; Sethi et al., 2015; Yang et al., 1998). In addition, the human tissue expression

data were consistent with many of the reported phenotypes observed in p73- and p63-deficient mice (Holembowski et al., 2014; Marshall et al., 2016; Mills et al., 1999; Nemajerova et al., 2016; Yang et al., 1999, 2000). For both *p73* and *p63*, alternative promoter usage isoform expression had a larger range of variation between tissues than alternative splicing isoform expression. Outside of p63γ expression in skeletal muscle, we observed little evidence for tissue-specific expression of the alternative splicing isoforms of *p73* and *p63*. Nearly all tissues expressed predominantly α isoforms, with minor amounts of β +/- γ isoforms, and little of any other isoform.

Most human tissues that express high levels of p73 and/or p63 have an observable phenotype in the respective tissues of the corresponding knockout mouse models. We identified several tissues in our study that were an exception to this and had interesting isoform expression patterns. The adult cerebellum expressed high levels of TAp73α. Previous studies have determined that the cerebellum of *p73*-/- mice have a normal gross morphology (Pozniak et al., 2002) and that multiple subtypes of medulloblastoma, a cancer that arises from arises from cerebellar progenitor cells, are driven by overexpression of TAp73α (Niklison-Chirou et al., 2017). In these tumors, TAp73α overexpression is reported to support mitochondrial respiration by regulating the expression of genes involved in glutamine metabolism (e.g. *GLS2*) (Niklison-Chirou et al., 2017). Future studies to determine which cell types in the cerebellum express p73

and if *p73*-/- mice exhibit cerebellar phenotypes would be helpful. In addition, the high levels of TAp63γ expression in skeletal muscle stood out, because it was the only example of a tissue in which p73α and p63α was not the predominant isoform expressed. The role of TAp63γ in skeletal muscle is unknown, but a prior study determined that p63 has a cytoplasmic staining pattern in skeletal muscle and localizes to the Z bands of sarcomeres (Martin et al., 2011). It would be interesting to analyze embryonic skeletal muscle from *p63*-/- mice to determine if there are any gross morphological defects.

Our study provided preliminary evidence supporting the existence of a previously unreported p73 TSS in multiple epithelial tissue. Further studies using alternative methods for identifying TSS are needed to establish whether or not the TSS exists *in vivo*. If confirmed, it will be important to determine the relative expression level and biological differences between ΔNp73 and E4p73 in physiologically-relevant contexts. In this Chapter, we determined the p73 mRNA isoforms expressed in epithelial tissues with basal cell populations. We made pragmatic use of this knowledge in the selection of one tissue, the skin, to serve as a model for the experimental results and discoveries presented in Chapter IV.

CHAPTER IV

p73 REGULATES EPIDERMAL WOUND HEALING AND INDUCED KERATINOCYTE PROGRAMMING

Introduction

The p53 family of transcription factors (p53, p63, and p73) play critical roles in cell cycle regulation, DNA damage response, and cellular differentiation (el-Deiry et al., 1993; Kaghad et al., 1997; Marshall et al., 2016; Mills et al., 1999; Nemajerova et al., 2016; Osada et al., 1998; Westfall et al., 2003; Yang et al., 1998, 1999). All three family members share structural and functional homology in their transactivation (TA), DNA-binding, and oligomerization domains (Yang et al., 2002). Due to the high degree of sequence homology in their DNA-binding domains, family members bind to similar genomic regions and regulate overlapping target genes. Both p73 and p63 have two distinct promoters that encode for either a longer (TA) or shorter (ΔN) transactivation domain (Kaghad et al., 1997; Yang et al., 1998). In general, TA isoforms induce canonical p53 activity (e.g. cell cycle arrest, DNA repair, and apoptosis) while ΔN isoforms can repress these activities by acting in a dominant-negative manner towards TA isoforms (Grob et al., 2001; Yang et al., 1998). ΔN isoforms can also induce the expression of specific target genes on their own (Ihrie et al., 2005; Liu et al., 2004; Wu et al., 2003). Adding further complexity, both TA and ΔN isoforms can be alternatively spliced in their C-terminus to produce

variants (e.g. α, β, γ) with differing transcriptional activity (De Laurenzi et al., 1998; Yang et al., 1998). In addition to sharing overlapping target genes, p73 and p63 isoforms can form stable heterodimers through association of their oligomerization domains (Davison et al., 1999; Joerger et al., 2009).

The complicated interplay between p73 and p63 proteins has made studying the individual roles of each protein challenging. The development of knockout mouse models has provided insight to the distinct biological roles of p63 and p73. Mice lacking p63 (*p63*-/-) fail to develop stratified epithelia, epithelial appendages, and limbs; and die shortly after birth due to desiccation (Mills et al., 1999; Yang et al., 1999). Studies have collectively shown that p63 (specifically ΔNp63α) is expressed in basal progenitor cell populations of ectodermal tissues and is essential for stem cell maintenance, proliferation, and development (Mills et al., 1999; Senoo et al., 2007; Truong et al., 2006; Yang et al., 1999). Mice lacking p73 (*p73*-/-) have a diverse set of phenotypes including hydrocephalus, hippocampal dysgenesis, sterility, chronic infections, and premature aging (Marshall et al., 2016; Nemajerova et al., 2016; Rufini et al., 2012; Santos Guasch et al., 2018; Yang et al., 2000). Many of these phenotypes are primarily due to the loss of multiciliated cells, which require a TAp73-mediated transcriptional program to develop. We previously reported that 50% of p63-expressing basal epithelial cells in the trachea co-express p73 and that tracheas from *p73*-/- mice exhibit a 35% reduction in the number of basal

epithelial cells (Marshall et al., 2016). However, the role of p73 in basal progenitor cells is largely unknown. Studies of somatic cell reprogramming have provided clues by showing that p73 is required for effective generation of induced pluripotent stem cells (iPSCs) with Yamanaka factors (Lin et al., 2012; Martin-Lopez et al., 2017). Mouse embryonic fibroblasts lacking p73 have impaired mesenchymal-to-epithelial transition (a rate-limiting step during reprogramming), resulting in iPSCs with a defective epithelial phenotype (Martin-Lopez et al., 2017).

The skin has proven to be an excellent model system for studying basal cell function during homeostasis and after injury (e.g. wounding). The skin forms a barrier that protects the body from physical, microbial, and chemical assaults as well as unregulated loss of water and solutes (Proksch et al., 2008b). The epidermis [also referred to herein as the interfollicular epidermis (IFE)] is the primary component of the skin barrier and consists of a multi-layered stratified epithelium with appendages. Basal stem cells in the innermost layer of the epidermis are essential for maintaining tissue homeostasis and give rise to cells that detach from the basal layer, exit the cell cycle, and undergo a differentiation program. During this process, keratinocytes migrate towards the surface of the skin and undergo a tightly controlled series of gene expression changes that result in the production of dead squames, which are essential for maintaining the skin barrier (Blanpain and Fuchs, 2009). Following wounding, it is essential to quickly repair the epidermis and restore the

barrier function of the skin. Stem cells of the skin, located in the basal layer of the epidermis and the hair follicle (HF) bulge, regulate this process (Ge and Fuchs, 2018). Stem cells near the wound are activated to migrate into the wound bed and proliferate, helping reepithelialize the wound epidermis (Ito et al., 2005; Levy et al., 2007b).

We used the skin as a model system to investigate the role of p73 in basal epithelial cells and discovered that p73 is required for timely healing of cutaneous wounds. Wounds in *p73*-/- mice healed slower and demonstrated decreased proliferation and increased levels of biomarkers associated with the DNA damage response in basal keratinocytes at the epidermal wound edge. In addition, p73 expression increased in the basal keratinocytes at the wound edge of *p73*+/+ mice. Through analysis of single-cell transcriptomic data, we found that p73 was expressed by epidermal and HF stem cells, the cell types that regulate wound healing. Using a model of somatic cell reprogramming, we determined that ΔNp73 enhances the expression of keratinocyte genes involved in skin development, proliferation, and wound healing.

Results

Analysis of p73 Expression in Human and Murine Skin

To determine which tissues express p73, we analyzed transcriptomic data from 37 human tissues (Uhlen et al., 2010). We observed expression [>1 transcript per million (TPM)] of *TP73* in many tissues with basal cell populations, including: skin, esophagus, prostate, tonsil, salivary gland, and lung (Figure 4.1). Across all tissues, expression of *TP73* was significantly ($p = 0.0003$) correlated with expression of *TP63* (Figure 4.1), a marker of basal epithelial cells. Given that *TP73* and *TP63* co-expression was highest in the skin, there are robust model systems for studying this organ, and we previously determined which p73 isoforms are expressed in this tissue (Chapter III, Tables 3.1 and 3.2), we focused our analysis on the role of p73 in the skin and its interplay with p63.

Prior work from our laboratory has shown that some pan-p73 antibodies cross-react with p63 (Rosenbluth et al., 2009). In order to validate that the pan-p73 antibody (EP436Y) used in our studies did not cross-react with p63 and confound our results, we conducted immunoblot analyses on a diverse set of primary and transformed human epithelial cells using p73 (EP436Y), p63 (AF1916), and p63α (H-129) antibodies (Figure 4.2). Cells selected for analysis expressed varying levels of p73 and p63 mRNA in public databases and included a triple-negative breast cancer cell line that did not express either p73 or p63 mRNA (HCC70). We found that

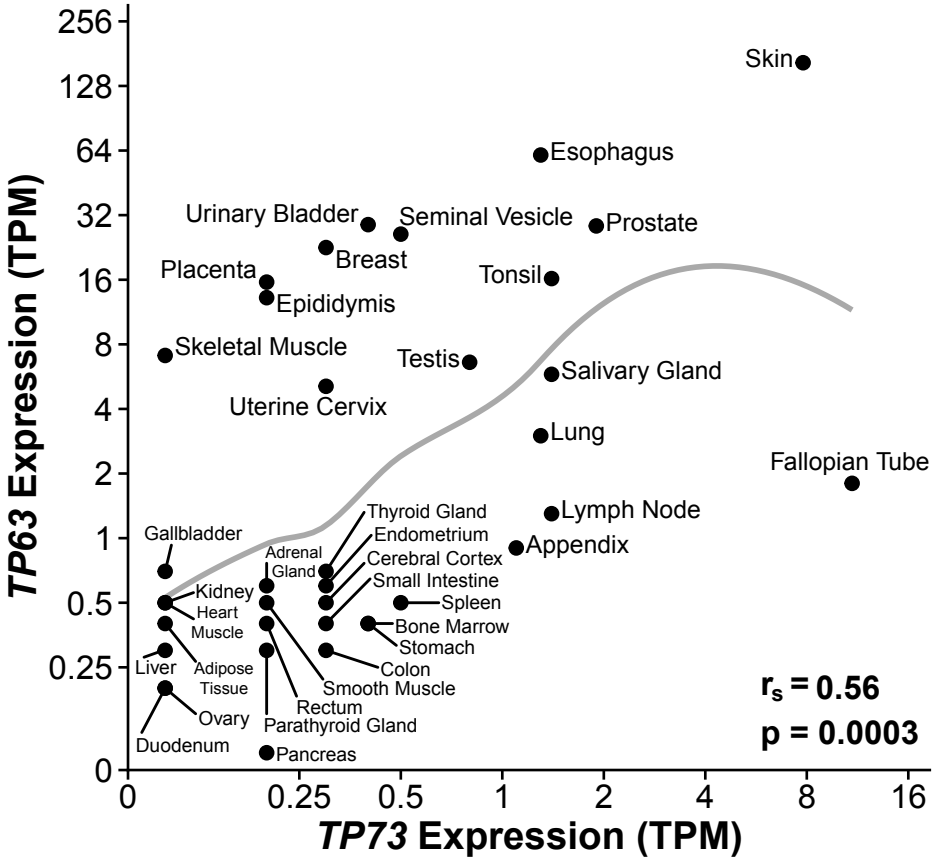

Figure 4.1. p73 and p63 Gene Expression in Human Tissue. Scatter plot of *TP63* versus *TP73* RNA-seq expression (units = TPM) by human tissue type (n = 37) from the Human Protein Atlas (172 total samples). Mean expression (TPM + 0.1) for each tissue is plotted on a log2 scale with a LOESS smooth local regression line (gray). Correlation between *TP63* and *TP73* was quantified using Spearman's rank correlation coefficient (r_s).

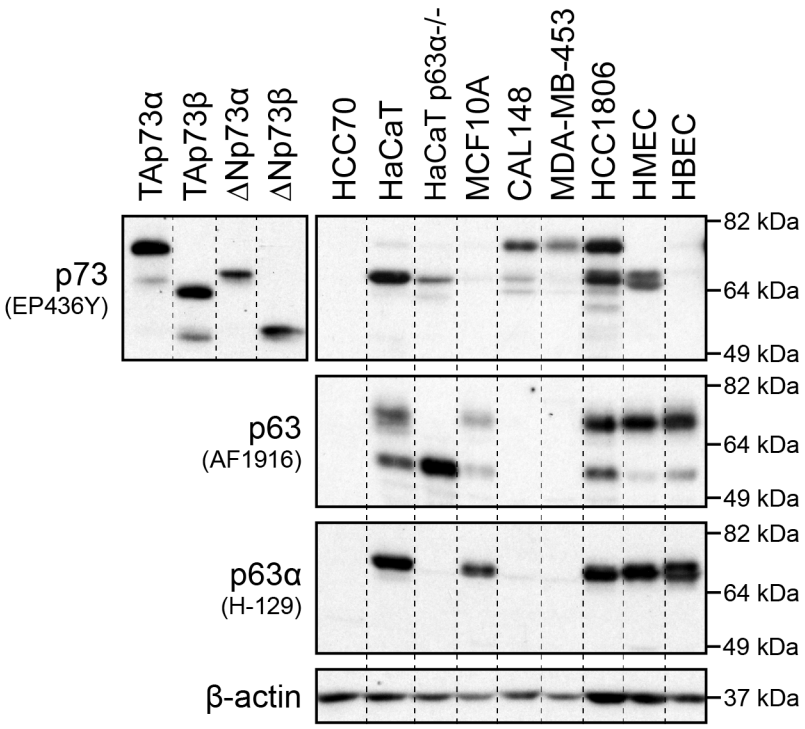

Figure 4.2. Validation of p73 and p63 Antibody Sensitivity and Specificity. Immunoblot of p73 (EP436Y), p63 (AF1916), and p63α (H-129) protein expression in a diverse set of primary and transformed human epithelial cells with varying levels of p73 and p63 mRNA expression. Human p73 isoform controls (generated by ectopic overexpression in 293FT cells) were included in the analysis to assess the sensitivity of the pan-p73 antibody. HCC70 (triple-negative breast cancer) cells lack expression of p73 and p63 mRNA and were selected to evaluate antibody specificity. HaCaT p63α-/- cells lack p63α expression as a result of CRISPR-Cas9 genomic editing.

p73 EP436Y recognized all four human p73 isoform controls, detected protein expression levels consistent with the known p73 and p63 mRNA levels, lacked non-specific detection in cells (HCC70) that do not express p73 RNA, and did not cross-react with p63 (Figure 4.2). These results validate the specificity of p73 EP436Y and are consistent with previous reports of the antibody's specificity in immunofluorescence (IF) analyses (Marshall et al., 2016; Santos Guasch et al., 2018).

We performed IF staining for p73 and p63α on human and murine skin to determine cell expression patterns (Figure 4.3A). In both species, p73 expression was nuclear and limited to a subset of p63-positive cells in the IFE, outer root sheath (ORS) of the HF, hair bulb, and sebaceous gland (Figure 4.3A). We did not detect p73 expression in the hair shaft (HS) or the suprabasal layer of the IFE. Both species expressed p73 in the basal layer of the IFE, but expression in the suprabasal layer was primarily limited to human skin (Figure 4.3A). In human skin, p73 was strongly co-expressed with p63α in the stem cell compartment of the HF, termed the bulge (Figure 4.3A, top panel). The bulge is a specific area of the ORS containing HF stem cells that is located between the attachment site of the arrector pili muscle and the opening of the sebaceous gland (Cotsarelis et al., 1990). We also saw expression of p73 in the bulge region of murine HFs. IF staining for p73 and p63α in murine skin (Figure 4.3A, bottom panel) was consistent with immunoblot analysis of the tissue (Figure 4.3B).

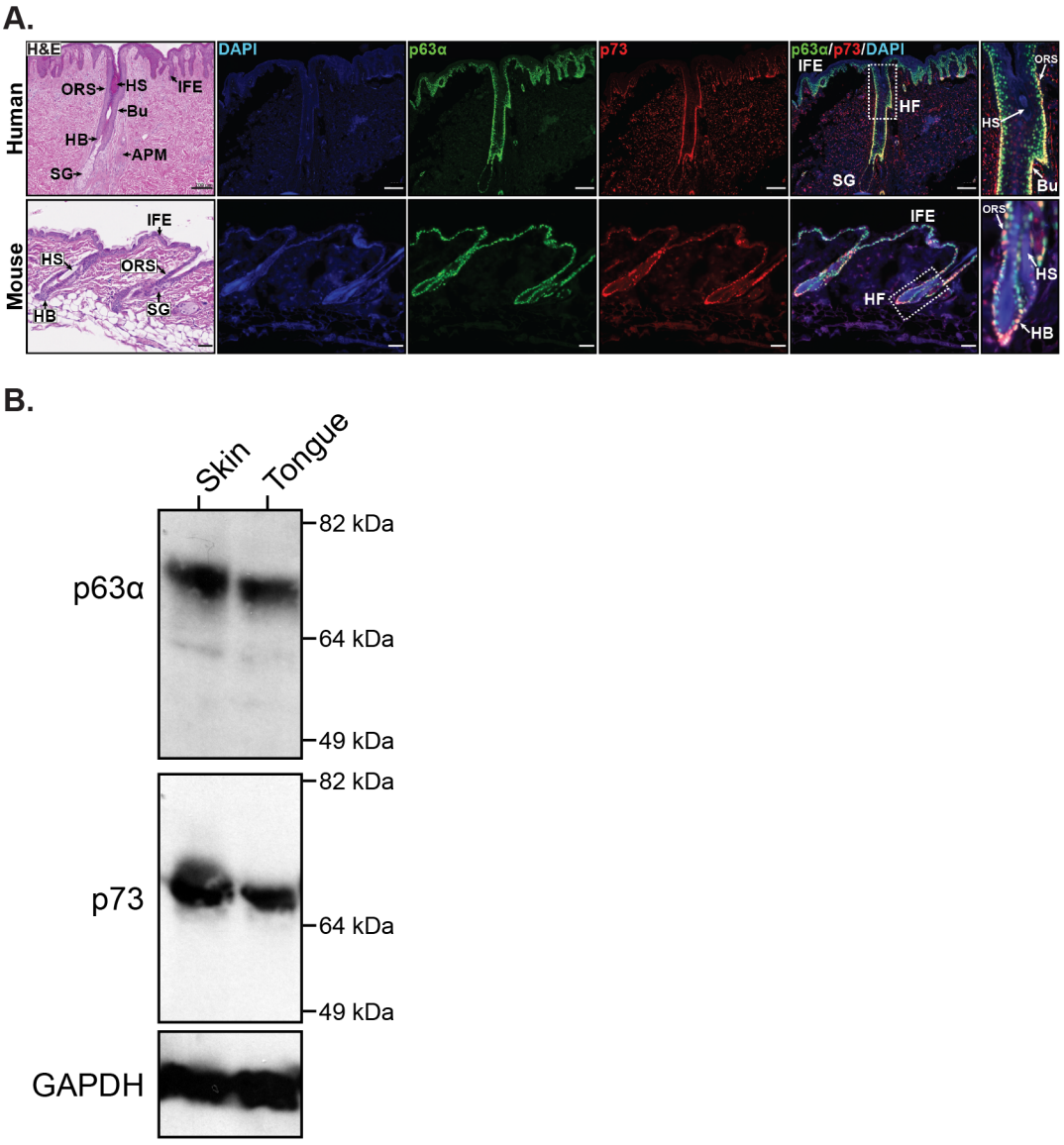

Figure 4.3. p73 Protein Expression and Localization in Human and Murine Skin. (A) Representative micrographs of H&E and IF staining on serial human (top) and mouse (bottom) skin sections; DAPI (blue), p63α (green), and p73 (red). Regions of the skin in micrographs are labeled as: interfollicular epidermis (IFE), hair follicle (HF), outer root sheath (ORS), HF bulge (Bu), hair bulb (HB), sebaceous gland (SG), hair shaft (HS), and arrector pili muscle (APM). Scale bars represent 200 μm for human and 50 μm for murine tissue. (B) Immunoblot of p63α and p73 protein expression in murine skin and tongue. Tissue was harvested from p73+/+ mice for immunoblot analysis. All data represented was collected by Clayton Marshall.

The IF results indicate that p73 expression in the skin is limited to a subset of p63-positive basal cells in the IFE and HF, and imply a role for p73 in basal keratinocytes.

p73 is Co-expressed with p63 Throughout Murine Embryonic Skin Development

To determine if p73 is co-expressed with p63 during skin development in a pattern similar to that of adult murine tissue (Figure 4.3A, bottom panel), we performed IF staining for p73 and p63α in murine skin at several time points during embryogenesis. Similar to adult mice (Figure 4.3A, bottom panel), p73 was coordinately expressed with p63α in basal cells at all developmental time points analyzed (Figure 4.4). During early embryonic stages (E12.5 and E13.5), p73 was expressed at low levels in the single-layered epidermis. At later time points during epidermal stratification (E14.5 and E16.5), expression of p73 increased and was restricted to cells in the basal layer, while p63α was expressed in both the basal and suprabasal layers (Figure 4.4). HF morphogenesis is the process in which specific subsets of basal cells within the epidermis divide perpendicularly to the basement membrane and grow downward into the dermis to form HFs. p73 was highly expressed during HF morphogenesis (E16.5-P1) in the ORS and hair bulb of developing HFs (Figure 4.4). By postnatal day 1 (P1), p73 expression in the basal IFE was reduced and

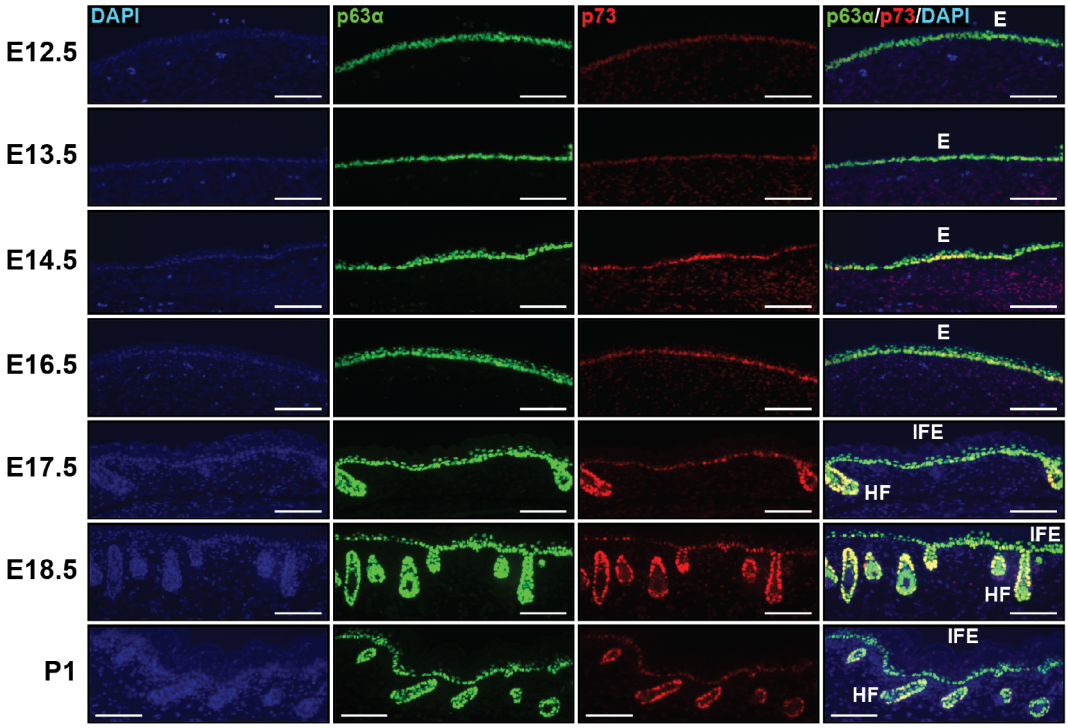

Figure 4.4. p73 and p63α Protein Expression and Localization During Murine Embryonic Skin Development. Representative micrographs of IF staining for DAPI (blue), p63α (green), and p73 (red) in skin specimens at the indicated stages of murine development. Scale bars represent 50 μm. Regions of the skin in micrographs are labeled as: epidermis (E), IFE, and HF. All data represented was collected by Clayton Marshall.

limited to only a subset of cells (Figure 4.4), similar to the IF staining seen in adult mice (Figure 4.3A, bottom panel).

p73-/- Murine Skin has a Normal Morphological Appearance

To evaluate if p73 plays a role in skin morphogenesis, we analyzed the skin of *p73*-/- mice (Marshall et al., 2016; Santos Guasch et al., 2018). Analysis of H&E-stained tissues showed no overt morphological differences between the back skin of adult *p73*+/+ and *p73*-/- mice (Figure 4.5A). Likewise, IF staining for markers of epidermal differentiation (K5, p63α, K14, E-cadherin, and K10) in *p73*+/+ and *p73*-/- mice demonstrated no significant difference in expression or localization (Figures 4.5B-E). HFs in Figure 4.5 that appear disconnected from the epidermis represent an artifact of sectioning. These results suggest that p73 is not required for proper epidermal morphogenesis or differentiation in mice.

p73-/- Mice Exhibit Delayed Wound Healing

Given the lack of phenotypic differences in the skin of *p73*-/- mice under homeostatic conditions and the importance of basal keratinocytes, which express p73, in wound healing, we examined the role of p73 in the skin after epidermal wounding. We generated full-thickness wounds (diameter = 0.5 mm) on the backs of adult *p73*+/+ and *p73*-/- mice and analyzed the wound-healing process at post-wound days 0, 3, 7, and 10. Over the 10-day time course, the rate of wound closure was significantly

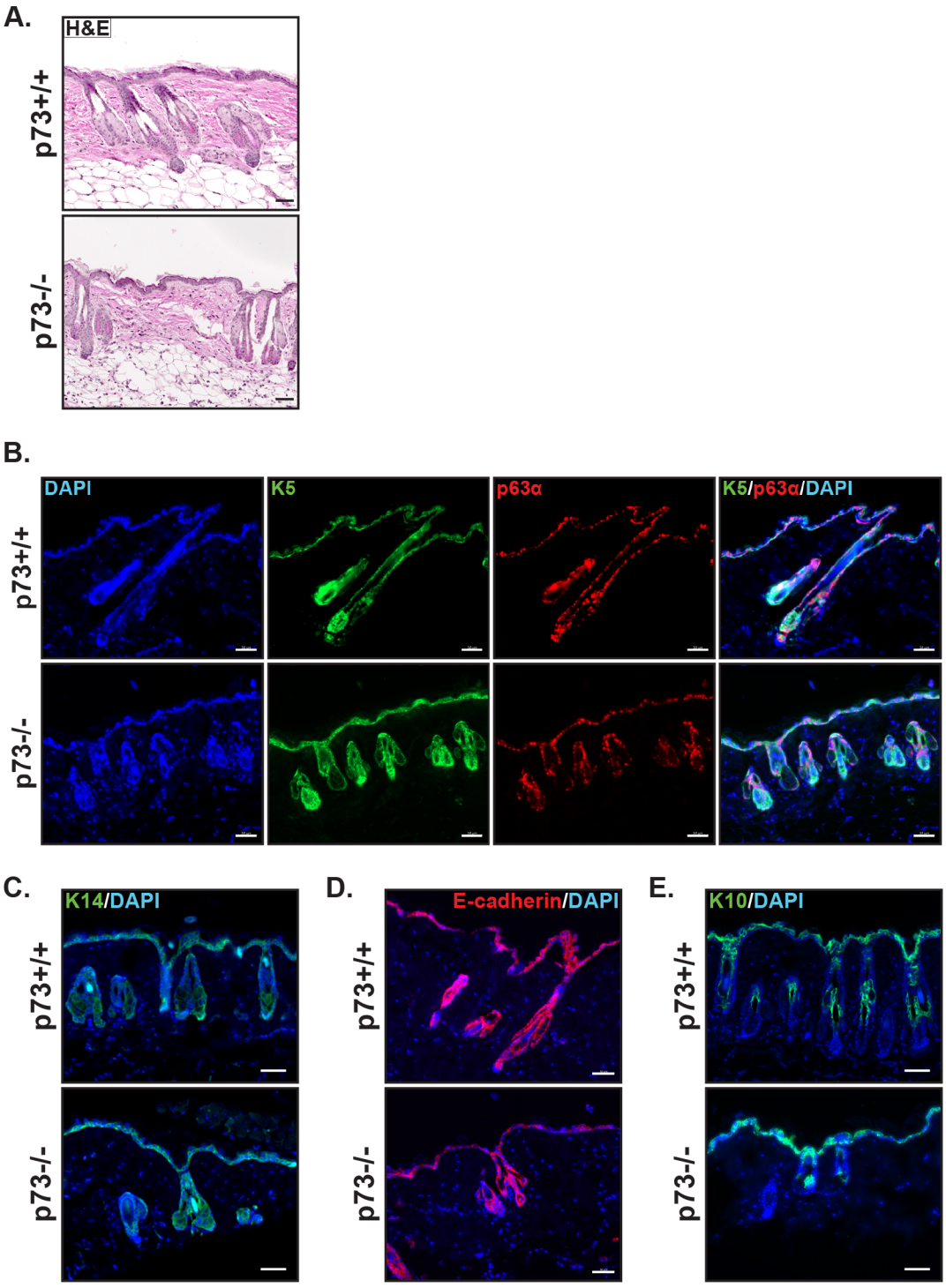

Figure 4.5. Expression Patterns of Epidermal Differentiation Markers in p73+/+ and p73-/- Murine Skin. (A) Representative H&E micrographs of p73+/+ (top) and p73-/- (bottom) murine skin. (B-E) Representative micrographs of IF staining in p73+/+ (top) and p73-/- (bottom) murine skin for DAPI (blue) and: (B) K5 (green) and p63α (red), (C) K14 (green), (D) E-cadherin (red), (E) K10 (green). All scale bars represent 50 μm. All data represented was collected by Clayton Marshall.

(p = 0.004) decreased in *p73*-/- mice compared with *p73*+/+ mice, with the largest difference (p = 0.0125) occurring on post-wound day 7 (Figure 4.6).

To gain insight to the molecular processes underlying the wound healing defect in *p73*-/- mice, we conducted IF and immunohistochemistry (IHC) staining on wounded skin sections from *p73*+/+ and *p73*-/- mice at post-wound days 3, 7, and 10. Semiquantitative scores of staining were generated by a pathologist using QuPath software (Bankhead et al., 2017) and reflect both the percentage of stained nuclei and staining intensity. In *p73*+/+ mice, p73 IF staining was increased in wounded compared to unwounded skin, and this difference was largest (p = 0.00007) at post-wound day 7 (Figure 4.7A). The increase of p73 expression after wounding was primarily due to increased expression in basal keratinocytes at the epidermal wound edge and in the newly-formed wound epidermis (Figure 4.7B). These periwound basal keratinocytes had a diffuse and continuous p73 expression pattern, in contrast with the intermittent p73 expression detected in basal keratinocytes of unwounded skin (Figures 4.7B). Adjacent normal (non-wounded) epidermis had less p73 IF staining than the epidermal wound edge (Figure 4.8) and overall had a similar staining pattern as unwounded skin (Figure 4.7B).

Timely wound healing is dependent on a rapid proliferation response by basal keratinocytes at the epidermal wound edge. We found that expression of Ki67, a marker of proliferation, was increased in the skin after wounding by IF for both genotypes (Figure 4.9A). The increase of Ki67

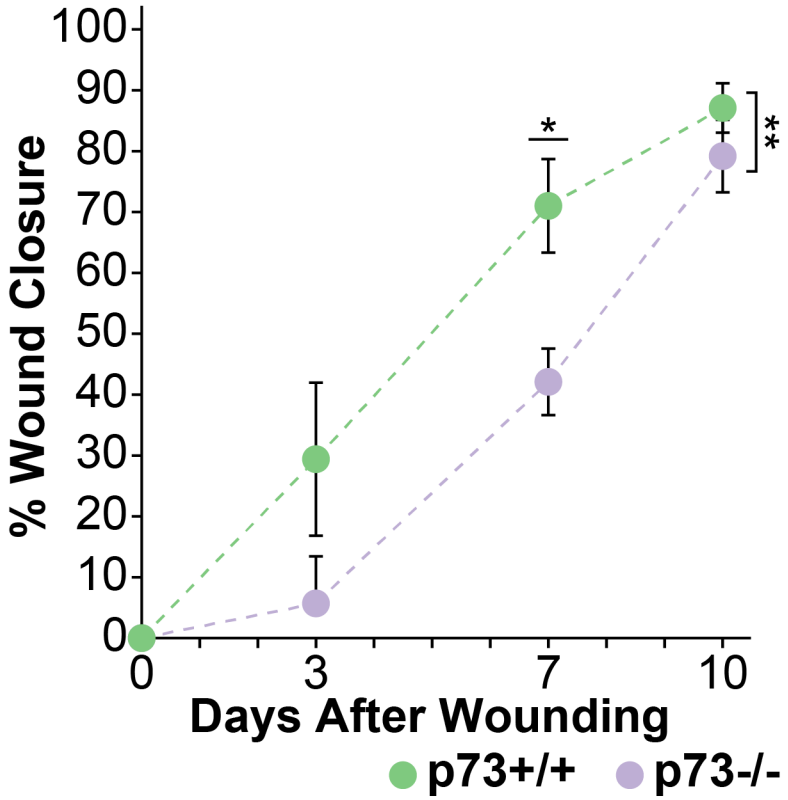

Figure 4.6. Wound Closure in p73+/+ and p73-/- Mice After Epidermal Wounding. Graph of percentage (%) wound closure relative to initial wound size in p73+/+ and p73-/- mice at 0, 3, 7, and 10 days after wounding. The mean area of eight wounds is shown with error bars representing SEM. *p-value < 0.05, **p-value < 0.01. All data represented was generated through collaboration with Clayton Marshall.

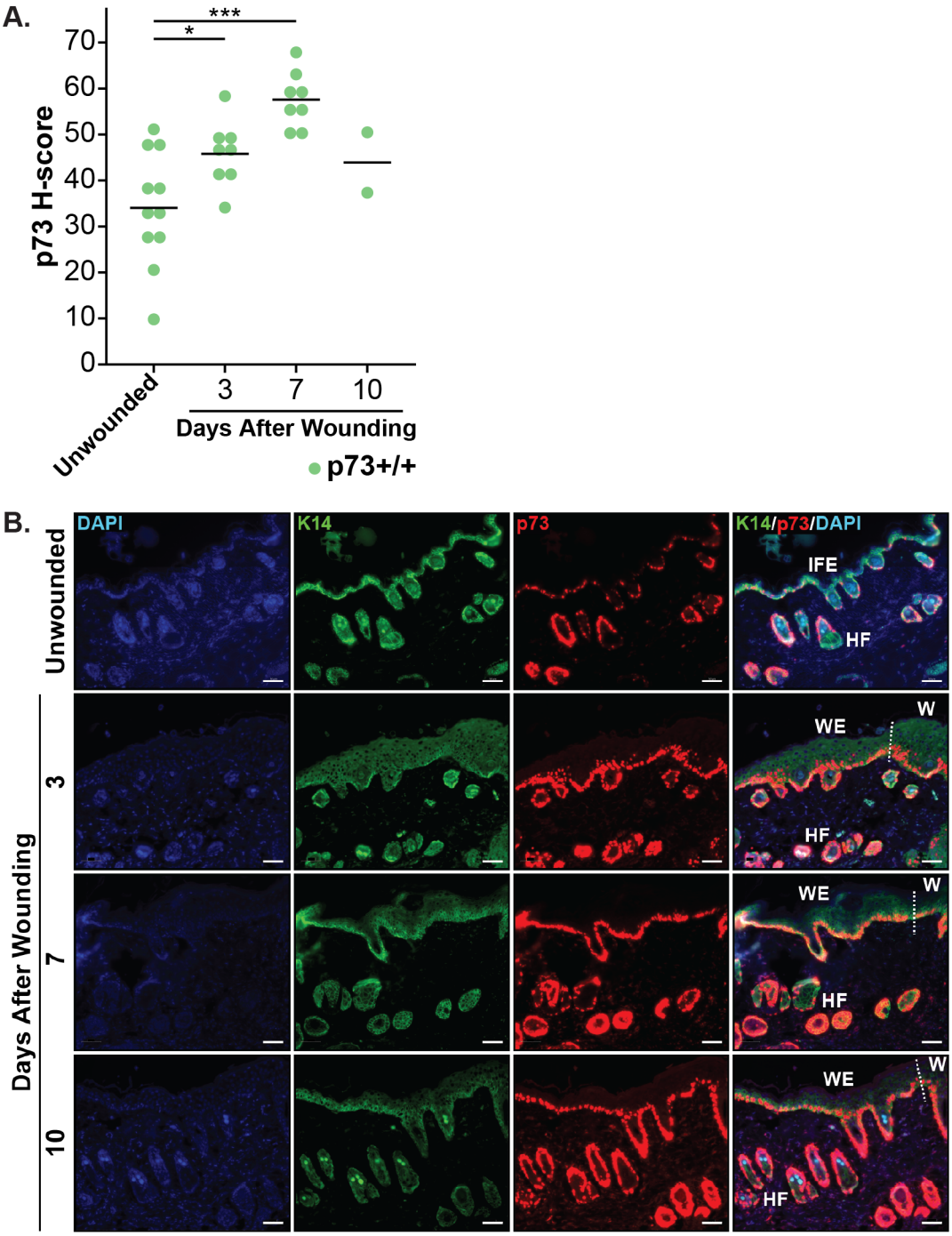

Figure 4.7. p73 Protein Expression and Localization in p73+/+ Skin After Epidermal Wounding. (A) Dot plot of p73 H-score in unwounded and wounded (days 3, 7, and 10) skin specimens from p73+/+ mice. *p-value < 0.05, ***p-value < 0.001. (B) Representative micrographs of IF staining for DAPI (blue), K14 (green), and p73 (red) in unwounded and wounded (days 3, 7, and 10) skin specimens from p73+/+ mice. All scale bars represent 50 μm. Regions of the skin are labeled as: IFE, HF, epidermal wound edge (WE), newly-formed wound epidermis (W), and adjacent normal epidermis (AN). The white dotted lines indicate the border between the WE and W or AN. All IF staining represented was collected by Clayton Marshall and quantified by Paula Gonzalez Ericsson.

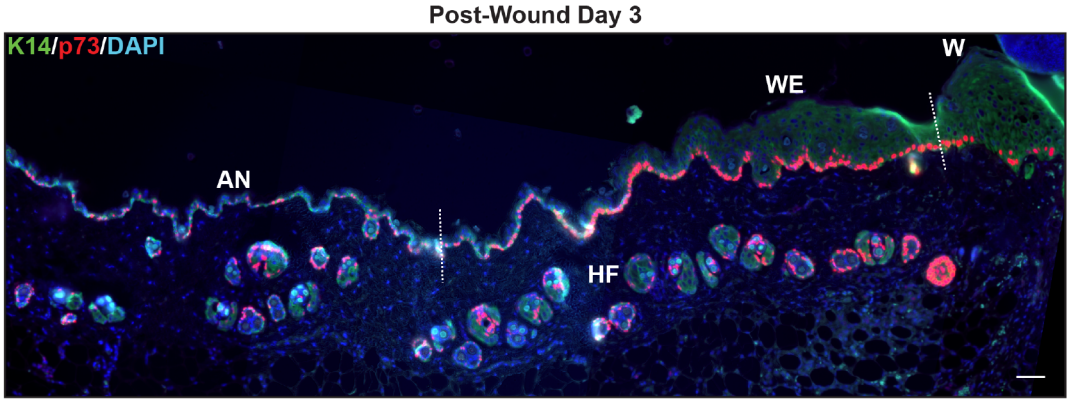

Figure 4.8. p73 Protein Expression and Localization in p73+/+ Wounded and Adjacent Normal Skin 3 Days After Epidermal Wounding. Representative micrograph (zoomed out view) of IF staining for DAPI (blue), K14 (green), and p73 (red) in a skin specimen from a p73+/+ mouse at post-wound day 3. The scale bars represent 50 μm. Regions of the skin are labeled as: IFE, HF, epidermal wound edge (WE), newly-formed wound epidermis (W), and adjacent normal epidermis (AN). The white dotted lines indicate the border between the WE and W or AN. All data represented was collected by Clayton Marshall.

expression in wounded skin was localized to the epidermal wound edge, adjacent HFs, and newly-formed wound epidermis (Figure 4.9B). At post-wound day 3, we detected a significant decrease ($p = 0.00003$) in the percentage of Ki67-positive cells in the skin of *p73*-/- compared to *p73*+/+ mice (Figures 4.9A and B), consistent with the observation that the largest difference in wound closure between the two genotypes occurred at post-wound day 7 (Figure 4.6). The reduction of Ki67 staining in *p73*-/- wounds at post-wound day 3 was primarily due to decreased staining in the basal keratinocytes at the epidermal wound edge and in the newly-formed wound epidermis, and, to a lesser extent, adjacent HFs (Figure 4.9B). We did not detect a difference in Ki67 expression between the unwounded skin of *p73*+/+ and *p73*-/- mice (Figures 4.9A and B).

Previous work has shown that DNA damage contributes to the decline in stem cell function in aged tissues (Oh et al., 2014) and that p73 regulates the response to DNA damage (Flores et al., 2002; Tomasini et al., 2008; Wilhelm et al., 2010). γH2AX is a marker of the DNA damage response and replication stress (Rogakou et al., 1998; Ward and Chen, 2001). In both *p73*+/+ and *p73*-/- mice, levels of γH2AX in the skin increased after wounding by IHC (Figures 4.10A and B). The increase of γH2AX staining was detected in the epidermal wound edge, adjacent HFs, and newly-formed wound epidermis (Figure 4.10B). We observed a significant increase ($p = 0.007$) of γH2AX levels in *p73*-/- versus *p73*+/+ wounds at post-wound day 10 (Figures 4.10A and B). Collectively, these

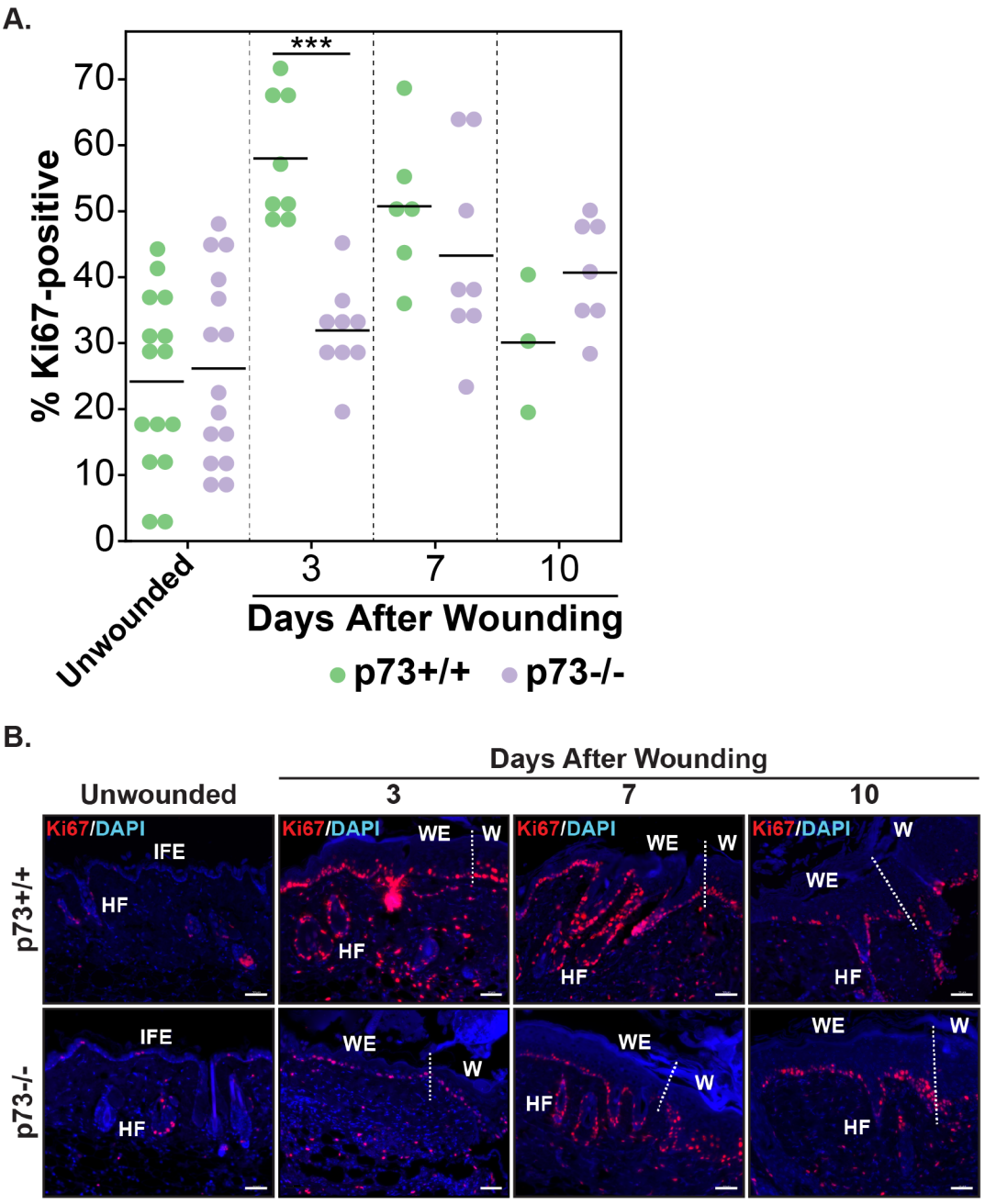

Figure 4.9. Ki67 Protein Expression and Localization in p73+/+ and p73-/- Skin After Epidermal Wounding. (A) Dot plot of the percentage (%) of Ki67-positive cells in unwounded and wounded (days 3, 7, and 10) skin specimens from p73+/+ and p73-/- mice. ***p-value < 0.001. (B) Representative micrographs of IF staining for DAPI (blue) and Ki67 (red) in unwounded and wounded (days 3, 7, and 10) skin specimens from p73+/+ and p73-/- mice. All scale bars represent 50 μm. Regions of the skin are labeled as: IFE, HF, epidermal wound edge (WE), and newly-formed wound epidermis (W). The dotted lines indicate the border between the WE and W. All IF staining represented was collected by Clayton Marshall and quantified by Paula Gonzalez Ericsson.

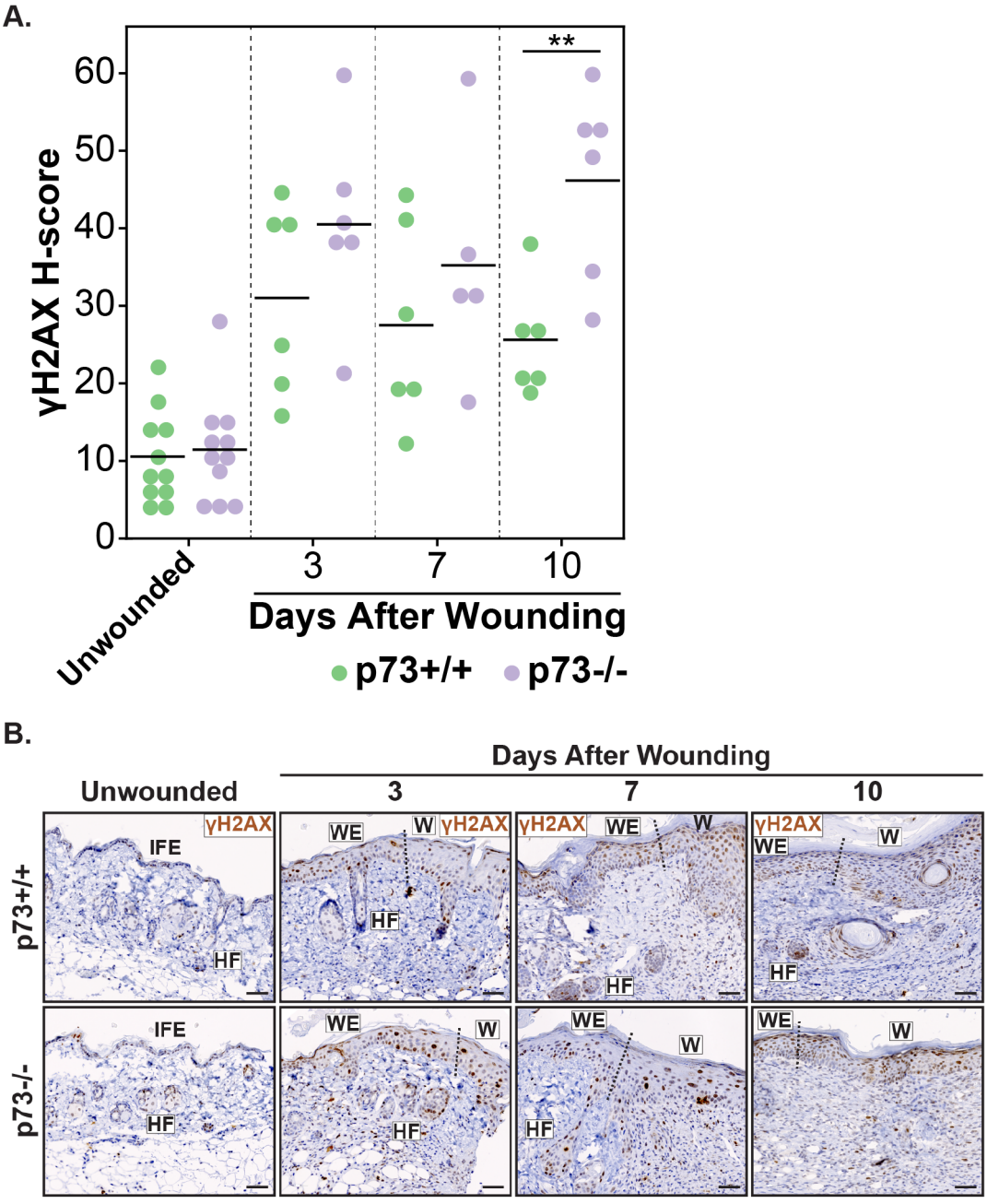

Figure 4.10. γH2AX Protein Expression and Localization in p73+/+ and p73-/- Skin After Epidermal Wounding. (A) Dot plot of γH2AX H-score in unwounded and wounded (days 3, 7, and 10) skin specimens from p73+/+ and p73-/- mice. **p-value < 0.01. (B) Representative micrographs of immunohistochemistry (IHC) staining for γH2AX in unwounded and wounded (days 3, 7, and 10) skin specimens from p73+/+ and p73-/- mice. All scale bars represent 50 μm. Regions of the skin are labeled as: IFE, HF, epidermal wound edge (WE), and newly-formed wound epidermis (W). The dotted lines indicate the border between the WE and W. All data represented was collected by Paula Gonzalez Ericsson.

data establish a role for p73 in epidermal wound healing, in part through regulation of proliferation and the DNA damage response in basal keratinocytes.

p73 is Expressed by Epidermal and Hair Follicle Stem Cells

Epidermal and HF stem cells regulate tissue homeostasis and wound healing in the skin (Ge and Fuchs, 2018). After epidermal injury, both epidermal and HF stem cells contribute to the wound-healing process by undergoing local migration and proliferation to ensure rapid repair of the epidermis and reestablishment of the skin barrier (Ito et al., 2005). Based on the observation that the expression pattern of p73 overlaps with regions of the skin where the stem cell populations reside (Figure 4.3A) and that *p73*-/- mice have delayed epidermal wound healing (Figure 4.6) due in part to decreased basal keratinocyte proliferation (Figure 4.9A), we determined p73 expression in epidermal and HF stem cells using transcriptomic data sets. We analyzed single-cell RNA-seq (scRNA-seq) data from 2,310 murine back skin cells (Tabula Muris Consortium et al., 2018) that were isolated by *Itga6* (skin epithelial integrin) and/or *Cd34* (bulge HF stem cell marker) expression using fluorescence-activated cell sorting (FACS). Cluster analysis was performed with Seurat (Butler et al., 2018) and identified seven distinct cell clusters. We visualized the data using uniform manifold approximation and projection (UMAP) (Becht et al., 2018), a nonlinear dimensionality reduction technique that preserves both local and

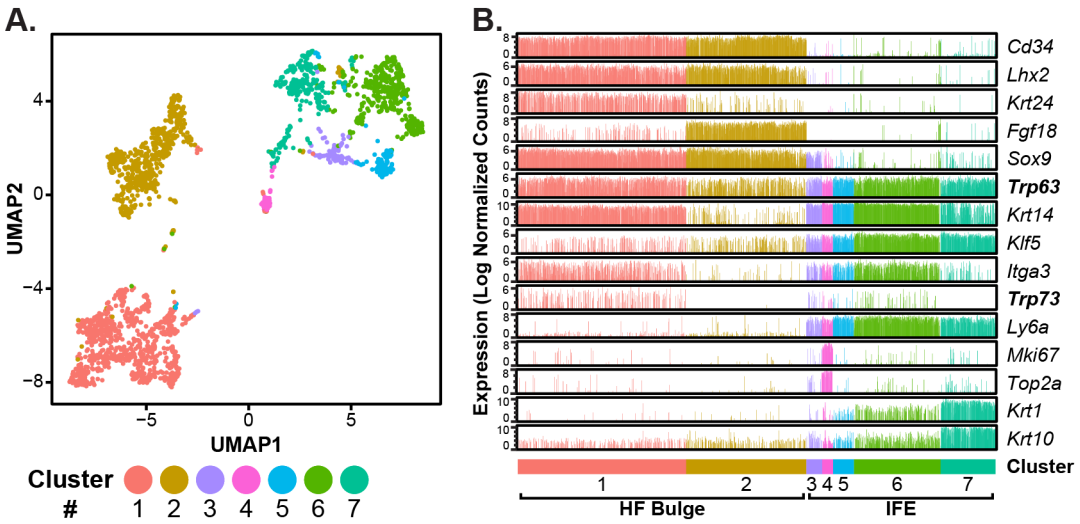

C.

#	Cell Type	n	p73+ p63- (%)	p73- p63+ (%)	p73+ p63+ (%)	p73- p63- (%)
1	Outer Bulge	812	1.6	67.7	22.8	7.9
2	Inner Bulge	577	0	65.7	0.2	34.1
3	Basal Stem IFE	75	2.7	78.7	14.7	4.0
4	Basal Proliferating IFE	52	0	75.0	19.2	5.8
5	Basal IFE	100	1.0	91.0	7.0	1.0
6	Basal IFE	417	1.0	83.2	10.8	5.0
7	Differentiating IFE	268	0	94.8	0	5.2

Figure 4.11. Analysis of p73 mRNA Expression in Individual Epidermal and Hair Follicle Keratinocytes. (A) UMAP (Uniform Manifold Approximation and Projection) plot of 2310 murine keratinocyte (back skin) single cell transcriptomes from the Tabula Muris dataset. Each dot represents an individual cell and is colored according to cluster membership. (B) Bar graphs of RNA expression for keratinocyte cell type markers from (A). Each bar represents one cell and is colored by cluster number from (A). (C) Table summarizing *Trp73* and *Trp63* expression and co-expression in single murine keratinocyte cells from (A) by cluster number. Each cluster number is annotated with: the primary cell type of the cluster (based on cell type marker expression), the number (n) of cells belonging to the cluster, and the percentage (%) of cells with each p73/p63 expression status.

global data structure (Figure 4.11A). Cells were separated along UMAP1 based on their region of origin within the skin, either HF bulge (Cd34+) or IFE (Ly6a+) (Figures 4.11A and B). HF bulge cells were divided into two clusters, one that expressed outer bulge markers (cluster #1, e.g. *Krt24*) and another that expressed inner bulge markers (cluster #2, e.g. *Fgf18*) (Figures 4.11A and B) (Joost et al., 2016). IFE cells were divided between five clusters (Figures 4.11A and B). Cluster #7 was distinguished by the expression of the differentiation markers *Krt1* and *Krt10* (Figure 4.11B). The remaining IFE clusters all expressed basal cell markers (e.g. *Krt14* and *Itga3*) (Figure 4.11B). Among these, cluster #3 was characterized by stem markers (e.g. *Sox9*) and cluster #4 by proliferation markers (e.g. *Mki67* and *Top2a*) (Figure 4.11B). Clusters #5 and #6 lacked distinguishing cell type markers (Figure 4.11B), but cluster #5 was unique in being the only cluster composed almost exclusively of cells from one stage (telogen) of the hair cycle.

We determined if each skin cell expressed *Trp73* and *Trp63* and summarized the results by cluster number (Figure 4.11C). Most (>85%) cells that expressed *Trp73* also expressed *Trp63* (Figure 4.11C). The percentage of cells with *Trp73* expression (p73+/p63- and p73+/p63+) was highest in the outer bulge cluster (Figure 4.11C), the stem cell compartment of the HF (Cotsarelis et al., 1990). *Trp73* was expressed by a subset of cells in all of the basal IFE clusters (Figure 4.11C), the stem cell compartment of the epidermis. The basal proliferating IFE cluster had the

second-highest percentage of cells that expressed *Trp73* (Figure 4.11C), consistent with a prior study that found increased expression of *Trp73* by non-label-retaining keratinocytes (i.e. those that divide more frequently) of the murine IFE (Sada et al., 2016). The inner bulge and differentiating IFE clusters did not express *Trp73* (Figure 4.11C). *Trp73* was expressed in a lower percentage of cells within each cluster than *Trp63* (Figure 4.11C), consistent with its lower expression levels in the tissue (Figure 4.1). *Trp63* was expressed by greater than 90% of cells in each cluster (p73-/p63+ and p73+/p63+) except for the inner bulge (Figure 4.11C).

Given that the outer bulge cluster had the highest percentage of cells that expressed p73 and p63 (Figure 4.11C), we decided to further study *Trp73* expression in defined HF stem cell populations. To do so, we analyzed an additional scRNA-seq dataset (Yang et al., 2017) that profiled diverse types of murine HF stem cells at different stages of the hair cycle. In telogen (quiescent stage), a large percentage of bulge HF stem cells and hair germ cells (56.4% and 59.2% respectively) expressed *Trp73* (Figure 4.12). During the transition from telogen to anagen I, hair germ cells are activated to proliferate (Greco et al., 2009); a large percentage of these cells (59.6%) retained expression of *Trp73* (Figure 4.12). As anagen proceeds, the hair germ gives rise to transit-amplifying cells, which are highly proliferative and go on to produce the hair shaft and inner root sheath (Hsu et al., 2014). *Trp73* expression was lower in transit-amplifying cells during anagen II and VI (29.1% and 22.4% respectively) (Figure 4.12).

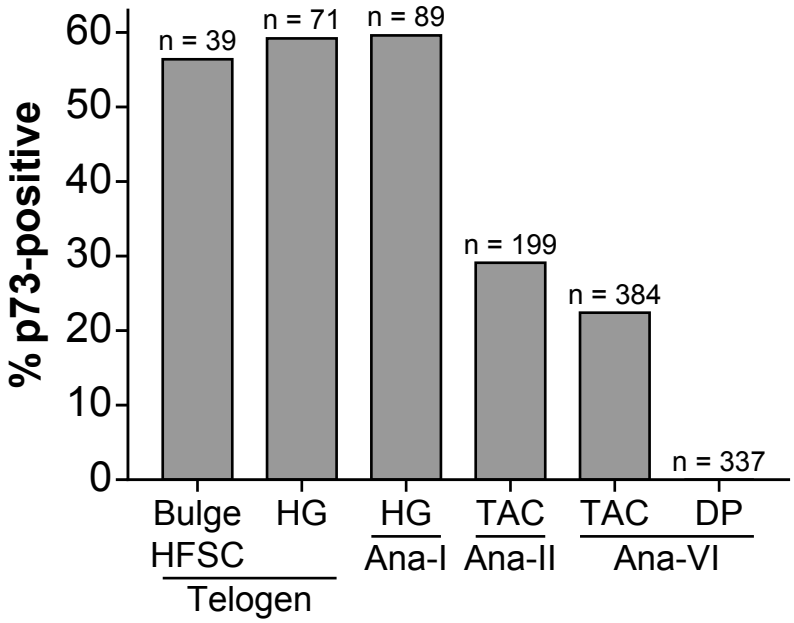

Figure 4.12. p73 mRNA Expression in Individual Hair Follicle Stem Cells. Bar graph of the percentage (%) of p73-positive cells in different classes of murine HF cells by single-cell RNA-seq (scRNA-seq). Hair cycle stages include: telogen, anagen I (Ana-I), anagen II (Ana-II), and anagen VI (Ana-VI). Cell types include: bulge HF stem cells (HFSC), hair germ (HG) cells, transit-amplifying cells (TAC), and dermal papilla (DP) cells. The number of cells analyzed for each cell type is listed above each bar.

Anagen VI dermal papilla cells (mesenchymal) did not express *Trp73*, as anticipated (Figure 4.12). These results indicate that *Trp73* is expressed in HF stem cell populations during different stages of the hair cycle under homeostatic conditions, particularly bulge HF stem cells and hair germ cells.

scRNA-seq produces data with more technical noise and biological variation than bulk RNA-seq (Chen et al., 2019). To validate the scRNA-seq results, we analyzed bulk RNA-seq data from murine bulge HF and epidermal stem cells isolated by FACS with marker-based sorting (*Itga6*, *Cd34*, and *Ly6a*) (Ge et al., 2017). Both bulge HF and epidermal stem cells expressed *Trp73* (Figure 4.13A), consistent with the scRNA-seq results (Figures 4.11C and 4.12). In order to assess *TP73* expression in human keratinocytes, we analyzed bulk RNA-seq data from primary human keratinocytes (HK) cultured and differentiated *in vitro* (Cavazza et al., 2016; Kouwenhoven et al., 2015). *TP73* was expressed by progenitor-enriched (isolated by rapid collagen IV adherence) and unenriched basal HKs, but not by HKs after 6 days of differentiation (Figure 4.13B), consistent with the p73 IF staining pattern observed in human skin (Figure 4.3A, top panel). These results collectively indicate that p73 is expressed by murine bulge HF and epidermal stem cells and basal HKs.

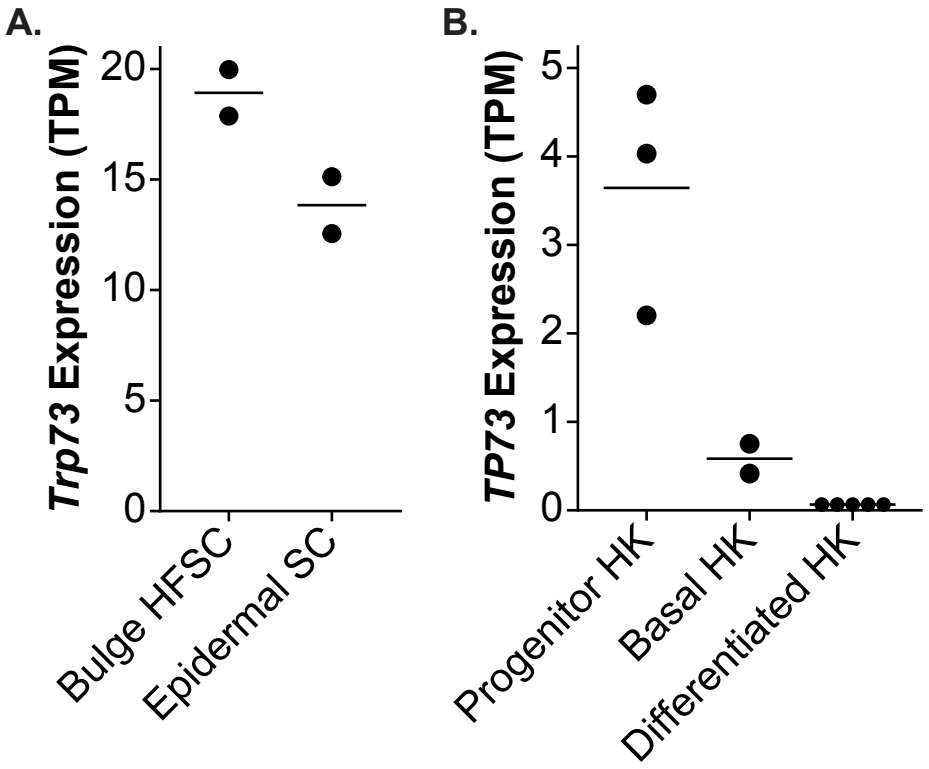

Figure 4.13. p73 mRNA Expression in Keratinocyte Populations. (A) Dot plot of *Trp73* expression (TPM) in murine bulge HF stem cells and epidermal stem cells (SC) by bulk RNA-seq. Cells were isolated by fluorescence-activated cell sorting (FACS) with marker-based sorting. Horizontal lines represent the mean. (B) Dot plot of *TP73* expression (TPM) in primary human keratinocytes (HK) grown and differentiated *in vitro* for 6 or 7 days. HKs were enriched for progenitors based on rapid collagen IV adherence. Horizontal lines represent the mean.

ΔNp73 Enhances p63-Mediated Expression of Keratinocyte Genes During Cellular Reprogramming of Human Dermal Fibroblasts to a Basal Keratinocyte-like State

Prior work has shown that p73 is required for effective generation of iPSCs with Yamanaka factors and that iPSCs lacking p73 have an attenuated epithelial phenotype (Martin-Lopez et al., 2017). To study the role of p73 in epidermal programming, we used an induced basal keratinocyte (iKC) model system first described by Chen and colleagues (Chen et al., 2014). In this system, skin lineage-specific transcription factors KLF4 and ΔNp63α are expressed in neonatal human dermal fibroblasts (HDFn) to generate iKCs. To recapitulate the system, we infected HDFn cells with lentiviruses encoding KLF4, ΔNp63α, KLF4 + ΔNp63α, or empty vector controls (Figure 4.14A). We grew the cells for 3 days after the initial infection and performed RNA-seq. Cells infected with KLF4 + ΔNp63α lentivirus had increased expression of basal keratinocyte genes (e.g. *KRT14*, *ITGA3*) and reduced expression of fibroblast genes (e.g. *MME*, *VIM*) compared to control infections (Figure 4.14B). Also, the differentially expressed genes (n = 755) between HDFn cells infected with KLF4 + ΔNp63α versus control lentivirus were enriched for several Genome Ontology (GO) categories related to basal keratinocytes, including cell-substrate junction, extracellular structure organization, epidermis development, and epithelial cell development (Figure 4.14C). Our iKC results were consistent with those described in the original iKC report

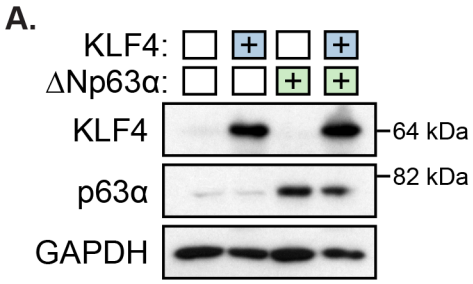

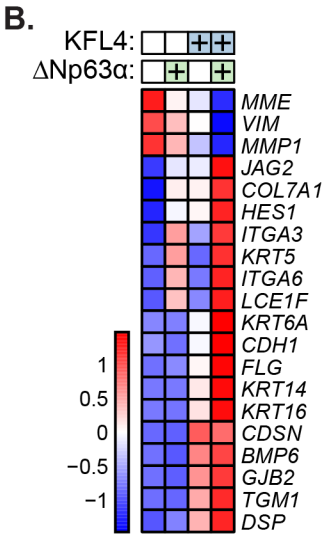

C.

Enriched GO Categories: KLF4 + ΔNp63α vs Control

#	Name	FDR
1	Proteinaceous extracellular matrix	6.4E-13
2	Cell-substrate junction	2.4E-11
3	Focal adhesion	1.5E-10
4	Cell-substrate adherens junction	1.9E-10
5	Extracellular matrix organization	3.5E-10
6	Extracellular structure organization	3.7E-10
7	Cell projection membrane	1.8E-07
8	Blood vessel morphogenesis	3.9E-07
9	Epidermis development	1.1E-06
10	Cell-cell adherens junction	1.4E-06
11	Actin cytoskeleton	1.8E-06
12	Cell junction organization	1.9E-06
13	Actin-based cell projection	4.0E-06
14	Ossification	6.4E-06
15	Epithelial cell development	7.4E-06
16	Cell adhesion molecule binding	8.3E-06
17	Cell leading edge	1.1E-05
18	Angiogenesis	1.5E-05
19	Epithelial cell proliferation	1.5E-05
20	Establishment of skin barrier	2.2E-05

Figure 4.14. Reproducing the Induced Keratinocyte (iKC) Model System. (A) Immunoblot of KLF4 and p63α protein expression in HDFn cells infected with lentivirus encoding KLF4, ΔNp63α, KLF4 + ΔNp63α, or empty vector control. Cells were grown for 3 days and protein was harvested for immunoblot analysis. (B) Heatmap of the expression of iKC-related genes in HDFn cells infected with lentivirus encoding KLF4, ΔNp63α, KLF4 + ΔNp63α, or empty vector control. Cells were grown for 3 days and RNA was harvested for RNA-seq analysis. (C) Table listing the top 20 enriched GO categories for genes differentially expressed between KLF4 + ΔNp63α and empty vector control infections from (B). Hailing Jin and Spencer Lea provided technical assistance in reproducing the iKC model system.

(Chen et al., 2014), indicating that we had a reliable model system in which to evaluate the role of ΔNp73 in induced basal keratinocyte programming.

We infected HDFn cells with lentivirus encoding ΔNp73 isoforms (ΔNp73α and ΔNp73β) or empty vector control in combination with KLF4 + ΔNp63α and performed immunoblot analysis to verify protein expression (Figure 4.15A). We evaluated ΔNp73 isoforms because they are the most highly expressed isoforms in human skin (Chapter III, Table 3.1) and have been shown to regulate the initiation phase (involving mesenchymal-to-epithelial transition) of reprogramming murine embryonic fibroblasts into iPSCs (Martin-Lopez et al., 2017). Three days after infection of the HDFn cells with ΔNp73-expressing lentivirus, we harvested cells, isolated RNA, and performed qRT-PCR for keratinocyte genes that are markers of the iKC state (*KRT14*, *KRT5*, *SFN*, and *FLG*) (Figure 4.15B). Co-expression of ΔNp73 isoforms with KLF4 + ΔNp63α led to increased expression of keratinocyte genes compared to KLF4 + ΔNp63α with empty vector control infections (Figure 4.15B). These results imply that ΔNp73 regulates the expression of keratinocyte genes in coordination with ΔNp63α and, in turn, conversion to the iKC state. For all four genes analyzed by qRT-PCR, we found that ΔNp73β induced higher levels of gene expression than ΔNp73α (Figure 4.15B). These results are consistent with published reports of ΔNp73β having greater transcriptional activity than ΔNp73α (Liu et al., 2004) and suggest that the role of ΔNp73 isoforms in the iKC model is due to transactivation of target gene expression.

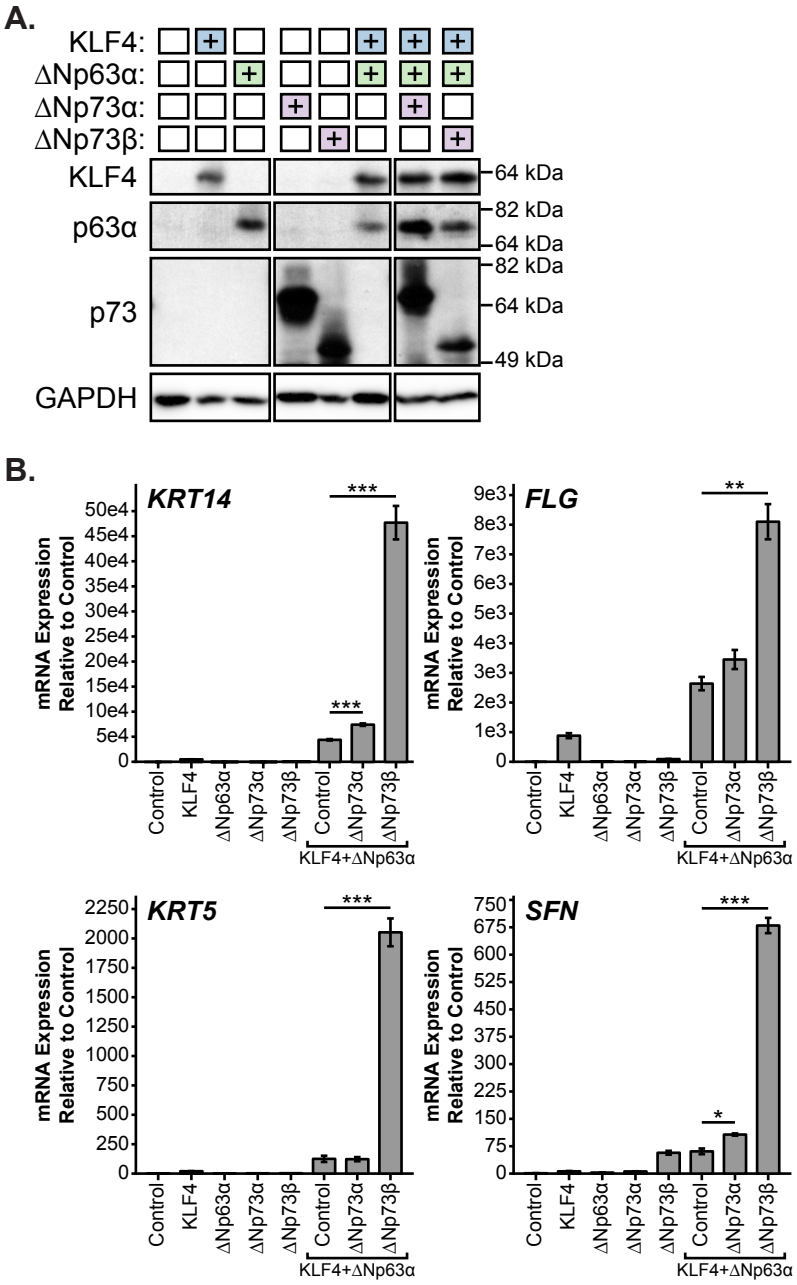

Figure 4.15. ΔNp73 Transcriptional Activity During iKC Reprogramming of Human Dermal Fibroblasts. (A) Immunoblot of KLF4, p63α, and p73 protein expression in HDFn cells infected with lentivirus encoding ΔNp73 isoforms (ΔNp73α and ΔNp73β) or empty vector control in combination with KLF4 and ΔNp63α. Cells were grown for 3 days and protein was harvested for immunoblot analysis. (B) Bar graphs of RNA expression for the indicated iKC marker genes in HDFn cells infected in (A). Cells were grown for 3 days and RNA was harvested for qRT-PCR analysis. Expression data are represented as the fold increase relative to control. The mean of three replicates is shown with error bars representing SEM. *p-value < 0.05, **p-value < 0.01, ***p-value < 0.001.

In order to identify additional ΔNp73-regulated genes in the iKC model system, we infected HDFn cells with lentivirus encoding ΔNp73β isoforms or empty vector control in combination with KLF4 + ΔNp63α. We used ΔNp73β because it was the strongest inducer of keratinocyte gene expression in our qRT-PCR experiments (Figure 4.15B). After 6 days, we isolated RNA from the cells and performed RNA-seq. Consistent with our qRT-PCR analysis (Figure 4.15B), infection of HDFn cells with ΔNp73β in combination with KLF4 + ΔNp63α led to increased expression of *KRT14*, *KRT5*, *FLG,* and *SFN* as compared to KLF4 + ΔNp63α with control or control alone. Also, combination infections with ΔNp73β led to increased expression of additional basal keratinocyte genes (e.g. *ITGA3*, *ITGB4*, *KRT6A*, *KRT16*, *COL7A1*, and *CDH1*) and decreased expression of fibroblast genes (e.g. *VIM*, *MME*, and *MMP1*). We performed principal component analysis (PCA) on the RNA-seq data and the samples appeared to be ordered by degree of conversion to the iKC state along PC1, which was responsible for the majority (88%) of the variance in the data (Figure 4.16A). To further investigate, we determined the top 250 genes contributing to PC1 and plotted their expression in a heatmap (Figure 4.16B). We identified two main sets of PC1 genes (Figure 4.16B). The larger subset of genes increased in expression along PC1 and included many basal keratinocyte-related genes (Figure 4.16B). The smaller subset of genes decreased in expression along PC1 and included many fibroblast-related genes (Figure 4.16B). These data suggest that the

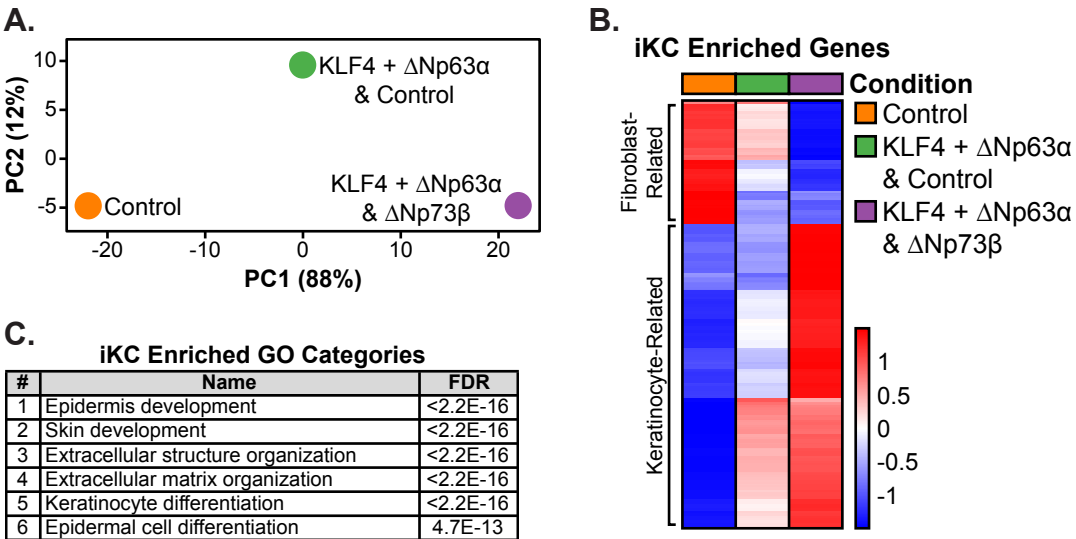

C.

iKC Enriched GO Categories

#	Name	FDR
1	Epidermis development	<2.2E-16
2	Skin development	<2.2E-16
3	Extracellular structure organization	<2.2E-16
4	Extracellular matrix organization	<2.2E-16
5	Keratinocyte differentiation	<2.2E-16
6	Epidermal cell differentiation	4.7E-13
7	Cornification	6.2E-12
8	Cell adhesion molecule binding	5.8E-11
9	Extracellular matrix	8.8E-11
10	Cornified envelope	1.1E-10
11	Keratinization	1.4E-10
12	Collagen-containing extracellular matrix	1.5E-09
13	Extracellular matrix structural constituent	2.8E-09
14	Cell-cell junction	2.5E-07
15	Extracellular matrix component	1.3E-06
16	Hemidesmosome assembly	3.2E-06
17	Cell-cell adherens junction	4.7E-06
18	Epithelial cell proliferation	1.7E-05
19	Integrin complex	3.0E-05
20	Cell junction organization	3.0E-05

D.

iKC Enriched Pathways

#	Name	FDR
1	Reactome: Formation of cornified envelope	6.7E-12
2	Extracellular matrix organization	2.5E-09
3	Keratinization	3.3E-08
4	Assembly of collagen fibrils	3.3E-08
5	Cell junction organization	2.8E-07
6	Type I hemidesmosome assembly	1.1E-06
7	Integrin cell surface interactions	1.0E-05
8	Cell-Cell communication	1.2E-05
9	Collagen degradation	6.6E-05
10	Epithelial mesenchymal transition	1.2E-04

Figure 4.16. ΔNp73-Regulated Genes and Pathways During iKC Reprogramming. (A) Principal component analysis (PCA) plot of RNA-seq from HDFn cells infected with lentivirus encoding ΔNp73β or empty vector control in combination with KLF4 and ΔNp63 α. Cells were grown for 6 days and RNA was harvested for RNA-seq analysis. The percentage (%) of variance contributed by each PC is listed in parentheses. (B) Heatmap of the expression of the top 250 genes contributing to PC1 from (A). (C and D) Tables listing the enriched Genome Ontology (GO) categories and pathways among the top 250 genes contributing to PC1 from (A).

top 250 genes contributing to PC1 largely recapitulate the core genes involved in reprogramming to the iKC state and that ΔNp73β enhances this reprogramming process.

To determine gene sets associated with reprogramming HDFn cells to the iKC state, we performed enrichment analysis on the top 250 PC1 genes using WebGestalt (Wang et al., 2017). The top 20 enriched Genome Ontology (GO) categories included many related to keratinocytes, including epidermis development, skin development, extracellular structure organization, cornification, cell adhesion molecule-binding, and cell-cell junction (Figure 4.16C). Also, the top ten enriched pathways in WebGestalt contained many related to keratinocytes, including formation of the cornified envelope, extracellular matrix organization, keratinization, and cell junction organization (Figure 4.16D). To investigate the genes underlying the enriched GO categories in Figure 4.16C, we determined which of the top 250 PC1 genes were annotated with GO categories related to skin development, cell junctions, cornification, and proliferation. We identified a set of 44 genes involved in these biological processes that underlie most of the observed GO category enrichment (Figure 4.17). Of interest, we found that ΔNp73β increased the expression of 18 genes with known roles in cellular proliferation (Figure 4.17), including *MKI67* and *TOP2A*, which is consistent with our data showing that *p73*-/- wounds have reduced proliferation (Figure 4.9A) and that basal proliferating cells have the highest percentage of p73 expression among IFE clusters (Figure 4.11C). Given

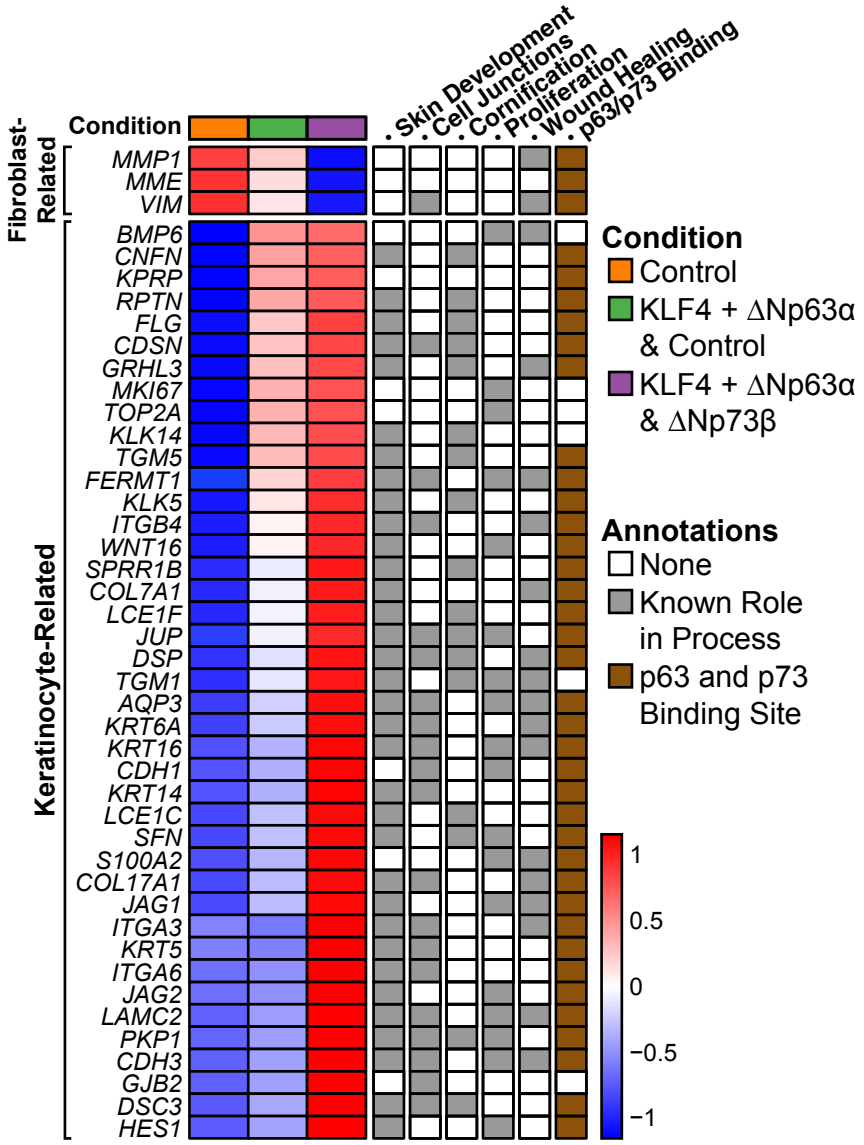

Figure 4.17. Core Set of 44 ΔNp73-Regulated and Skin-Associated Genes During iKC Reprogramming. Heatmap with the expression of a set of 44 genes that underlie the enrichment of GO categories observed in Figure 4.16C. Genes are annotated based on known roles in iKC-related processes (gray box) and the presence of a p63/p73 ChIP-seq peak within 50 kb of its TSS in multiple basal cell types (brown box).

the observed delay in wound healing in *p73*-/- mice (Figure 4.6), we assessed if any of the core set of 44 genes had known roles in wound healing. We found that 18 of these genes have roles in wound healing, including *ITGA3* (Reynolds et al., 2008), *ITGB4* (Liu et al., 2010; Turcan et al., 2016), *KRT6A* (Wojcik et al., 2000), *KRT16* (Lessard et al., 2013; Patel et al., 2006), *COL7A1* (Nyström et al., 2013), *S100A2* (Pan et al., 2018), *AQP3* (Hara-Chikuma and Verkman, 2008), *TGM1* (Inada et al., 2000), *FERMT1* (Jobard et al., 2003; Siegel et al., 2003), and *GRHL3* (Caddy et al., 2010) (Figure 4.17).

To determine if p73 binds near the transcriptional start site (TSS) of any of the 44 genes involved in reprogramming to the iKC state, we analyzed p73- and p63-binding in ChIP-seq datasets from three basal cell models: HK [primary human keratinocytes; (Kouwenhoven et al., 2015)], HaCaT [immortalized keratinocyte; newly generated herein], and HCC1806 [tumor-derived basal breast epithelial cells; newly generated herein and (Santos Guasch et al., 2018)]. As part of our analyses, we leveraged previous findings that endogenous p73 and p63 have similar genomic-binding profiles when co-expressed (Yang et al., 2010) and that heterotetramers of p73 and p63 are more thermodynamically stable than either homotetramer (Gebel et al., 2016). We also validated the previous finding by Yang and colleagues (Yang et al., 2010) using our own HCC1806 p73 and p63 ChIP-seq data (Figure 4.18). Genes displayed in

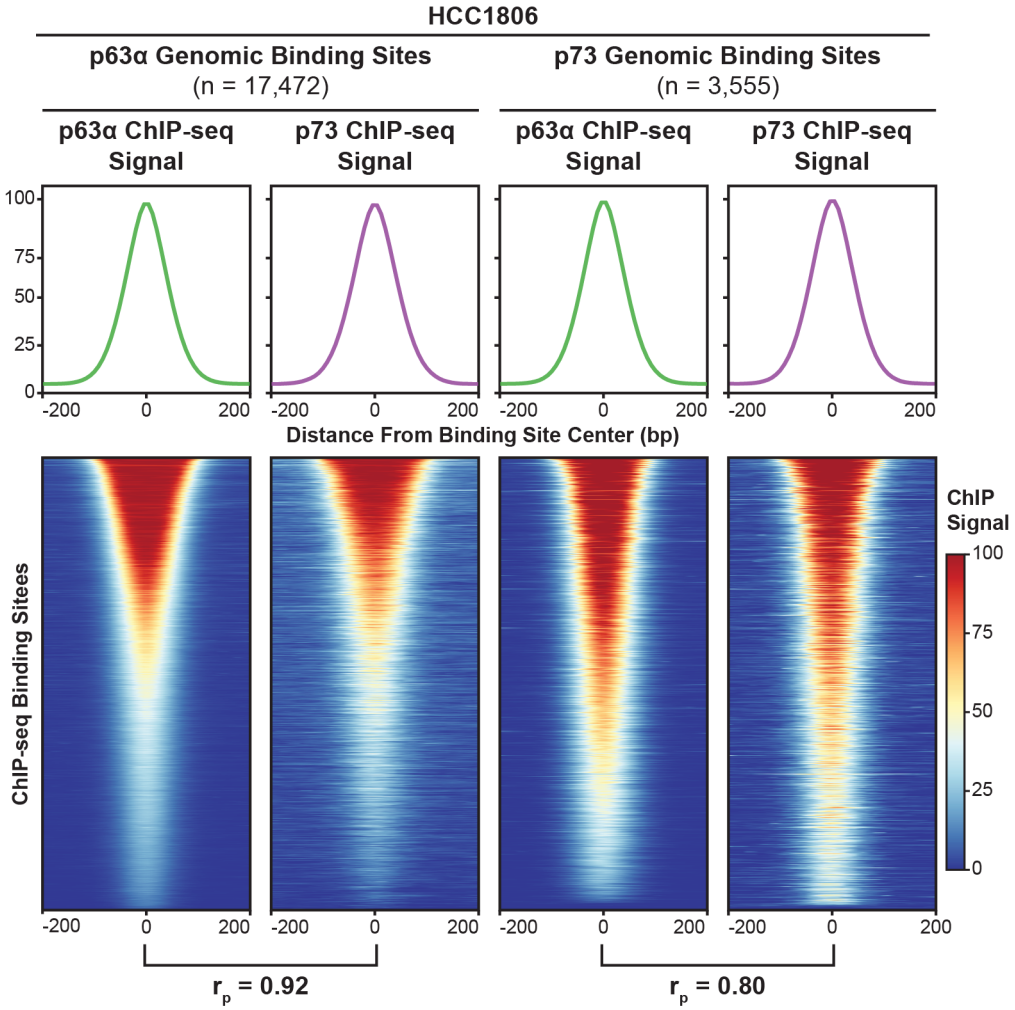

Figure 4.18. Analysis of p73 and p63α Genomic Binding Profiles in HCC1806 Cells. Profile plots (top panel) and heatmaps (bottom panel) of p63α and p73 ChIP-seq signal in HCC1806 cells at p63α (left) and p73 (right) genomic binding sites. Correlation between p63α and p73 ChIP-seq signal was quantified using Pearson's correlation coefficient (r_p). All data represented was generated through collaboration with Clayton Marshall.

Figure 4.17 were annotated as having a p63/p73 ChIP-seq peak if they met the following criteria: (1) had a p63/p73 ChIP-seq peak that overlapped in two out of the three cell types analyzed; and (2) the overlapping peak was located within 50 kb of the TSS of the gene and contained a canonical p63/p73 DNA binding motif. From the set of 44 genes involved in the iKC state, we found that 38 met our criteria for having a p63/p73-binding site (Figure 4.17). Of immediate interest were 13 of these keratinocyte-related genes with known roles in wound healing (Figure 4.17). Collectively, these findings support the conclusion that ΔNp73, in coordination with ΔNp63, acts as a regulator of the iKC state through direct and indirect regulation of key genes involved in skin development, cell junctions, cornification, proliferation, and wound healing.

ΔNp73 Enhances p63-Mediated Expression of Keratinocyte Genes During Induced Keratinocyte Reprogramming of Mesenchymal Breast Cancer Cells

To rule out a cell-type specific phenotype and determine if ΔNp73 could increase the expression of iKC marker genes in non-primary cells, we infected MDA-MB-231 cells (mesenchymal triple-negative breast cancer cell line) with lentivirus encoding ΔNp73 (ΔNp73α and ΔNp73β) or empty vector control in combination with KLF4 + ΔNp63α (Figure 4.19A). After 4 days we harvested cells, isolated RNA, and performed qRT-PCR for keratinocyte genes (*KRT14*, *KRT5*, *FLG,* and *SFN*) that were regulated in a

p73-dependent manner in HDFn cells. Expression of ΔNp73 isoforms in combination with KLF4 + ΔNp63α had a similar effect in MDA-MB-231 cells (Figure 4.19B) as it did in HDFn cells (Figure 4.15B). ΔNp73 isoforms increased the expression of *KRT14*, *KRT5*, *FLG,* and *SFN*; for all four of these genes, ΔNp73β induced higher levels of expression than ΔNp73α (Figure 4.19B). These results indicate that ΔNp73 isoforms can regulate the expression of iKC marker genes in coordination with ΔNp63α in cell types from different tissues of origin as well as both primary and transformed cell states.

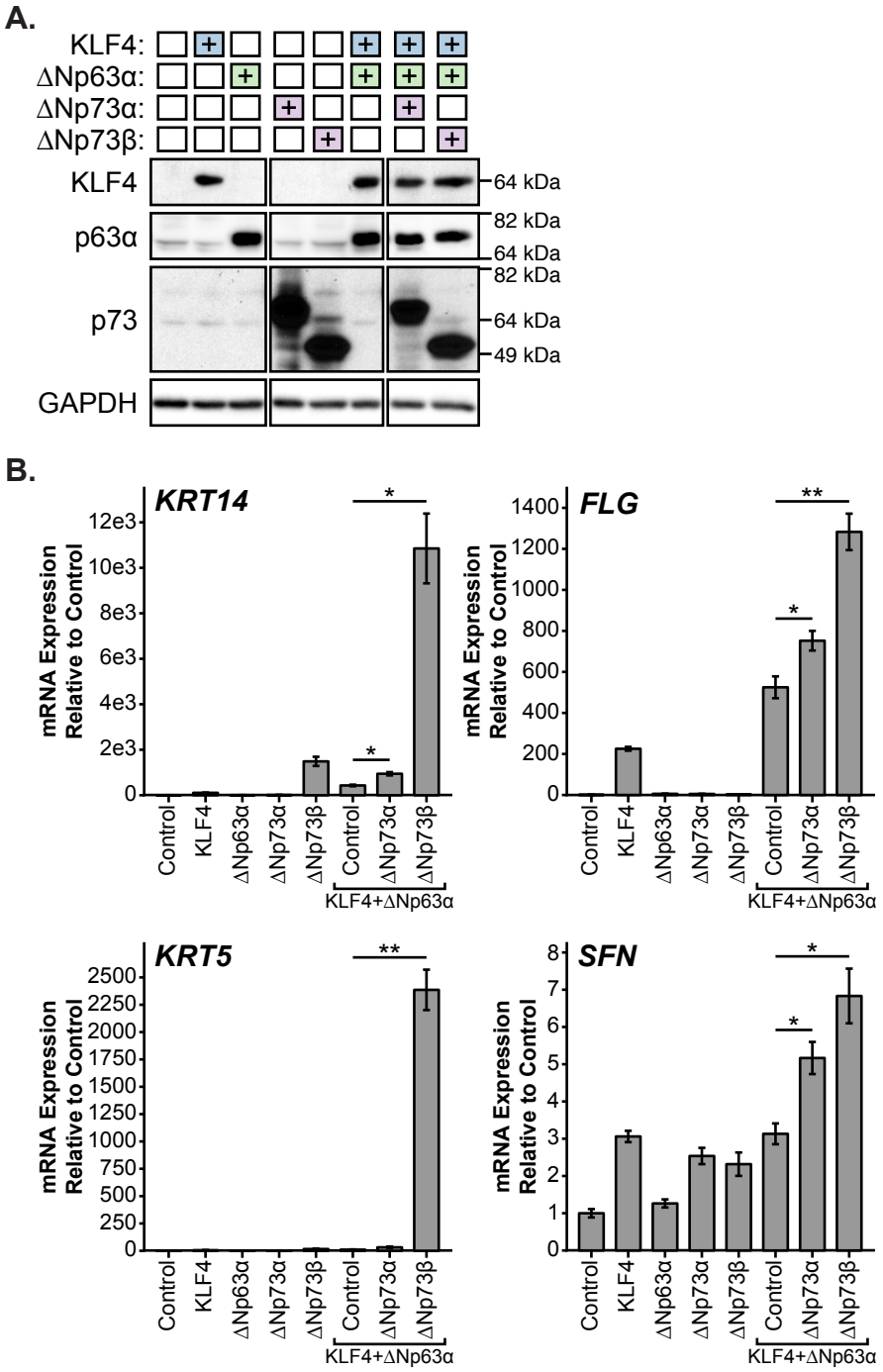

Figure 4.19. ΔNp73 Transcriptional Activity During iKC Reprogramming of Mesenchymal Breast Cancer Cells. (A) Immunoblot of KLF4, p63α, and p73 protein expression in MDA-MB-231 cells infected with lentivirus encoding ΔNp73 isoforms (ΔNp73 α and ΔNp73β) or empty vector control in combination with KLF4 and ΔNp63α. Cells were grown for 4 days and protein was harvested for immunoblot analysis. (B) Bar graphs of RNA expression for the indicated iKC marker genes in MDA-MB-231 cells infected in (A). Cells were grown for 4 days and RNA was harvested for qRT-PCR analysis. Expression data are represented as the fold increase relative to control. The mean of three replicates is shown with error bars representing SEM. *p-value < 0.05, **p-value < 0.01.

Conclusion

We discovered that p73 is required for timely cutaneous wound healing in mice. *p73*-/- mice exhibited delayed wound healing, due in part to decreased proliferation and increased activation of the DNA damage response in basal keratinocytes at the epidermal wound edge. In wild-type mice, this same cell population exhibited increased p73 expression after wounding. Further, we found that p73 was expressed by epidermal and HF stem cells, which regulate wound healing (Ge and Fuchs, 2018). Using a model system for reprogramming fibroblasts to keratinocyte-like cells, we found that ΔNp73, in conjunction with ΔNp63, regulates the expression of keratinocyte genes and conversion to a keratinocyte-like state. We identified a core set of 44 genes directly or indirectly regulated by ΔNp73 that are involved in skin development, cell junctions, cornification, proliferation, and wound healing.

Our study provides insight to the role of p73 in basal keratinocytes and the skin overall and highlights the importance of studying the functional interplay of p73 and p63. Our results provide a mechanism for the wound healing phenotype observed in *p73*-/- mice and build on observations from previous studies linking ΔNp73 to stem cell activity in the basal cells of the (Lin et al., 2012; Martin-Lopez et al., 2017) trachea (Marshall et al., 2016), iPSCs (Lin et al., 2012; Martin-Lopez et al., 2017), neural stem cells (Talos et al., 2010), and cancer stem cells (Meier et al., 2016). We propose a model in which ΔNp73 is required for effective function of adult skin stem

cells after stress, through coordinate regulation with ΔNp63 of a progenitor cell transcriptional program.

CHAPTER V

CONCLUSIONS AND FUTURE DIRECTIONS

Introduction

The work presented within this dissertation was carried out with the goal of expanding our knowledge of the biological roles of p73 in basal epithelial cells, the stem cell population of many tissues. The primary impetus for the work was a discovery made during our prior study linking p73 to multiciliogenesis (Marshall et al., 2016), namely, that p73 is expressed by basal epithelial cells in the murine trachea and that tracheas from *p73*-/- mice exhibit a 35% reduction in the number of basal epithelial cells number despite a loss of multiciliated cells, the most common cell type in the tissue. These data imply that basal cell maintenance and differentiation are regulated by loss of p73. Findings from previous studies support this implication: (1) p73 is expressed by basal epithelial cells in many tissue types (Puig et al., 2003); and (2) p73 regulates stem cell maintenance and/or activity in a variety of biological contexts (Agostini et al., 2010; Alexandrova et al., 2013; Gonzalez-Cano et al., 2010; Lin et al., 2012; Martin-Lopez et al., 2017; Rufini et al., 2012; Talos et al., 2010), including basal epidermal stem cells (Sada et al., 2016). With these findings in mind, we decided to focus on the basal epithelial cells in the skin.

Determining which p73 isoforms are expressed in a given cell or tissue model is an important step in deciphering the functional roles of p73 in the model because the proteins encoded by different p73 isoforms have distinct biological properties (Nemajerova et al., 2016; Romano et al., 2012; Su et al., 2009; Wilhelm et al., 2010). In Chapter III, I presented our methodology to quantify p73 isoform expression, through analysis of exon junction-spanning reads corresponding to alternative promoter usage and splicing isoforms, and used it to analyze the largest publicly available RNA-seq dataset of human tissue. In the skin, we determined that ΔNp73 is the predominantly expressed isoform.

In Chapter IV, I described the findings from a series of experiments designed to evaluate the role of p73 in basal keratinocyte function. We showed that p73-deficient mice exhibit delayed wound healing despite morphologically normal-appearing skin. The delay in wound healing was accompanied by decreased proliferation in basal keratinocytes at the epidermal wound edge. In wild-type mice, this same cell population exhibited increased p73 expression after wounding. Through analysis of transcriptomic data, we found that p73 was expressed by epidermal and hair follicle stem cells, cell types required for wound healing. Moreover, using a model to reprogram fibroblasts into keratinocyte-like cells (iKC), we discovered that ΔNp73 regulates the expression of a gene network involved in wound healing, proliferation, and skin development. Collectively, our data establish a role for p73 in cutaneous wound healing, in part

through regulation of genes with roles in timely wound healing and proliferation. In the remainder of this Chapter, I discuss questions that arise from our findings and describe hypotheses that can be experimentally tested to further our understanding of the roles and regulation of p73 in basal keratinocytes and, more broadly, in basal epithelial cells.

p73 and Stem Cells

Adult tissue stem cells have an important role in tissue maintenance and regeneration after injury (Ermolaeva et al., 2018). The stem cell function of these long-lived cells decreases with age due to the accumulation of cellular damage and contributes to the declining functional capacities observed in aging tissues (Ermolaeva et al., 2018). The delayed healing, reduced proliferation, and increased levels of the DNA damage response observed in the epidermal wounds of *p73*-/- mice implies that p73 regulates the activity of adult skin stem cells after injury. While we did not detect an overt difference in the morphology or the expression pattern of epidermal differentiation markers in the skin of adult *p73*-/- mice, we cannot rule out that p73 also regulates adult skin stem cells during homeostasis, which in turn could impact the functional abilities of these cells after injury. A role for p73 in the regulation of adult stem cells is consistent with previous studies showing that p73 regulates neural stem cell maintenance (Agostini et al., 2010; Talos et al., 2010) and protects against aging through regulation of cellular metabolism and the oxidative stress response (Du et

al., 2013; Marini et al., 2018; Rufini et al., 2012). Additional studies utilizing alternate wounding (e.g. partial-thickness wounding) and genetic (e.g. p73 isoform-specific knockout mice) models will be needed to further explore the roles of p73 in adult skin stem cells. Questions still unanswered include: (1) What roles does p73 play in epidermal and HF stem cells after injury and how do they differ between the cell types?; (2) What is the relative contribution of p73 isoforms to the wound healing phenotypes observed in *p73*-/- mice?; (3) Does p73 have any roles in stem cell maintenance in the skin, similar to p63 (Su et al., 2009; Yang et al., 1999)?; and (4) What role, if any, does p73 have regulation of the immune system response during wound healing? Based on the increased p73 staining at post-wound day 3 in the newly-formed wound epidermis, a time point at which basal keratinocytes are migrating into the wound to close the gap, and recent work demonstrating that p73 regulates migration(Fernandez-Alonso et al., 2015; Santos Guasch et al., 2018), we hypothesize that p73 also regulates the migration of keratinocytes during epithelialization.

Interplay of p73 and p63

Through analysis of single cell expression in the skin (IF and scRNA-seq), we observed that nearly all p73-positive basal keratinocytes co-expressed p63. Since p73 and p63 can hetero-oligomerize (Davison et al., 1999; Gebel et al., 2016), it is difficult to properly study the function of p73 in these cells without also taking into account p63. Moving forward, it is

important to characterize p73 and p63 isoform expression at the cellular level in order to better understand the interplay between these family members and how they vary between individual cells. Our ability to study p73 isoform expression in the single-cell analyses was limited by the low number of exon-exon spanning reads from the 5' end of mRNA transcripts in current scRNA-seq data sets and the lack of p73 isoform-specific antibodies. From our analysis of GTEx data, we determined that ΔNp73 is the most highly expressed N-terminal isoform (both α and β) in adult human skin during homeostasis. Further studies are needed to determine if p73 isoform expression patterns vary amongst cell types in the skin (e.g. epidermal versus HF stem cells) and if ΔNp73 is the predominantly expressed isoform in basal cells across tissue types. If the latter is confirmed, it is tempting to posit that p73 isoform switching might be involved in signaling tracheal basal cells (ΔNp73+) to differentiate into multiciliated cells (TAp73+) (Marshall et al., 2016).

In our experiments reprogramming fibroblasts into keratinocyte-like cells, we discovered that ΔNp73 isoforms, in particular ΔNp73β, significantly enhanced the expression of keratinocyte genes (e.g. *KRT14*, *KRT5*) and conversion to a keratinocyte-like state. Rather than causing gene expression changes in unique genes like KLF4, ΔNp73 largely amplified the magnitude of ΔNp63-induced gene expression, suggesting that ΔNp73 and ΔNp63 have similar transcriptional activity in this context. We observed similar results in reprogramming MDA-MB-231 cells,

suggesting that this phenotype is not cell-type specific. Similarly, while validating the iKC model, we found that KLF4 significantly enhanced the expression of genes that were differentially expressed in ΔNp63-only conditions. Going forward, it will be important to determine how interplay between KLF4, ΔNp63, and ΔNp73 affects target gene regulation, as all three transcription factors are co-expressed by basal keratinocytes, and how ΔNp73 has such large effects on target gene expression in the iKC model system. Among the top ΔNp73-regulated genes, we identified an enrichment for genes involved in proliferation and wound healing; this knowledge may be useful in studying the mechanisms underlying the wound healing defect in *p73*-/- mice. Additional studies will be required to determine which of the ΔNp73-regulated genes are novel direct target genes in basal keratinocytes, as our analysis was limited to identifying genes that contained overlapping p63/p73 genomic-binding sites within 50 kb of the TSS in multiple basal cell types. In future studies, it will be important to determine the role of TAp73 isoforms in the iKC model system and the skin more broadly, since these isoforms are generally more transcriptionally active, expressed in human skin, and deleted along with ΔNp73 isoforms in our *p73*-/- mice with the wound healing defect. Our reprogramming studies are limited by their *in vitro* nature and reliance on ectopic overexpression of lineage-specific transcription factors; nevertheless, the results are of significant value since they provide insight

to the interplay between p73 and p63 in driving a keratinocyte-like transcriptional program.

Ankyloblepharon-ectodermal defects-cleft lip/palate (AEC) syndrome, a rare ectodermal dysplasia caused by heterozygous mutations in the C-terminus of *TP63*, is distinguished from other human *TP63*-associated disorders by the occurrence of severe skin erosions, especially those of the scalp (Julapalli et al., 2009; McGrath et al., 2001). A recent study determined that this unique symptom is due to the increased propensity of AEC-mutant p63 protein to aggregate intracellularly (Russo et al., 2018). Interestingly, the authors found that AEC-mutant p63 bound to and coaggregated with p73, likely inhibiting its transcriptional activity. The overlapping functions between ΔNp73 and ΔNp63 in our studies with the iKC model system provide a potential explanation for the severe skin phenotype observed in patients with AEC syndrome. Namely, the skin erosions are more severe in patients with AEC syndrome because they impaired function of both p63 and p73. Analogously, the lack of an overt phenotype in the skin of *p73*-/- mice during homeostasis might be due to the ability of p63, which is more highly expressed, to compensate for the loss of p73. In future studies, it would be interesting to determine if expression of ΔNp73 from the endogenous ΔNp63 promotor could rescue the ectodermal development defects observed in p63-/- mice. These studies would help clarify the biological differences between ΔNp63 and

ΔNp73 beyond differential regulation of mRNA expression levels in different tissues and cell types.

p73 mRNA Isoform Quantification

Our p73 mRNA isoform analysis provided preliminary evidence consistent with the existence of a previously unreported p73 TSS located upstream of the ‘5 end of exon 4 that may be expressed in multiple epithelial tissue types. Further experiments using alternate methods (e.g. CAGE sequencing, DNase I mapping, H3K4me3 ChIP-seq, mass spectrometry) will be required to definitely prove the TSS exists *in vivo*. If confirmed, this finding could catalyze the reinterpretation of studies comparing global *p73*-/- to TAp73-/- and ΔNp73-/- mouse models. Experiments designed to study the mechanistic and biological differences between ΔNp73 and E4p73 should be performed in physiologically-relevant contexts, and analyzed with and without ΔNp63 co-expressed, since most of the tissue types with evidence supporting E4p73 also co-express ΔNp63. A previous study reported that the first 13 amino acids of ΔNp73 play important roles in transcriptional regulation at canonical p53 target genes (Liu et al., 2004) and these amino acids would be absent from E4p73. Rinne and colleagues identified three patients with an AEC-like syndrome, caused by mutations in the exons of *TP63* that encode the ΔN domain, that express a truncated ΔNp63 protein (termed ΔΔNp63) analogous to E4p73

with reduced transcriptional activity at the KRT14 promoter (Rinne et al., 2008).

Conclusions

In conclusion, the research presented herein has uncovered a new role for p73 in the basal keratinocytes of the skin and provided insight into the co-regulation of gene expression by ΔNp63 and ΔNp73 when co-expressed by cells. Our work builds on prior studies link p73 to stem cells and supports a model in which ΔNp73 is required for effective function of adult skin stem cells after stress, through coordinate regulation with ΔNp63 of a progenitor cell transcriptional program. We hope this work will be valuable to the p53 family, skin biology, and stem cell fields and that our discoveries can be translated into improved outcomes for human diseases with potential links to p73 function such as cancer, COPD, infertility, and ectodermal dysplasia syndromes.

REFERENCES

Agostini, M., Tucci, P., Chen, H., Knight, R.A., Bano, D., Nicotera, P., McKeon, F., and Melino, G. (2010). p73 regulates maintenance of neural stem cell. Biochem. Biophys. Res. Commun. *403*, 13–17.

Alexandrova, E.M., Talos, F., and Moll, U.M. (2013). p73 is dispensable for commitment to neural stem cell fate, but is essential for neural stem cell maintenance and for blocking premature differentiation. Cell Death Differ. *20*, 368.

Anders, S., Pyl, P.T., and Huber, W. (2015). HTSeq--a Python framework to work with high-throughput sequencing data. Bioinformatics *31*, 166–169.

Aviv, T., Lin, Z., Lau, S., Rendl, L.M., Sicheri, F., and Smibert, C.A. (2003). The RNA-binding SAM domain of Smaug defines a new family of post-transcriptional regulators. Nat. Struct. Biol. *10*, 614–621.

Baker, S.J., Fearon, E.R., Nigro, J.M., Hamilton, S.R., Preisinger, A.C., Jessup, J.M., vanTuinen, P., Ledbetter, D.H., Barker, D.F., Nakamura, Y., et al. (1989). Chromosome 17 deletions and p53 gene mutations in colorectal carcinomas. Science *244*, 217–221.

Baker, S.J., Markowitz, S., Fearon, E.R., Willson, J.K., and Vogelstein, B. (1990). Suppression of human colorectal carcinoma cell growth by wild-type p53. Science *249*, 912–915.

Bankhead, P., Loughrey, M.B., Fernández, J.A., Dombrowski, Y., McArt, D.G., Dunne, P.D., McQuaid, S., Gray, R.T., Murray, L.J., Coleman, H.G., et al. (2017). QuPath: Open source software for digital pathology image analysis. Sci. Rep. *7*, 16878.

Bao, X., Rubin, A.J., Qu, K., Zhang, J., Giresi, P.G., Chang, H.Y., and Khavari, P.A. (2015). A novel ATAC-seq approach reveals lineage-specific reinforcement of the open chromatin landscape via cooperation between BAF and p63. Genome Biol. *16*, 284.

Barak, Y., Juven, T., Haffner, R., and Oren, M. (1993). mdm2 expression is induced by wild type p53 activity. EMBO J. *12*, 461–468.

Barbaro, V., Testa, A., Di Iorio, E., Mavilio, F., Pellegrini, G., and De Luca, M. (2007). C/EBPδ regulates cell cycle and self-renewal of human limbal stem cells. The Journal of Cell Biology *177*, 1037–1049.

Barbieri, C.E., and Pietenpol, J.A. (2005). p53 family members: similar biochemistry, different biology. Cancer Biol. Ther. *4*, 419–420.

Batut, P., and Gingeras, T.R. (2013). RAMPAGE: promoter activity profiling by paired-end sequencing of 5'-complete cDNAs. Curr. Protoc. Mol. Biol. *104*, Unit 25B.11.

Batut, P., Dobin, A., Plessy, C., Carninci, P., and Gingeras, T.R. (2013). High-fidelity promoter profiling reveals widespread alternative promoter usage and transposon-driven developmental gene expression. Genome Res. *23*, 169–180.

Becht, E., McInnes, L., Healy, J., Dutertre, C.-A., Kwok, I.W.H., Ng, L.G., Ginhoux, F., and Newell, E.W. (2018). Dimensionality reduction for visualizing single-cell data using UMAP. Nat. Biotechnol.

Beeler, J.S., Marshall, C.B., Gonzalez-Ericsson, P.I., Shaver, T.M., Santos Guasch, G.L., Lea, S.T., Johnson, K.N., Jin, H., Venters, B.J., Sanders, M.E., et al. (2019). p73 regulates epidermal wound healing and induced keratinocyte programming. PLoS One *14*, e0218458.

Belyi, V.A., Ak, P., Markert, E., Wang, H., Hu, W., Puzio-Kuter, A., and Levine, A.J. (2010). The origins and evolution of the p53 family of genes. Cold Spring Harb. Perspect. Biol. *2*, a001198.

Bergamaschi, D., Samuels, Y., Jin, B., Duraisingham, S., Crook, T., and Lu, X. (2004). ASPP1 and ASPP2: common activators of p53 family members. Mol. Cell. Biol. *24*, 1341–1350.

Blandino, G., and Dobbelstein, M. (2004). p73 and p63: why do we still need them? Cell Cycle *3*, 886–894.

Blanpain, C., and Fuchs, E. (2009). Epidermal homeostasis: a balancing act of stem cells in the skin. Nat. Rev. Mol. Cell Biol. *10*, 207–217.

van Bokhoven, H., Jung, M., Smits, A.P., van Beersum, S., Rüschendorf, F., van Steensel, M., Veenstra, M., Tuerlings, J.H., Mariman, E.C., Brunner, H.G., et al. (1999). Limb mammary syndrome: a new genetic disorder with mammary hypoplasia, ectrodactyly, and other Hand/Foot anomalies maps to human chromosome 3q27. Am. J. Hum. Genet. *64*, 538–546.

van Bokhoven, H., Hamel, B.C.J., Bamshad, M., Sangiorgi, E., Gurrieri, F., Duijf, P.H.G., Vanmolkot, K.R.J., van Beusekom, E., van Beersum, S.E.C., Celli, J., et al. (2001). p63 Gene Mutations in EEC Syndrome, Limb-Mammary Syndrome, and Isolated Split Hand–Split Foot Malformation Suggest a Genotype-Phenotype Correlation. The American Journal of Human Genetics *69*, 481–492.

Borrelli, S., Testoni, B., Callari, M., Alotto, D., Castagnoli, C., Romano, R.-A., Sinha, S., Viganò, A.M., and Mantovani, R. (2007). Reciprocal regulation of p63 by C/EBP delta in human keratinocytes. BMC Mol. Biol. *8*, 85.

Bourdon, J.-C., Fernandes, K., Murray-Zmijewski, F., Liu, G., Diot, A., Xirodimas, D.P., Saville, M.K., and Lane, D.P. (2005). p53 isoforms can regulate p53 transcriptional activity. Genes Dev. *19*, 2122–2137.

Bray, N.L., Pimentel, H., Melsted, P., and Pachter, L. (2016). Near-optimal probabilistic RNA-seq quantification. Nat. Biotechnol. *34*, 525–527.

Butler, A., Hoffman, P., Smibert, P., Papalexi, E., and Satija, R. (2018). Integrating single-cell transcriptomic data across different conditions, technologies, and species. Nat. Biotechnol. *36*, 411–420.

Caddy, J., Wilanowski, T., Darido, C., Dworkin, S., Ting, S.B., Zhao, Q., Rank, G., Auden, A., Srivastava, S., Papenfuss, T.A., et al. (2010). Epidermal wound repair is regulated by the planar cell polarity signaling pathway. Dev. Cell *19*, 138–147.

Carithers, L.J., Ardlie, K., Barcus, M., Branton, P.A., Britton, A., Buia, S.A., Compton, C.C., DeLuca, D.S., Peter-Demchok, J., Gelfand, E.T., et al. (2015). A Novel Approach to High-Quality Postmortem Tissue Procurement: The GTEx Project. Biopreserv. Biobank. *13*, 311–319.

Carroll, D.K., Carroll, J.S., Leong, C.-O., Cheng, F., Brown, M., Mills, A.A., Brugge, J.S., and Ellisen, L.W. (2006). p63 regulates an adhesion programme and cell survival in epithelial cells. Nat. Cell Biol. *8*, 551–561.

Cavazza, A., Miccio, A., Romano, O., Petiti, L., Malagoli Tagliazucchi, G., Peano, C., Severgnini, M., Rizzi, E., De Bellis, G., Bicciato, S., et al. (2016). Dynamic Transcriptional and Epigenetic Regulation of Human Epidermal Keratinocyte Differentiation. Stem Cell Reports *6*, 618–632.

Celli, J., Duijf, P., Hamel, B.C., Bamshad, M., Kramer, B., Smits, A.P., Newbury-Ecob, R., Hennekam, R.C., Van Buggenhout, G., van Haeringen, A., et al. (1999). Heterozygous germline mutations in the p53 homolog p63 are the cause of EEC syndrome. Cell *99*, 143–153.

Chen, G., Ning, B., and Shi, T. (2019). Single-Cell RNA-Seq Technologies and Related Computational Data Analysis. Front. Genet. *10*, 47.

Chen, X., Whitney, E.M., Gao, S.Y., and Yang, V.W. (2003). Transcriptional profiling of Krüppel-like factor 4 reveals a function in cell cycle regulation and epithelial differentiation. J. Mol. Biol. *326*, 665–677.

Chen, Y., Mistry, D.S., and Sen, G.L. (2014). Highly rapid and efficient conversion of human fibroblasts to keratinocyte-like cells. J. Invest. Dermatol. *134*, 335–344.

Chène, P. (2001). The role of tetramerization in p53 function. Oncogene *20*, 2611–2617.

Cheng, C.-C., Wang, D.-Y., Kao, M.-H., and Chen, J.-K. (2009). The growth-promoting effect of KGF on limbal epithelial cells is mediated by upregulation of ΔNp63α through the p38 pathway. Journal of Cell Science *122*, 4473–4480.

Cho, Y., Gorina, S., Jeffrey, P.D., and Pavletich, N.P. (1994). Crystal structure of a p53 tumor suppressor-DNA complex: understanding tumorigenic mutations. Science *265*, 346–355.

Chu, W.-K., Dai, P.-M., Li, H.-L., and Chen, J.-K. (2008). Glycogen synthase kinase-3beta regulates DeltaNp63 gene transcription through the beta-catenin signaling pathway. J. Cell. Biochem. *105*, 447–453.

Chua, H.L., Bhat-Nakshatri, P., Clare, S.E., Morimiya, A., Badve, S., and Nakshatri, H. (2007). NF-κB represses E-cadherin expression and enhances epithelial to mesenchymal transition of mammary epithelial cells: potential involvement of ZEB-1 and ZEB-2. Oncogene *26*, 711–724.

Conforti, F., Yang, A.L., Piro, M.C., Mellone, M., Terrinoni, A., Candi, E., Tucci, P., Thomas, G.J., Knight, R.A., Melino, G., et al. (2013). PIR2/Rnf144B regulates epithelial homeostasis by mediating degradation of p21WAF1 and p63. Oncogene *32*, 4758–4765.

Cotsarelis, G., Sun, T.T., and Lavker, R.M. (1990). Label-retaining cells reside in the bulge area of pilosebaceous unit: implications for follicular stem cells, hair cycle, and skin carcinogenesis. Cell *61*, 1329–1337.

Coulombe, P.A. (1997). Towards a molecular definition of keratinocyte activation after acute injury to stratified epithelia. Biochem. Biophys. Res. Commun. *236*, 231–238.

Coutandin, D., Löhr, F., Niesen, F.H., Ikeya, T., Weber, T.A., Schäfer, B., Zielonka, E.M., Bullock, A.N., Yang, A., Güntert, P., et al. (2009). Conformational stability and activity of p73 require a second helix in the tetramerization domain. Cell Death Differ. *16*, 1582–1589.

Davis, C.A., Hitz, B.C., Sloan, C.A., Chan, E.T., Davidson, J.M., Gabdank, I., Hilton, J.A., Jain, K., Baymuradov, U.K., Narayanan, A.K., et al. (2018). The Encyclopedia of DNA elements (ENCODE): data portal update. Nucleic Acids Res. *46*, D794–D801.

Davison, T.S., Vagner, C., Kaghad, M., Ayed, A., Caput, D., and Arrowsmith, C.H. (1999). p73 and p63 Are Homotetramers Capable of Weak Heterotypic Interactions with Each Other but Not with p53. Journal of Biological Chemistry *274*, 18709–18714.

el-Deiry, W.S., Kern, S.E., Pietenpol, J.A., Kinzler, K.W., and Vogelstein, B. (1992). Definition of a consensus binding site for p53. Nat. Genet. *1*, 45–49.

el-Deiry, W.S., Tokino, T., Velculescu, V.E., Levy, D.B., Parsons, R., Trent, J.M., Lin, D., Mercer, W.E., Kinzler, K.W., and Vogelstein, B. (1993). WAF1, a potential mediator of p53 tumor suppression. Cell *75*, 817–825.

De Laurenzi, V., Costanzo, A., Barcaroli, D., Terrinoni, A., Falco, M., Annicchiarico-Petruzzelli, M., Levrero, M., and Melino, G. (1998). Two new p73 splice variants, gamma and delta, with different transcriptional activity. J. Exp. Med. *188*, 1763–1768.

DeLuca, D.S., Levin, J.Z., Sivachenko, A., Fennell, T., Nazaire, M.-D., Williams, C., Reich, M., Winckler, W., and Getz, G. (2012). RNA-SeQC: RNA-seq metrics for quality control and process optimization. Bioinformatics *28*, 1530–1532.

DeYoung, M.P., Johannessen, C.M., Leong, C.-O., Faquin, W., Rocco, J.W., and Ellisen, L.W. (2006). Tumor-specific p73 up-regulation mediates p63 dependence in squamous cell carcinoma. Cancer Res. *66*, 9362–9368.

Di Como, C.J., Urist, M.J., Babayan, I., Drobnjak, M., Hedvat, C.V., Teruya-Feldstein, J., Pohar, K., Hoos, A., and Cordon-Cardo, C. (2002). p63 expression profiles in human normal and tumor tissues. Clin. Cancer Res. *8*, 494–501.

Diller, L., Kassel, J., Nelson, C.E., Gryka, M.A., Litwak, G., Gebhardt, M., Bressac, B., Ozturk, M., Baker, S.J., and Vogelstein, B. (1990). p53 functions as a cell cycle control protein in osteosarcomas. Mol. Cell. Biol. *10*, 5772–5781.

Dobbelstein, M., Wienzek, S., König, C., and Roth, J. (1999). Inactivation of the p53-homologue p73 by the mdm2-oncoprotein. Oncogene *18*, 2101–2106.

Dobin, A., Davis, C.A., Schlesinger, F., Drenkow, J., Zaleski, C., Jha, S., Batut, P., Chaisson, M., and Gingeras, T.R. (2013). STAR: ultrafast universal RNA-seq aligner. Bioinformatics *29*, 15–21.

Dodt, M., Roehr, J.T., Ahmed, R., and Dieterich, C. (2012). FLEXBAR-Flexible Barcode and Adapter Processing for Next-Generation Sequencing Platforms. Biology *1*, 895–905.

Dohn, M., Zhang, S., and Chen, X. (2001). p63alpha and DeltaNp63alpha can induce cell cycle arrest and apoptosis and differentially regulate p53 target genes. Oncogene *20*, 3193–3205.

Donehower, L.A., Harvey, M., Slagle, B.L., McArthur, M.J., Montgomery, C.A., Jr, Butel, J.S., and Bradley, A. (1992). Mice deficient for p53 are developmentally normal but susceptible to spontaneous tumours. Nature *356*, 215–221.

Du, W., Jiang, P., Mancuso, A., Stonestrom, A., Brewer, M.D., Minn, A.J., Mak, T.W., Wu, M., and Yang, X. (2013). TAp73 enhances the pentose phosphate pathway and supports cell proliferation. Nat. Cell Biol. *15*, 991–1000.

Ermolaeva, M., Neri, F., Ori, A., and Rudolph, K.L. (2018). Cellular and epigenetic drivers of stem cell ageing. Nat. Rev. Mol. Cell Biol. *19*, 594–610.

Fernandez-Alonso, R., Martin-Lopez, M., Gonzalez-Cano, L., Garcia, S., Castrillo, F., Diez-Prieto, I., Fernandez-Corona, A., Lorenzo-Marcos, M.E., Li, X., Claesson-Welsh, L., et al. (2015). p73 is required for endothelial cell differentiation, migration and the formation of vascular networks regulating VEGF and TGFβ signaling. Cell Death Differ. *22*, 1287–1299.

Ferone, G., Mollo, M.R., Thomason, H.A., Antonini, D., Zhou, H., Ambrosio, R., De Rosa, L., Salvatore, D., Getsios, S., van Bokhoven, H., et al. (2013). p63 control of desmosome gene expression and adhesion is compromised in AEC syndrome. Hum. Mol. Genet. *22*, 531–543.

Ferreira, P.G., Muñoz-Aguirre, M., Reverter, F., Sá Godinho, C.P., Sousa, A., Amadoz, A., Sodaei, R., Hidalgo, M.R., Pervouchine, D., Carbonell-Caballero, J., et al. (2018). The effects of death and post-mortem cold ischemia on human tissue transcriptomes. Nat. Commun. *9*, 490.

Ferretti, E., Li, B., Zewdu, R., Wells, V., Hebert, J.M., Karner, C., Anderson, M.J., Williams, T., Dixon, J., Dixon, M.J., et al. (2011). A conserved Pbx-Wnt-p63-Irf6 regulatory module controls face morphogenesis by promoting epithelial apoptosis. Dev. Cell *21*, 627–641.

Fessing, M.Y., Mardaryev, A.N., Gdula, M.R., Sharov, A.A., Sharova, T.Y., Rapisarda, V., Gordon, K.B., Smorodchenko, A.D., Poterlowicz, K., Ferone, G., et al. (2011). p63 regulates Satb1 to control tissue-specific chromatin remodeling during development of the epidermis. J. Cell Biol. *194*, 825–839.

Fields, S., and Jang, S.K. (1990). Presence of a potent transcription activating sequence in the p53 protein. Science *249*, 1046–1049.

Flores, E.R., Tsai, K.Y., Crowley, D., Sengupta, S., Yang, A., McKeon, F., and Jacks, T. (2002). p63 and p73 are required for p53-dependent apoptosis in response to DNA damage. Nature *416*, 560–564.

Fontemaggi, G., Gurtner, A., Strano, S., Higashi, Y., Sacchi, A., Piaggio, G., and Blandino, G. (2001). The transcriptional repressor ZEB regulates p73 expression at the crossroad between proliferation and differentiation. Mol. Cell. Biol. *21*, 8461–8470.

Frankish, A., Diekhans, M., Ferreira, A.-M., Johnson, R., Jungreis, I., Loveland, J., Mudge, J.M., Sisu, C., Wright, J., Armstrong, J., et al. (2019). GENCODE reference annotation for the human and mouse genomes. Nucleic Acids Res. *47*, D766–D773.

Fuchs, E. (2016). Epithelial Skin Biology: Three Decades of Developmental Biology, a Hundred Questions Answered and a Thousand New Ones to Address. Curr. Top. Dev. Biol. *116*, 357–374.

Fuchs, E., and Green, H. (1980). Changes in keratin gene expression during terminal differentiation of the keratinocyte. Cell *19*, 1033–1042.

Ge, Y., and Fuchs, E. (2018). Stretching the limits: from homeostasis to stem cell plasticity in wound healing and cancer. Nat. Rev. Genet. *19*, 311–325.

Ge, Y., Gomez, N.C., Adam, R.C., Nikolova, M., Yang, H., Verma, A., Lu, C.P.-J., Polak, L., Yuan, S., Elemento, O., et al. (2017). Stem Cell Lineage Infidelity Drives Wound Repair and Cancer. Cell *169*, 636–650.e14.

Gebel, J., Luh, L.M., Coutandin, D., Osterburg, C., Löhr, F., Schäfer, B., Frombach, A.-S., Sumyk, M., Buchner, L., Krojer, T., et al. (2016). Mechanism of TAp73 inhibition by ΔNp63 and structural basis of p63/p73 hetero-tetramerization. Cell Death Differ. *23*, 1930–1940.

Gonzales, K.A.U., and Fuchs, E. (2017). Skin and Its Regenerative Powers: An Alliance between Stem Cells and Their Niche. Developmental Cell *43*, 387–401.

Gonzalez-Cano, L., Herreros-Villanueva, M., Fernandez-Alonso, R., Ayuso-Sacido, A., Meyer, G., Garcia-Verdugo, J.M., Silva, A., Marques, M.M., and Marin, M.C. (2010). p73 deficiency results in impaired self renewal and premature neuronal differentiation of mouse neural progenitors independently of p53. Cell Death Dis. *1*, e109.

Gordon, W.M., Zeller, M.D., Klein, R.H., Swindell, W.R., Ho, H., Espetia, F., Gudjonsson, J.E., Baldi, P.F., and Andersen, B. (2014). A GRHL3-regulated repair pathway suppresses immune-mediated epidermal hyperplasia. J. Clin. Invest. *124*, 5205–5218.

Greco, V., Chen, T., Rendl, M., Schober, M., Pasolli, H.A., Stokes, N., Dela Cruz-Racelis, J., and Fuchs, E. (2009). A two-step mechanism for stem cell activation during hair regeneration. Cell Stem Cell *4*, 155–169.

Grespi, F., Amelio, I., Tucci, P., Annicchiarico-Petruzzelli, M., and Melino, G. (2012). Tissue-specific expression of p73 C-terminal isoforms in mice. Cell Cycle *11*, 4474–4483.

Grob, T.J., Novak, U., Maisse, C., Barcaroli, D., Lüthi, A.U., Pirnia, F., Hügli, B., Graber, H.U., De Laurenzi, V., Fey, M.F., et al. (2001). Human delta Np73 regulates a dominant negative feedback loop for TAp73 and p53. Cell Death Differ. *8*, 1213–1223.

GTEx Consortium (2013). The Genotype-Tissue Expression (GTEx) project. Nat. Genet. *45*, 580–585.

GTEx Consortium, Laboratory, Data Analysis &Coordinating Center (LDACC)—Analysis Working Group, Statistical Methods groups—Analysis Working Group, Enhancing GTEx (eGTEx) groups, NIH Common Fund, NIH/NCI, NIH/NHGRI, NIH/NIMH, NIH/NIDA, Biospecimen Collection Source Site—NDRI, et al. (2017). Genetic effects on gene expression across human tissues. Nature *550*, 204–213.

Gurtner, G.C., Werner, S., Barrandon, Y., and Longaker, M.T. (2008). Wound repair and regeneration. Nature *453*, 314–321.

Hara-Chikuma, M., and Verkman, A.S. (2008). Aquaporin-3 facilitates epidermal cell migration and proliferation during wound healing. J. Mol. Med. *86*, 221–231.

Harmes, D.C., Bresnick, E., Lubin, E.A., Watson, J.K., Heim, K.E., Curtin, J.C., Suskind, A.M., Lamb, J., and DiRenzo, J. (2003). Positive and negative regulation of deltaN-p63 promoter activity by p53 and deltaN-p63-alpha contributes to differential regulation of p53 target genes. Oncogene *22*, 7607–7616.

Harrow, J., Frankish, A., Gonzalez, J.M., Tapanari, E., Diekhans, M., Kokocinski, F., Aken, B.L., Barrell, D., Zadissa, A., Searle, S., et al. (2012). GENCODE: the reference human genome annotation for The ENCODE Project. Genome Res. *22*, 1760–1774.

Haupt, Y., Maya, R., Kazaz, A., and Oren, M. (1997). Mdm2 promotes the rapid degradation of p53. Nature *387*, 296–299.

Hearnes, J.M., Mays, D.J., Schavolt, K.L., Tang, L., Jiang, X., and Pietenpol, J.A. (2005). Chromatin immunoprecipitation-based screen to identify functional genomic binding sites for sequence-specific transactivators. Mol. Cell. Biol. *25*, 10148–10158.

Herfs, M., Hubert, P., Suarez-Carmona, M., Reschner, A., Saussez, S., Berx, G., Savagner, P., Boniver, J., and Delvenne, P. (2010). Regulation of p63 isoforms by snail and slug transcription factors in human squamous cell carcinoma. Am. J. Pathol. *176*, 1941–1949.

Hibi, K., Trink, B., Patturajan, M., Westra, W.H., Caballero, O.L., Hill, D.E., Ratovitski, E.A., Jen, J., and Sidransky, D. (2000). AIS is an oncogene amplified in squamous cell carcinoma. Proc. Natl. Acad. Sci. U. S. A. *97*, 5462–5467.

Higashikawa, K., Yoneda, S., Tobiume, K., Taki, M., Shigeishi, H., and Kamata, N. (2007). Snail-induced down-regulation of DeltaNp63alpha acquires invasive phenotype of human squamous cell carcinoma. Cancer Res. *67*, 9207–9213.

Holembowski, L., Kramer, D., Riedel, D., Sordella, R., Nemajerova, A., Dobbelstein, M., and Moll, U.M. (2014). TAp73 is essential for germ cell adhesion and maturation in testis. J. Cell Biol. *204*, 1173–1190.

Hsu, Y.-C., Li, L., and Fuchs, E. (2014). Transit-amplifying cells orchestrate stem cell activity and tissue regeneration. Cell *157*, 935–949.

Hu, H., Xia, S.-H., Li, A.-D., Xu, X., Cai, Y., Han, Y.-L., Wei, F., Chen, B.-S., Huang, X.-P., Han, Y.-S., et al. (2002). Elevated expression of p63 protein in human esophageal squamous cell carcinomas. Int. J. Cancer *102*, 580–583.

Hwang, B., Lee, J.H., and Bang, D. (2018). Single-cell RNA sequencing technologies and bioinformatics pipelines. Exp. Mol. Med. *50*, 96.

Ianakiev, P., Kilpatrick, M.W., Toudjarska, I., Basel, D., Beighton, P., and Tsipouras, P. (2000). Split-Hand/Split-Foot Malformation Is Caused by Mutations in the p63 Gene on 3q27. The American Journal of Human Genetics *67*, 59–66.

Ihrie, R.A., Marques, M.R., Nguyen, B.T., Horner, J.S., Papazoglu, C., Bronson, R.T., Mills, A.A., and Attardi, L.D. (2005). Perp is a p63-regulated gene essential for epithelial integrity. Cell *120*, 843–856.

Inada, R., Matsuki, M., Yamada, K., Morishima, Y., Shen, S.C., Kuramoto, N., Yasuno, H., Takahashi, K., Miyachi, Y., and Yamanishi, K. (2000). Facilitated wound healing by activation of the Transglutaminase 1 gene. Am. J. Pathol. *157*, 1875–1882.

Ingraham, C.R., Kinoshita, A., Kondo, S., Yang, B., Sajan, S., Trout, K.J., Malik, M.I., Dunnwald, M., Goudy, S.L., Lovett, M., et al. (2006). Abnormal skin, limb and craniofacial morphogenesis in mice deficient for interferon regulatory factor 6 (Irf6). Nat. Genet. *38*, 1335–1340.

Inoue, S., Tomasini, R., Rufini, A., Elia, A.J., Agostini, M., Amelio, I., Cescon, D., Dinsdale, D., Zhou, L., Harris, I.S., et al. (2014). TAp73 is required for spermatogenesis and the maintenance of male fertility. Proc. Natl. Acad. Sci. U. S. A. *111*, 1843–1848.

Irwin, M., Marin, M.C., Phillips, A.C., Seelan, R.S., Smith, D.I., Liu, W., Flores, E.R., Tsai, K.Y., Jacks, T., Vousden, K.H., et al. (2000). Role for the p53 homologue p73 in E2F-1-induced apoptosis. Nature *407*, 645–648.

Ito, M., Liu, Y., Yang, Z., Nguyen, J., Liang, F., Morris, R.J., and Cotsarelis, G. (2005). Stem cells in the hair follicle bulge contribute to wound repair but not to homeostasis of the epidermis. Nature Medicine *11*, 1351–1354.

Janes, S.M., Ofstad, T.A., Campbell, D.H., Watt, F.M., and Prowse, D.M. (2004). Transient activation of FOXN1 in keratinocytes induces a transcriptional programme that promotes terminal differentiation: contrasting roles of FOXN1 and Akt. J. Cell Sci. *117*, 4157–4168.

Jeffrey, P.D., Gorina, S., and Pavletich, N.P. (1995). Crystal structure of the tetramerization domain of the p53 tumor suppressor at 1.7 angstroms. Science *267*, 1498–1502.

Jiang, P., Du, W., and Yang, X. (2013). A critical role of glucose-6-phosphate dehydrogenase in TAp73-mediated cell proliferation. Cell Cycle *12*, 3720–3726.

Jobard, F., Bouadjar, B., Caux, F., Hadj-Rabia, S., Has, C., Matsuda, F., Weissenbach, J., Lathrop, M., Prud'homme, J.-F., and Fischer, J. (2003). Identification of mutations in a new gene encoding a FERM family protein with a pleckstrin homology domain in Kindler syndrome. Hum. Mol. Genet. *12*, 925–935.

Joerger, A.C., Rajagopalan, S., Natan, E., Veprintsev, D.B., Robinson, C.V., and Fersht, A.R. (2009). Structural evolution of p53, p63, and p73: implication for heterotetramer formation. Proc. Natl. Acad. Sci. U. S. A. *106*, 17705–17710.

Johnson, J.L., Najor, N.A., and Green, K.J. (2014). Desmosomes: regulators of cellular signaling and adhesion in epidermal health and disease. Cold Spring Harb. Perspect. Med. *4*, a015297.

Joost, S., Zeisel, A., Jacob, T., Sun, X., La Manno, G., Lönnerberg, P., Linnarsson, S., and Kasper, M. (2016). Single-Cell Transcriptomics Reveals that Differentiation and Spatial Signatures Shape Epidermal and Hair Follicle Heterogeneity. Cell Syst *3*, 221–237.e9.

Joost, S., Jacob, T., Sun, X., Annusver, K., La Manno, G., Sur, I., and Kasper, M. (2018). Single-Cell Transcriptomics of Traced Epidermal and Hair Follicle Stem Cells Reveals Rapid Adaptations during Wound Healing. Cell Rep. *25*, 585–597.e7.

Jost, C.A., Marin, M.C., and Kaelin, W.G., Jr (1997). p73 is a simian [correction of human] p53-related protein that can induce apoptosis. Nature *389*, 191–194.

Julapalli, M.R., Scher, R.K., Sybert, V.P., Siegfried, E.C., and Bree, A.F. (2009). Dermatologic findings of ankyloblepharon-ectodermal defects-cleft lip/palate (AEC) syndrome. Am. J. Med. Genet. A *149A*, 1900–1906.

Jung, Y.-S., Qian, Y., Yan, W., and Chen, X. (2013). Pirh2 E3 ubiquitin ligase modulates keratinocyte differentiation through p63. J. Invest. Dermatol. *133*, 1178–1187.

Kaghad, M., Bonnet, H., Yang, A., Creancier, L., Biscan, J.C., Valent, A., Minty, A., Chalon, P., Lelias, J.M., Dumont, X., et al. (1997). Monoallelically expressed gene related to p53 at 1p36, a region frequently deleted in neuroblastoma and other human cancers. Cell *90*, 809–819.

Kandoth, C., McLellan, M.D., Vandin, F., Ye, K., Niu, B., Lu, C., Xie, M., Zhang, Q., McMichael, J.F., Wyczalkowski, M.A., et al. (2013). Mutational landscape and significance across 12 major cancer types. Nature *502*, 333–339.

Kim, C.A., Phillips, M.L., Kim, W., Gingery, M., Tran, H.H., Robinson, M.A., Faham, S., and Bowie, J.U. (2001). Polymerization of the SAM domain of TEL in leukemogenesis and transcriptional repression. EMBO J. *20*, 4173–4182.

Kitayner, M., Rozenberg, H., Kessler, N., Rabinovich, D., Shaulov, L., Haran, T.E., and Shakked, Z. (2006). Structural basis of DNA recognition by p53 tetramers. Mol. Cell *22*, 741–753.

Klein, R.H., Lin, Z., Hopkin, A.S., Gordon, W., Tsoi, L.C., Liang, Y., Gudjonsson, J.E., and Andersen, B. (2017). GRHL3 binding and enhancers rearrange as epidermal keratinocytes transition between functional states. PLoS Genet. *13*, e1006745.

Koster, M.I., Dai, D., Marinari, B., Sano, Y., Costanzo, A., Karin, M., and Roop, D.R. (2007). p63 induces key target genes required for epidermal morphogenesis. Proc. Natl. Acad. Sci. U. S. A. *104*, 3255–3260.

Koster, M.I., Marinari, B., Payne, A.S., Kantaputra, P.N., Costanzo, A., and Roop, D.R. (2009). ΔNp63 knockdown mice: A mouse model for AEC syndrome. American Journal of Medical Genetics Part A *149A*, 1942–1947.

Kouwenhoven, E.N., Oti, M., Niehues, H., van Heeringen, S.J., Schalkwijk, J., Stunnenberg, H.G., van Bokhoven, H., and Zhou, H. (2015). Transcription factor p63 bookmarks and regulates dynamic enhancers during epidermal differentiation. EMBO Rep. *16*, 863–878.

Kurokawa, I., Mizutani, H., Kusumoto, K., Nishijima, S., Tsujita-Kyutoku, M., Shikata, N., and Tsubura, A. (2006). Cytokeratin, filaggrin, and p63 expression in reepithelialization during human cutaneous wound healing. Wound Repair Regen. *14*, 38–45.

Lane, D.P. (1992). Cancer. p53, guardian of the genome. Nature *358*, 15–16.

Lane, D.P., and Crawford, L.V. (1979). T antigen is bound to a host protein in SV40-transformed cells. Nature *278*, 261–263.

Langmead, B., and Salzberg, S.L. (2012). Fast gapped-read alignment with Bowtie 2. Nat. Methods *9*, 357–359.

Leinonen, R., Sugawara, H., Shumway, M., and International Nucleotide Sequence Database Collaboration (2011). The sequence read archive. Nucleic Acids Res. *39*, D19–D21.

Leong, C.-O., Vidnovic, N., DeYoung, M.P., Sgroi, D., and Ellisen, L.W. (2007). The p63/p73 network mediates chemosensitivity to cisplatin in a biologically defined subset of primary breast cancers. J. Clin. Invest. *117*, 1370–1380.

Lessard, J.C., Piña-Paz, S., Rotty, J.D., Hickerson, R.P., Kaspar, R.L., Balmain, A., and Coulombe, P.A. (2013). Keratin 16 regulates innate immunity in response to epidermal barrier breach. Proc. Natl. Acad. Sci. U. S. A. *110*, 19537–19542.

Levy, D., Adamovich, Y., Reuven, N., and Shaul, Y. (2007a). The Yes-associated protein 1 stabilizes p73 by preventing Itch-mediated ubiquitination of p73. Cell Death Differ. *14*, 743–751.

Levy, V., Lindon, C., Zheng, Y., Harfe, B.D., and Morgan, B.A. (2007b). Epidermal stem cells arise from the hair follicle after wounding. FASEB J. *21*, 1358–1366.

Li, B., and Dewey, C.N. (2011). RSEM: accurate transcript quantification from RNA-Seq data with or without a reference genome. BMC Bioinformatics *12*, 323.

Li, H., and Durbin, R. (2009). Fast and accurate short read alignment with Burrows-Wheeler transform. Bioinformatics *25*, 1754–1760.

Li, H., Handsaker, B., Wysoker, A., Fennell, T., Ruan, J., Homer, N., Marth, G., Abecasis, G., Durbin, R., and 1000 Genome Project Data Processing Subgroup (2009). The Sequence Alignment/Map format and SAMtools. Bioinformatics *25*, 2078–2079.

Li, N., Li, H., Cherukuri, P., Farzan, S., Harmes, D.C., and DiRenzo, J. (2006). TA-p63-gamma regulates expression of DeltaN-p63 in a manner that is sensitive to p53. Oncogene *25*, 2349–2359.

Li, N., Singh, S., Cherukuri, P., Li, H., Yuan, Z., Ellisen, L.W., Wang, B., Robbins, D., and DiRenzo, J. (2008). Reciprocal intraepithelial interactions between TP63 and hedgehog signaling regulate quiescence and activation of progenitor elaboration by mammary stem cells. Stem Cells *26*, 1253–1264.

Liao, Y., Smyth, G.K., and Shi, W. (2014). featureCounts: an efficient general purpose program for assigning sequence reads to genomic features. Bioinformatics *30*, 923–930.

Liefer, K.M., Koster, M.I., Wang, X.J., Yang, A., McKeon, F., and Roop, D.R. (2000). Down-regulation of p63 is required for epidermal UV-B-induced apoptosis. Cancer Res. *60*, 4016–4020.

Lin, Y., Cheng, Z., Yang, Z., Zheng, J., and Lin, T. (2012). DNp73 improves generation efficiency of human induced pluripotent stem cells. BMC Cell Biol. *13*, 9.

Liu, C., Liu, H.-J., Xiang, Y., Tan, Y.-R., Zhu, X.-L., and Qin, X.-Q. (2010). Wound repair and anti-oxidative capacity is regulated by ITGB4 in airway epithelial cells. Mol. Cell. Biochem. *341*, 259–269.

Liu, G., Nozell, S., Xiao, H., and Chen, X. (2004). DeltaNp73beta is active in transactivation and growth suppression. Mol. Cell. Biol. *24*, 487–501.

Livak, K.J., and Schmittgen, T.D. (2001). Analysis of relative gene expression data using real-time quantitative PCR and the 2(-Delta Delta C(T)) Method. Methods *25*, 402–408.

Love, M.I., Huber, W., and Anders, S. (2014). Moderated estimation of fold change and dispersion for RNA-seq data with DESeq2. Genome Biol. *15*, 550.

Machanick, P., and Bailey, T.L. (2011). MEME-ChIP: motif analysis of large DNA datasets. Bioinformatics *27*, 1696–1697.

Malkin, D., Li, F.P., Strong, L.C., Fraumeni, J.F., Jr, Nelson, C.E., Kim, D.H., Kassel, J., Gryka, M.A., Bischoff, F.Z., and Tainsky, M.A. (1990). Germ line p53 mutations in a familial syndrome of breast cancer, sarcomas, and other neoplasms. Science *250*, 1233–1238.

Mangiulli, M., Valletti, A., Caratozzolo, M.F., Tullo, A., Sbisà, E., Pesole, G., and D'Erchia, A.M. (2009). Identification and functional characterization of two new transcriptional variants of the human p63 gene. Nucleic Acids Res. *37*, 6092–6104.

Marabese, M., Vikhanskaya, F., Rainelli, C., Sakai, T., and Broggini, M. (2003). DNA damage induces transcriptional activation of p73 by removing C-EBPalpha repression on E2F1. Nucleic Acids Res. *31*, 6624–6632.

Mardaryev, A.N., Gdula, M.R., Yarker, J.L., Emelianov, V.U., Poterlowicz, K., Sharov, A.A., Sharova, T.Y., Scarpa, J.A., Joffe, B., Solovei, I., et al. (2014). p63 and Brg1 control developmentally regulated higher-order chromatin remodelling at the epidermal differentiation complex locus in epidermal progenitor cells. Development *141*, 101–111.

Marini, A., Rotblat, B., Sbarrato, T., Niklison-Chirou, M.V., Knight, J.R.P., Dudek, K., Jones, C., Bushell, M., Knight, R.A., Amelio, I., et al. (2018). TAp73 contributes to the oxidative stress response by regulating protein synthesis. Proc. Natl. Acad. Sci. U. S. A. *115*, 6219–6224.

Marshall, C.B., Mays, D.J., Beeler, J.S., Rosenbluth, J.M., Boyd, K.L., Santos Guasch, G.L., Shaver, T.M., Tang, L.J., Liu, Q., Shyr, Y., et al. (2016). p73 Is Required for Multiciliogenesis and Regulates the Foxj1-Associated Gene Network. Cell Rep. *14*, 2289–2300.

Martin, S.E., Temm, C.J., Goheen, M.P., Ulbright, T.M., and Hattab, E.M. (2011). Cytoplasmic p63 immunohistochemistry is a useful marker for muscle differentiation: an immunohistochemical and immunoelectron microscopic study. Mod. Pathol. *24*, 1320–1326.

Martin-Lopez, M., Maeso-Alonso, L., Fuertes-Alvarez, S., Balboa, D., Rodríguez-Cortez, V., Weltner, J., Diez-Prieto, I., Davis, A., Wu, Y., Otonkoski, T., et al. (2017). p73 is required for appropriate BMP-induced mesenchymal-to-epithelial transition during somatic cell reprogramming. Cell Death Dis. *8*, e3034.

Massion, P.P., Taflan, P.M., Jamshedur Rahman, S.M., Yildiz, P., Shyr, Y., Edgerton, M.E., Westfall, M.D., Roberts, J.R., Pietenpol, J.A., Carbone, D.P., et al. (2003). Significance of p63 amplification and overexpression in lung cancer development and prognosis. Cancer Res. *63*, 7113–7121.

McCarty, K.S., Jr, Miller, L.S., Cox, E.B., Konrath, J., and McCarty, K.S., Sr (1985). Estrogen receptor analyses. Correlation of biochemical and immunohistochemical methods using monoclonal antireceptor antibodies. Arch. Pathol. Lab. Med. *109*, 716–721.

McGrath, J.A., Duijf, P.H., Doetsch, V., Irvine, A.D., de Waal, R., Vanmolkot, K.R., Wessagowit, V., Kelly, A., Atherton, D.J., Griffiths, W.A., et al. (2001). Hay-Wells syndrome is caused by heterozygous missense mutations in the SAM domain of p63. Hum. Mol. Genet. *10*, 221–229.

Meier, C., Hardtstock, P., Joost, S., Alla, V., and Pützer, B.M. (2016). p73 and IGF1R Regulate Emergence of Aggressive Cancer Stem-like Features via miR-885-5p Control. Cancer Res. *76*, 197–205.

Mercer, W.E., Shields, M.T., Amin, M., Sauve, G.J., Appella, E., Romano, J.W., and Ullrich, S.J. (1990). Negative growth regulation in a glioblastoma tumor cell line that conditionally expresses human wild-type p53. Proc. Natl. Acad. Sci. U. S. A. *87*, 6166–6170.

Michalovitz, D., Halevy, O., and Oren, M. (1990). Conditional inhibition of transformation and of cell proliferation by a temperature-sensitive mutant of p53. Cell *62*, 671–680.

Mills, A.A., Zheng, B., Wang, X.J., Vogel, H., Roop, D.R., and Bradley, A. (1999). p63 is a p53 homologue required for limb and epidermal morphogenesis. Nature *398*, 708–713.

Montoro, D.T., Haber, A.L., Biton, M., Vinarsky, V., Lin, B., Birket, S.E., Yuan, F., Chen, S., Leung, H.M., Villoria, J., et al. (2018). A revised airway epithelial hierarchy includes CFTR-expressing ionocytes. Nature *560*, 319–324.

Mori, R., Tanaka, K., de Kerckhove, M., Okamoto, M., Kashiyama, K., Tanaka, K., Kim, S., Kawata, T., Komatsu, T., Park, S., et al. (2014). Reduced FOXO1 expression accelerates skin wound healing and attenuates scarring. Am. J. Pathol. *184*, 2465–2479.

Murray-Zmijewski, F., Lane, D.P., and Bourdon, J.-C. (2006). p53/p63/p73 isoforms: an orchestra of isoforms to harmonise cell differentiation and response to stress. Cell Death Differ. *13*, 962–972.

Nakagawa, T., Takahashi, M., Ozaki, T., Watanabe Ki, K.-I., Todo, S., Mizuguchi, H., Hayakawa, T., and Nakagawara, A. (2002). Autoinhibitory regulation of p73 by Delta Np73 to modulate cell survival and death through a p73-specific target element within the Delta Np73 promoter. Mol. Cell. Biol. *22*, 2575–2585.

Natan, E., and Joerger, A.C. (2012). Structure and kinetic stability of the p63 tetramerization domain. J. Mol. Biol. *415*, 503–513.

Nemajerova, A., Kramer, D., Siller, S.S., Herr, C., Shomroni, O., Pena, T., Gallinas Suazo, C., Glaser, K., Wildung, M., Steffen, H., et al. (2016). TAp73 is a central transcriptional regulator of airway multiciliogenesis. Genes Dev. *30*, 1300–1312.

Nemajerova, A., Amelio, I., Gebel, J., Dötsch, V., Melino, G., and Moll, U.M. (2018). Non-oncogenic roles of TAp73: from multiciliogenesis to metabolism. Cell Death & Differentiation *25*, 144–153.

Ng, W.L., Chen, G., Wang, M., Wang, H., Story, M., Shay, J.W., Zhang, X., Wang, J., Amin, A.R.M.R., Hu, B., et al. (2014). OCT4 as a target of miR-34a stimulates p63 but inhibits p53 to promote human cell transformation. Cell Death Dis. *5*, e1024.

Nguyen, B.-C., Lefort, K., Mandinova, A., Antonini, D., Devgan, V., Della Gatta, G., Koster, M.I., Zhang, Z., Wang, J., Tommasi di Vignano, A., et al. (2006). Cross-regulation between Notch and p63 in keratinocyte commitment to differentiation. Genes Dev. *20*, 1028–1042.

Niklison-Chirou, M.V., Erngren, I., Engskog, M., Haglöf, J., Picard, D., Remke, M., McPolin, P.H.R., Selby, M., Williamson, D., Clifford, S.C., et al. (2017). TAp73 is a marker of glutamine addiction in medulloblastoma. Genes Dev. *31*, 1738–1753.

Nyström, A., Velati, D., Mittapalli, V.R., Fritsch, A., Kern, J.S., and Bruckner-Tuderman, L. (2013). Collagen VII plays a dual role in wound healing. J. Clin. Invest. *123*, 3498–3509.

Oh, J., Lee, Y.D., and Wagers, A.J. (2014). Stem cell aging: mechanisms, regulators and therapeutic opportunities. Nat. Med. *20*, 870–880.

Olsen, T.K., and Baryawno, N. (2018). Introduction to Single-Cell RNA Sequencing. Current Protocols in Molecular Biology *122*, e57.

Osada, M., Ohba, M., Kawahara, C., Ishioka, C., Kanamaru, R., Katoh, I., Ikawa, Y., Nimura, Y., Nakagawara, A., Obinata, M., et al. (1998). Cloning and functional analysis of human p51, which structurally and functionally resembles p53. Nat. Med. *4*, 839–843.

Osada, M., Park, H.L., Nagakawa, Y., Yamashita, K., Fomenkov, A., Kim, M.S., Wu, G., Nomoto, S., Trink, B., and Sidransky, D. (2005). Differential recognition of response elements determines target gene specificity for p53 and p63. Mol. Cell. Biol. *25*, 6077–6089.

Oshlack, A., and Wakefield, M.J. (2009). Transcript length bias in RNA-seq data confounds systems biology. Biol. Direct *4*, 14.

Pan, S.-C., Li, C.-Y., Kuo, C.-Y., Kuo, Y.-Z., Fang, W.-Y., Huang, Y.-H., Hsieh, T.-C., Kao, H.-Y., Kuo, Y., Kang, Y.-R., et al. (2018). The p53-S100A2 Positive Feedback Loop Negatively Regulates Epithelialization in Cutaneous Wound Healing. Sci. Rep. *8*, 5458.

Patel, G.K., Wilson, C.H., Harding, K.G., Finlay, A.Y., and Bowden, P.E. (2006). Numerous keratinocyte subtypes involved in wound re-epithelialization. J. Invest. Dermatol. *126*, 497–502.

Pellegrini, G., Dellambra, E., Golisano, O., Martinelli, E., Fantozzi, I., Bondanza, S., Ponzin, D., McKeon, F., and De Luca, M. (2001). p63 identifies keratinocyte stem cells. Proc. Natl. Acad. Sci. U. S. A. *98*, 3156–3161.

Perez, C.A., Ott, J., Mays, D.J., and Pietenpol, J.A. (2007). p63 consensus DNA-binding site: identification, analysis and application into a p63MH algorithm. Oncogene *26*, 7363–7370.

Pietenpol, J.A., Tokino, T., Thiagalingam, S., el-Deiry, W.S., Kinzler, K.W., and Vogelstein, B. (1994). Sequence-specific transcriptional activation is essential for growth suppression by p53. Proc. Natl. Acad. Sci. U. S. A. *91*, 1998–2002.

Ponting, C.P. (1995). SAM: a novel motif in yeast sterile and Drosophila polyhomeotic proteins. Protein Sci. *4*, 1928–1930.

Pozniak, C.D., Barnabé-Heider, F., Rymar, V.V., Lee, A.F., Sadikot, A.F., and Miller, F.D. (2002). p73 is required for survival and maintenance of CNS neurons. J. Neurosci. *22*, 9800–9809.

Proksch, E., Brandner, J.M., and Jensen, J.-M. (2008). The skin: an indispensable barrier. Experimental Dermatology *17*, 1063–1072.

Puig, P., Capodieci, P., Drobnjak, M., Verbel, D., Prives, C., Cordon-Cardo, C., and Di Como, C.J. (2003). p73 Expression in human normal and tumor tissues: loss of p73alpha expression is associated with tumor progression in bladder cancer. Clin. Cancer Res. *9*, 5642–5651.

Ramírez, F., Dündar, F., Diehl, S., Grüning, B.A., and Manke, T. (2014). deepTools: a flexible platform for exploring deep-sequencing data. Nucleic Acids Res. *42*, W187–W191.

Raycroft, L., Wu, H.Y., and Lozano, G. (1990). Transcriptional activation by wild-type but not transforming mutants of the p53 anti-oncogene. Science *249*, 1049–1051.

Reynolds, L.E., Conti, F.J., Silva, R., Robinson, S.D., Iyer, V., Rudling, R., Cross, B., Nye, E., Hart, I.R., Dipersio, C.M., et al. (2008). alpha3beta1 integrin-controlled Smad7 regulates reepithelialization during wound healing in mice. J. Clin. Invest. *118*, 965–974.

Rinaldi, L., Datta, D., Serrat, J., Morey, L., Solanas, G., Avgustinova, A., Blanco, E., Pons, J.I., Matallanas, D., Von Kriegsheim, A., et al. (2016). Dnmt3a and Dnmt3b Associate with Enhancers to Regulate Human Epidermal Stem Cell Homeostasis. Cell Stem Cell *19*, 491–501.

Rinne, T., Brunner, H.G., and van Bokhoven, H. (2007). p63-associated disorders. Cell Cycle *6*, 262–268.

Rinne, T., Clements, S.E., Lamme, E., Duijf, P.H.G., Bolat, E., Meijer, R., Scheffer, H., Rosser, E., Tan, T.Y., McGrath, J.A., et al. (2008). A novel translation re-initiation mechanism for the p63 gene revealed by amino-terminal truncating mutations in Rapp-Hodgkin/Hay-Wells-like syndromes. Hum. Mol. Genet. *17*, 1968–1977.

Rizzo, J.M., Romano, R.-A., Bard, J., and Sinha, S. (2015). RNA-seq studies reveal new insights into p63 and the transcriptomic landscape of the mouse skin. J. Invest. Dermatol. *135*, 629–632.

Rocco, J.W., Leong, C.-O., Kuperwasser, N., DeYoung, M.P., and Ellisen, L.W. (2006). p63 mediates survival in squamous cell carcinoma by suppression of p73-dependent apoptosis. Cancer Cell *9*, 45–56.

Rogakou, E.P., Pilch, D.R., Orr, A.H., Ivanova, V.S., and Bonner, W.M. (1998). DNA double-stranded breaks induce histone H2AX phosphorylation on serine 139. J. Biol. Chem. *273*, 5858–5868.

Romano, R.-A., Birkaya, B., and Sinha, S. (2007). A functional enhancer of keratin14 is a direct transcriptional target of deltaNp63. J. Invest. Dermatol. *127*, 1175–1186.

Romano, R.-A., Smalley, K., Magraw, C., Serna, V.A., Kurita, T., Raghavan, S., and Sinha, S. (2012). ΔNp63 knockout mice reveal its indispensable role as a master regulator of epithelial development and differentiation. Development *139*, 772–782.

Rosenbluth, J.M., Johnson, K., Tang, L., Triplett, T., and Pietenpol, J.A. (2009). Evaluation of p63 and p73 antibodies for cross-reactivity. Cell Cycle *8*, 3702–3706.

Rosenbluth, J.M., Mays, D.J., Jiang, A., Shyr, Y., and Pietenpol, J.A. (2011). Differential regulation of the p73 cistrome by mammalian target of rapamycin reveals transcriptional programs of mesenchymal differentiation and tumorigenesis. Proc. Natl. Acad. Sci. U. S. A. *108*, 2076–2081.

Rossi, M., De Laurenzi, V., Munarriz, E., Green, D.R., Liu, Y.-C., Vousden, K.H., Cesareni, G., and Melino, G. (2005). The ubiquitin–protein ligase Itch regulates p73 stability. The EMBO Journal *24*, 836–848.

Rossi, M., Aqeilan, R.I., Neale, M., Candi, E., Salomoni, P., Knight, R.A., Croce, C.M., and Melino, G. (2006). The E3 ubiquitin ligase Itch controls the protein stability of p63. Proc. Natl. Acad. Sci. U. S. A. *103*, 12753–12758.

Rufini, A., Niklison-Chirou, M.V., Inoue, S., Tomasini, R., Harris, I.S., Marino, A., Federici, M., Dinsdale, D., Knight, R.A., Melino, G., et al. (2012). TAp73 depletion accelerates aging through metabolic dysregulation. Genes Dev. *26*, 2009–2014.

Russo, C., Osterburg, C., Sirico, A., Antonini, D., Ambrosio, R., Würz, J.M., Rinnenthal, J., Ferniani, M., Kehrloesser, S., Schäfer, B., et al. (2018). Protein aggregation of the p63 transcription factor underlies severe skin fragility in AEC syndrome. Proc. Natl. Acad. Sci. U. S. A. *115*, E906–E915.

Sada, A., Jacob, F., Leung, E., Wang, S., White, B.S., Shalloway, D., and Tumbar, T. (2016). Defining the cellular lineage hierarchy in the interfollicular epidermis of adult skin. Nat. Cell Biol. *18*, 619–631.

Saha, A., Kim, Y., Gewirtz, A.D.H., Jo, B., Gao, C., McDowell, I.C., GTEx Consortium, Engelhardt, B.E., and Battle, A. (2017). Co-expression networks reveal the tissue-specific regulation of transcription and splicing. Genome Res. *27*, 1843–1858.

Santos Guasch, G.L., Beeler, J.S., Marshall, C.B., Shaver, T.M., Sheng, Q., Johnson, K.N., Boyd, K.L., Venters, B.J., Cook, R.S., and Pietenpol, J.A. (2018). p73 Is Required for Ovarian Follicle Development and Regulates a Gene Network Involved in Cell-to-Cell Adhesion. iScience *8*, 236–249.

Sarantopoulou, D., Nayak, S., Brooks, T.G., Lahens, N.F., and Grant, G.R. (2019). Comparative evaluation of full-length isoform quantification from RNA-Seq. bioRxiv.

Sasaki, Y., Naishiro, Y., Oshima, Y., Imai, K., Nakamura, Y., and Tokino, T. (2005). Identification of pigment epithelium-derived factor as a direct target of the p53 family member genes. Oncogene *24*, 5131–5136.

Schavolt, K.L., and Pietenpol, J.A. (2007). p53 and Delta Np63 alpha differentially bind and regulate target genes involved in cell cycle arrest, DNA repair and apoptosis. Oncogene *26*, 6125–6132.

Seelan, R.S., Irwin, M., van der Stoop, P., Qian, C., Kaelin, W.G., Jr, and Liu, W. (2002). The human p73 promoter: characterization and identification of functional E2F binding sites. Neoplasia *4*, 195–203.

Senoo, M., Pinto, F., Crum, C.P., and McKeon, F. (2007). p63 Is essential for the proliferative potential of stem cells in stratified epithelia. Cell *129*, 523–536.

Serber, Z., Lai, H.C., Yang, A., Ou, H.D., Sigal, M.S., Kelly, A.E., Darimont, B.D., Duijf, P.H.G., Van Bokhoven, H., McKeon, F., et al. (2002). A C-terminal inhibitory domain controls the activity of p63 by an intramolecular mechanism. Mol. Cell. Biol. *22*, 8601–8611.

Serrano, M., Lin, A.W., McCurrach, M.E., Beach, D., and Lowe, S.W. (1997). Oncogenic ras provokes premature cell senescence associated with accumulation of p53 and p16INK4a. Cell *88*, 593–602.

Sethi, I., Romano, R.-A., Gluck, C., Smalley, K., Vojtesek, B., Buck, M.J., and Sinha, S. (2015). A global analysis of the complex landscape of isoforms and regulatory networks of p63 in human cells and tissues. BMC Genomics *16*, 584.

Shieh, S.Y., Ikeda, M., Taya, Y., and Prives, C. (1997). DNA damage-induced phosphorylation of p53 alleviates inhibition by MDM2. Cell *91*, 325–334.

Shimomura, Y., Wajid, M., Shapiro, L., and Christiano, A.M. (2008). P-cadherin is a p63 target gene with a crucial role in the developing human limb bud and hair follicle. Development *135*, 743–753.

Siegel, D.H., Ashton, G.H.S., Penagos, H.G., Lee, J.V., Feiler, H.S., Wilhelmsen, K.C., South, A.P., Smith, F.J.D., Prescott, A.R., Wessagowit, V., et al. (2003). Loss of kindlin-1, a human homolog of the Caenorhabditis elegans actin-extracellular-matrix linker protein UNC-112, causes Kindler syndrome. Am. J. Hum. Genet. *73*, 174–187.

Sniezek, J.C., Matheny, K.E., Westfall, M.D., and Pietenpol, J.A. (2004). Dominant Negative p63 Isoform Expression in Head and Neck Squamous Cell Carcinoma. The Laryngoscope *114*, 2063–2072.

Srivastava, S., Zou, Z.Q., Pirollo, K., Blattner, W., and Chang, E.H. (1990). Germ-line transmission of a mutated p53 gene in a cancer-prone family with Li-Fraumeni syndrome. Nature *348*, 747–749.

Stark, H.-J., Boehnke, K., Mirancea, N., Willhauck, M.J., Pavesio, A., Fusenig, N.E., and Boukamp, P. (2006). Epidermal homeostasis in long-term scaffold-enforced skin equivalents. J. Investig. Dermatol. Symp. Proc. *11*, 93–105.

Stark, R., Grzelak, M., and Hadfield, J. (2019). RNA sequencing: the teenage years. Nat. Rev. Genet.

Stiewe, T., and Pützer, B.M. (2000). Role of the p53-homologue p73 in E2F1-induced apoptosis. Nature Genetics *26*, 464–469.

Su, X., Paris, M., Gi, Y.J., Tsai, K.Y., Cho, M.S., Lin, Y.-L., Biernaskie, J.A., Sinha, S., Prives, C., Pevny, L.H., et al. (2009). TAp63 prevents premature aging by promoting adult stem cell maintenance. Cell Stem Cell *5*, 64–75.

Suh, E.-K., Yang, A., Kettenbach, A., Bamberger, C., Michaelis, A.H., Zhu, Z., Elvin, J.A., Bronson, R.T., Crum, C.P., and McKeon, F. (2006). p63 protects the female germ line during meiotic arrest. Nature *444*, 624–628.

Tabula Muris Consortium, Overall coordination, Logistical coordination, Organ collection and processing, Library preparation and sequencing, Computational data analysis, Cell type annotation, Writing group, Supplemental text writing group, and Principal investigators (2018). Single-cell transcriptomics of 20 mouse organs creates a Tabula Muris. Nature *562*, 367–372.

Talos, F., Abraham, A., Vaseva, A.V., Holembowski, L., Tsirka, S.E., Scheel, A., Bode, D., Dobbelstein, M., Brück, W., and Moll, U.M. (2010). p73 is an essential regulator of neural stem cell maintenance in embryonal and adult CNS neurogenesis. Cell Death Differ. *17*, 1816–1829.

Thanos, C.D., and Bowie, J.U. (1999). p53 Family members p63 and p73 are SAM domain-containing proteins. Protein Sci. *8*, 1708–1710.

Thorvaldsdóttir, H., Robinson, J.T., and Mesirov, J.P. (2013). Integrative Genomics Viewer (IGV): high-performance genomics data visualization and exploration. Brief. Bioinform. *14*, 178–192.

Thurfjell, N., Coates, P.J., Boldrup, L., Lindgren, B., Bäcklund, B., Uusitalo, T., Mahani, D., Dabelsteen, E., Dahlqvist, A., Sjöström, B., et al. (2005). Function and importance of p63 in normal oral mucosa and squamous cell carcinoma of the head and neck. Adv. Otorhinolaryngol. *62*, 49–57.

Tissir, F., Ravni, A., Achouri, Y., Riethmacher, D., Meyer, G., and Goffinet, A.M. (2009). DeltaNp73 regulates neuronal survival in vivo. Proc. Natl. Acad. Sci. U. S. A. *106*, 16871–16876.

Tomasini, R., Tsuchihara, K., Wilhelm, M., Fujitani, M., Rufini, A., Cheung, C.C., Khan, F., Itie-Youten, A., Wakeham, A., Tsao, M.-S., et al. (2008). TAp73 knockout shows genomic instability with infertility and tumor suppressor functions. Genes Dev. *22*, 2677–2691.

Tomasini, R., Tsuchihara, K., Tsuda, C., Lau, S.K., Wilhelm, M., Rufini, A., Tsao, M.-S., Iovanna, J.L., Jurisicova, A., Melino, G., et al. (2009). TAp73 regulates the spindle assembly checkpoint by modulating BubR1 activity. Proceedings of the National Academy of Sciences *106*, 797–802.

Truong, A.B., Kretz, M., Ridky, T.W., Kimmel, R., and Khavari, P.A. (2006). p63 regulates proliferation and differentiation of developmentally mature keratinocytes. Genes Dev. *20*, 3185–3197.

Turcan, I., Pasmooij, A.M.G., van den Akker, P.C., Lemmink, H., Halmos, G.B., Sinke, R.J., and Jonkman, M.F. (2016). Heterozygosity for a Novel Missense Mutation in the ITGB4 Gene Associated With Autosomal Dominant Epidermolysis Bullosa. JAMA Dermatol. *152*, 558–562.

Uhlen, M., Oksvold, P., Fagerberg, L., Lundberg, E., Jonasson, K., Forsberg, M., Zwahlen, M., Kampf, C., Wester, K., Hober, S., et al. (2010). Towards a knowledge-based Human Protein Atlas. Nat. Biotechnol. *28*, 1248–1250.

Velculescu, V.E., Zhang, L., Zhou, W., Vogelstein, J., Basrai, M.A., Bassett, D.E., Jr, Hieter, P., Vogelstein, B., and Kinzler, K.W. (1997). Characterization of the yeast transcriptome. Cell *88*, 243–251.

Venkatesh, B., Lee, A.P., Ravi, V., Maurya, A.K., Lian, M.M., Swann, J.B., Ohta, Y., Flajnik, M.F., Sutoh, Y., Kasahara, M., et al. (2014). Elephant shark genome provides unique insights into gnathostome evolution. Nature *505*, 174–179.

Wang, J., Vasaikar, S., Shi, Z., Greer, M., and Zhang, B. (2017). WebGestalt 2017: a more comprehensive, powerful, flexible and interactive gene set enrichment analysis toolkit. Nucleic Acids Res. *45*, W130–W137.

Wang, Z., Gerstein, M., and Snyder, M. (2009). RNA-Seq: a revolutionary tool for transcriptomics. Nat. Rev. Genet. *10*, 57–63.

Ward, I.M., and Chen, J. (2001). Histone H2AX is phosphorylated in an ATR-dependent manner in response to replicational stress. J. Biol. Chem. *276*, 47759–47762.

Warner, S.M.B., Hackett, T.-L., Shaheen, F., Hallstrand, T.S., Kicic, A., Stick, S.M., and Knight, D.A. (2013). Transcription factor p63 regulates key genes and wound repair in human airway epithelial basal cells. Am. J. Respir. Cell Mol. Biol. *49*, 978–988.

Weber, A., Bellmann, U., Bootz, F., Wittekind, C., and Tannapfel, A. (2002). Expression of p53 and its homologues in primary and recurrent squamous cell carcinomas of the head and neck. Int. J. Cancer *99*, 22–28.

Weinberg, R.L., Veprintsev, D.B., and Fersht, A.R. (2004). Cooperative binding of tetrameric p53 to DNA. J. Mol. Biol. *341*, 1145–1159.

Werner, S., and Grose, R. (2003). Regulation of wound healing by growth factors and cytokines. Physiol. Rev. *83*, 835–870.

Westfall, M.D., Mays, D.J., Sniezek, J.C., and Pietenpol, J.A. (2003). The Delta Np63 alpha phosphoprotein binds the p21 and 14-3-3 sigma promoters in vivo and has transcriptional repressor activity that is reduced by Hay-Wells syndrome-derived mutations. Mol. Cell. Biol. *23*, 2264–2276.

Wildung, M., Esser, T.U., Grausam, K.B., Wiedwald, C., Volceanov-Hahn, L., Riedel, D., Beuermann, S., Li, L., Zylla, J., Guenther, A.-K., et al. (2019). Transcription factor TAp73 and microRNA-449 complement each other to support multiciliogenesis. Cell Death Differ.

Wilhelm, M.T., Rufini, A., Wetzel, M.K., Tsuchihara, K., Inoue, S., Tomasini, R., Itie-Youten, A., Wakeham, A., Arsenian-Henriksson, M., Melino, G., et al. (2010). Isoform-specific p73 knockout mice reveal a novel role for delta Np73 in the DNA damage response pathway. Genes Dev. *24*, 549–560.

Wojcik, S.M., Bundman, D.S., and Roop, D.R. (2000). Delayed wound healing in keratin 6a knockout mice. Mol. Cell. Biol. *20*, 5248–5255.

Wu, G., Nomoto, S., Hoque, M.O., Dracheva, T., Osada, M., Lee, C.-C.R., Dong, S.M., Guo, Z., Benoit, N., Cohen, Y., et al. (2003). DeltaNp63alpha and TAp63alpha regulate transcription of genes with distinct biological functions in cancer and development. Cancer Res. *63*, 2351–2357.

Wu, H., Zeinab, R.A., Flores, E.R., and Leng, R.P. (2011). Pirh2, a ubiquitin E3 ligase, inhibits p73 transcriptional activity by promoting its ubiquitination. Mol. Cancer Res. *9*, 1780–1790.

Wu, S., Murai, S., Kataoka, K., and Miyagishi, M. (2008). Yin Yang 1 induces transcriptional activity of p73 through cooperation with E2F1. Biochem. Biophys. Res. Commun. *365*, 75–81.

Wu, X., Bayle, J.H., Olson, D., and Levine, A.J. (1993). The p53-mdm-2 autoregulatory feedback loop. Genes Dev. *7*, 1126–1132.

Yang, A., Kaghad, M., Wang, Y., Gillett, E., Fleming, M.D., Dötsch, V., Andrews, N.C., Caput, D., and McKeon, F. (1998). p63, a p53 homolog at 3q27-29, encodes multiple products with transactivating, death-inducing, and dominant-negative activities. Mol. Cell *2*, 305–316.

Yang, A., Schweitzer, R., Sun, D., Kaghad, M., Walker, N., Bronson, R.T., Tabin, C., Sharpe, A., Caput, D., Crum, C., et al. (1999). p63 is essential for regenerative proliferation in limb, craniofacial and epithelial development. Nature *398*, 714–718.

Yang, A., Walker, N., Bronson, R., Kaghad, M., Oosterwegel, M., Bonnin, J., Vagner, C., Bonnet, H., Dikkes, P., Sharpe, A., et al. (2000). p73-deficient mice have neurological, pheromonal and inflammatory defects but lack spontaneous tumours. Nature *404*, 99–103.

Yang, A., Kaghad, M., Caput, D., and McKeon, F. (2002). On the shoulders of giants: p63, p73 and the rise of p53. Trends Genet. *18*, 90–95.

Yang, A., Zhu, Z., Kettenbach, A., Kapranov, P., McKeon, F., Gingeras, T.R., and Struhl, K. (2010). Genome-wide mapping indicates that p73 and p63 co-occupy target sites and have similar dna-binding profiles in vivo. PLoS One *5*, e11572.

Yang, H., Adam, R.C., Ge, Y., Hua, Z.L., and Fuchs, E. (2017). Epithelial-Mesenchymal Micro-niches Govern Stem Cell Lineage Choices. Cell *169*, 483–496.e13.

Yonish-Rouach, E., Resnitzky, D., Lotem, J., Sachs, L., Kimchi, A., and Oren, M. (1991). Wild-type p53 induces apoptosis of myeloid leukaemic cells that is inhibited by interleukin-6. Nature *352*, 345–347.

Yu, Z., Lin, K.K., Bhandari, A., Spencer, J.A., Xu, X., Wang, N., Lu, Z., Gill, G.N., Roop, D.R., Wertz, P., et al. (2006). The Grainyhead-like epithelial transactivator Get-1/Grhl3 regulates epidermal terminal differentiation and interacts functionally with LMO4. Dev. Biol. *299*, 122–136.

Zeng, X., Chen, L., Jost, C.A., Maya, R., Keller, D., Wang, X., Kaelin, W.G., Jr, Oren, M., Chen, J., and Lu, H. (1999). MDM2 suppresses p73 function without promoting p73 degradation. Mol. Cell. Biol. *19*, 3257–3266.

Zhang, Y., Liu, T., Meyer, C.A., Eeckhoute, J., Johnson, D.S., Bernstein, B.E., Nusbaum, C., Myers, R.M., Brown, M., Li, W., et al. (2008). Model-based analysis of ChIP-Seq (MACS). Genome Biol. *9*, R137.

Zufferey, R., Nagy, D., Mandel, R.J., Naldini, L., and Trono, D. (1997). Multiply attenuated lentiviral vector achieves efficient gene delivery in vivo. Nat. Biotechnol. *15*, 871–875.